Universidad de Oviedo

FACULTAD DE CIENCIAS
Departamento de Física
Programa de Doctorado Física Fundamental y Aplicada

VARIABILIDAD HIDROGRÁFICA Y CIRCULACIÓN DEL OCÉANO PROFUNDO EN EL NOROESTE DE LA PENÍNSULA IBÉRICA

DEEP OCEAN HYDROGRAPHICAL VARIABILITY AND CIRCULATION IN THE NORTH-WEST IBERIA

TESIS DOCTORAL

Eva Prieto Bravo

Centro Oceanográfico de Gijón,
INSTITUTO ESPAÑOL DE OCEANOGRAFÍA

Oviedo, 2014.

Contents

Agradecimientos

El trabajo desarrollado durante esta tesis doctoral ha sido financiado por la beca de Formación de Personal Investigador (FPI) del Ministerio de Ciencia e Innovación asociada al proyecto COVACLAN (CTM2007-64600) del Instituto Español de Oceanografía.

En primer lugar, quiero agradecer a mis compañeros del equipo VACLAN y COVACLAN (Águeda, Ángel, Amaia, Cabanas, Chete, Elena's, Fernando, Gonzalo, Guillermo, Manuel, Menchu, Nacho, Raquel, Ricardo...), procedentes de los distintos Centros Oceanográficos de A Coruña, Cádiz, Santander y Vigo, por todo el esfuerzo y trabajo realizado desde el inicio del proyecto en 2003 (y el compartido desde mi incorporación en 2008), y a las tripulaciones del B/O Cornide de Saavedra y B/O Thalassa, aquellos que "nos llevan a medir el mar" y capean los temporales, por hacer que durante los dias de campaña todo llegara a *buen puerto*, nunca mejor dicho.

Al Grupo de Oceanografía Física de la Universidad de Vigo (Gabi, Kiko, Ramiro, Rocío...) con los que realicé mi estancia en 2009, y a los profesores del Máster en Física Aplicada. A Jorge y a Sara, por hacer que las Estrellas Galicia supieran mejor fuera de la Universidad y por nuestros conciertos de Jazz. Gracias al doctorado por darme la oportunidad de vivir durante una temporada en Galicia, no podía ser otro lugar: **toda ella es mar**.

Thanks to the Marine Physics and Ocean Climate Group of the National Oceanography Centre of Southampton where I was working during 2010 and 2011. Specially to N. Penny Holliday, for her support from the first day, her advices, comments and help for the writing process of one of submitted manuscripts. Also to Elaine McDonagh, Harry Bryden and to all the people who I met there, specially to Álvaro, Mary and Maxi.

Gracias al Grupo de Oceanografía Física del Centro Oceanográfico de Canarias con el que realicé mi estancia en 2012: a Eugenio, por transmitirme el entusiasmo por lo que hacemos a pesar de las dificultades, a Fran y Mire (no me caben en un párrafo todas las historias vividas en la Calle Salamanca), por todos los buenos momentos que me habéis dado, y porque estoy segura de que *"This must be the place"*. A Isis y Vero, por su disponibilidad para resolver cualquier duda. Porque nunca olvidaré la experiencia de trabajar sobre un volcán submarino en erupción.

Gracias a TODO el personal del Centro Oceanográfico de Gijón, por cuidarme desde el primer dia y por todas las horas compartidas en el comedor. A Elena y Jesús por involucrarse tanto en su (nuestro) trabajo y recibirnos cada mañana con una sonrisa; a Pili, por todas las charlas y por preocuparse tanto por el avance de la tesis y el retroceso de los kilos (jeje).. A mis compañeros de la sala Vip, ruta, café y cerve de viernes, porque sin ellos no hubiera sido lo mismo: Néstor, Ale, Dani, Eva V., Floren, Gonzalo, Leti, Lucie, Maite, Pili, Sara, Tamara, Virgi... A mis tres fundamentales, Juan, Paqui (veci!) y Sofi, porque a veces no era necesario ni hablar. Y a todas las personas con las que coincidí en algún momento de esta travesía.

A César, por su optimismo y su capacidad para hacerlo todo posible, por simplificar las cosas que yo veía complicadas y ayudarme a formarme en el duro mundo de la investigación. Por facilitarme la asistencia a cursos, congresos y campañas. Porque sabía que trabajando con él cualquier cosa iba a salir bien. A Alicia por sus ánimos, por estar siempre al tanto de todo y ayudarme en cualquier cosa que necesitara. Gracias a ambos por la confianza depositada en mi durante estos años. A Julio por su apoyo continuo como tutor en la Universidad de Oviedo y a Maria Ángeles, por su positivismo, generosidad y apoyo brindado, durante y después de la carrera. También a Jesús y Elena del Departamento de Física, por ayudarme y facilitarme el último empujón en el proceso de depósito.

A mis amigas, Eva y Raquel por su apoyo, por ser una via de escape, y en definitiva por estar siempre, a pesar de la distancia. A Fer, Jose y a Luis, por saber cuál era la pregunta que no se podía hacer y por todas las charlas sobre Matlab. Gracias por darme una perspectiva "desde fuera". Y a Juanín, por compartir parte de esta andadura conmigo. También a los que no entendían del todo a qué me dedicaba, y en general a todas las personas que se han interesado por mi trabajo o me han apoyado en algún momento.

Por último, quiero dedicarle este trabajo íntegramente a mi familia. A mis abuelos, mis tios y sobre todo a mis padres, por su apoyo incondicional y por los valores que me han inculcado hasta llegar aquí, y a mi hermana Sonia, por aportarme su visión práctica del mundo, por su vitalidad y por ser un ejemplo para mí.

"Si he logrado ver más lejos, ha sido porque he subido a hombros de gigantes."
I. Newton.

Resumen

El muestreo hidrográfico desde 2003 a lo largo de tres secciones oceanográficas profundas perpendiculares a la costa, 200 millas náuticas al oeste de cabo Finisterre en 43°N, 100 millas al norte de cabo Ortegal (8°O) y 100 al norte de Santander (3°47′O), ha permitido el análisis más detallado hasta la fecha de la variabilidad estacional e interanual de las propiedades termohalinas de las masas de agua en el noroeste de la península ibérica y sur del golfo de Vizcaya.

El muestreo semianual de la sección de Finisterre durante el periodo 2003-2010 ha revelado una fuerte estacionalidad en las propiedades termohalinas de todas las masas de agua de la termoclina permanente (hasta los 2000 dbar), caracterizada por una notable asimetría entre la región del talud y el océano abierto. En verano la vena de agua mediterránea aparece ceñida al talud y menor profundidad, reforzando su huella termohalina que a su vez disminuye en océano abierto. En invierno la situación se invierte y el agua mediterránea parece desprenderse del talud y propagarse hacia el oeste observándose incluso una rama secundaria alrededor del banco de Galicia. La estacionalidad en aguas intermedias alcanza valores de hasta 0.4°C y 0.08 en salinidad en la base del agua mediterránea, del orden del 20% de la variabilidad interanual observada durante todo el periodo. La descomposición de los cambios isobáricos en cambios isopicnos y cambios debidos al desplazamiento vertical de las isoneutras se muestra útil a la hora de analizar los patrones observados en función de (1) la estacionalidad a gran escala del giro subtropical como respuesta a la migración del sistema de altas presiones en el Atlántico Norte, (2) la dinámica del talud continental, caracterizada por el afloramiento en verano, el desarrollo de la Corriente Ibérica hacia el Polo en invierno y la propagación del agua mediterránea, y (3) la posible influencia de los cambios estacionales de las propiedades de las masas de agua adquiridas en sus regiones de formación.

Una vez cuantificada y extraída la estacionalidad se analizaron las series temporales de las propiedades de las diferentes masas de agua a lo largo de las tres secciones. La correlación entre cambios en la columna de agua, secciones y la propia autocorrelación de cada serie indican que las señales observadas son cambios robustos de las masas de agua a escala regional. Las series no muestran tendencias suaves sino que se caracterizan por transiciones que una vez producidas persisten durante campañas consecutivas. Como observaciones destacadas se incluye un aumento relativamente brusco de la salinidad de las aguas centrales en 2005 que permanece hasta la actualidad y una disminución de las propiedades termohalinas del agua con origen en el mar de Labrador desde el otoño de 2008 a 2010. Se observa una respuesta integrada a estados fuertes de la Oscilación del Atlántico Norte, destacando el calentamiento/salinificación de la columna de agua tras la fuerte caída del índice NAO en 2010. Este patrón es consistente con la respuesta esperada de la circulación a gran escala del Atlántico Norte, caracterizada por la propagación de aguas cálidas y salinas hacia el norte en la cuenca oriental durante un índice NAO negativo.

Las campañas de febrero y septiembre, caracterizadas por la estructura invierno/verano típica, disponen además de un conjunto de medidas directas de velocidad de corriente —perfilador acústico en roseta (LADCP), ADCP de casco y una línea de fondeo— que han servido para estimar transportes a través de la sección y comparar los diferentes métodos posibles. Se observan tres regiones bien diferenciadas, plataforma-talud caracterizada por transporte hacia el norte, el paso hasta el banco de Galicia con transporte sur y el oeste del banco de nuevo con transporte norte. Las corrientes en el paso hasta el banco de Galicia son predominantemente barotrópicas por lo que las estructuras que se observan en los campos geostróficos se ven advectadas.

Summary

Oceanic hydrography of the north-easternmost region of the North Atlantic subtropical gyre has been monitored since 2003 for the whole water column ($>$ 5000 m) by three sections extending zonally 200 nautical miles (nm) westwards of Cape Finisterre (43°N, western Iberia margin), and meridionally 100 nm off Cape Ortegal (8°W, southwestern Bay of Biscay) and 100 nm off Santander (3°47′W, southeastern Bay of Biscay), allowing for the analysis of the deep ocean variability from seasonal to interannual scales.

Semiannual time series of the Finisterre oceanographic section from 2003 to 2010 have shown that all water masses down to the permanent thermocline (2000 dbar) exhibit a consistent seasonal signature in their thermohaline properties with notable asymmetry between the slope region and the outer ocean. In summertime, Mediterranean Water (MW) gets tightly attached against the slope and is uplifted, reinforcing its thermohaline signature and diminishing its presence at the outer ocean. In wintertime the situation reverses, MW seems to detach from the slope and spreads out to the open ocean, even being observed a secondary branch around the Galicia Bank. Thermohaline seasonality at depth shows values up to 0.4°C and 0.08 in salinity at the lower MW, of the order of 20% of the overall interannual variability observed during the whole period. Decomposition of thermohaline changes at isobaric levels to changes along isoneutral surfaces and changes due to vertical displacements helped analyze the physical processes behind the observed seasonality in terms of (1) the large-scale seasonality of the subtropical gyre in response to the seasonal migration of the subtropical high pressure system, (2) the continental slope dynamics, characterized by summer upwelling, winter development of the Iberian Poleward Current and Mediterranean water spreading, and (3) the possible influence of seasonal changes of water mass properties at their formation sources.

Once signals were de-seasonalized, time series of property interannual changes of the different water masses were analyzed. Correlation of series in the vertical and among sections, autocorrelation and estimates of the effect of the noise induced by the mesoscale field, all indicate that observed signatures are robust changes of water masses at the regional scale. The hydrographic timeseries are not characterized by smooth trends but instead by shifts that persist through consecutive cruises. The most notable features include a shift to more saline central waters around 2005 after which they remained stable, and a decrease in thermohaline properties of the Labrador Sea Water from autumn 2008 to 2010. Years with a strong winter North Atlantic Oscillation (NAO) index are characterized by shifts in thermohaline properties across most of the intermediate levels, with the most notable event being the warming and increasing salinity that followed the large NAO index drop of 2010. These observations are consistent with current understanding of the large-scale functioning of the North Atlantic, which predicts a northeastwards expansion of subtropical temperate waters in the eastern boundary as a response to negative NAO forcing.

February and September cruises in 2008, exhibiting the typical winter/summer thermohaline distinct structures and also having a quite complete set of direct velocity measurements — Lowered Acoustic Current Profiler (LADCP), ship hull ADCP and an active mooring line — were explored to estimate transports across the section and compare different methods available. Three regions were evidenced, the continental shelf break-slope characterized by northwards transport, southwards circulation across most of the passage to the Galician Bank summit and then northwards flow again west of the seamount. Currents across the passage from Finisterre to the Galician Bank were markedly barotropic so mesoscale structures evidenced by geostrophy were being advected across the passage.

Glossary

AC Azores Current

BT Bottom-Track

CC Canary Current

CTD Conductivity-Temperature-Depth

ENACW Eastern North Atlantic Central Water

ENADW Eastern North Atlantic Deep Water

IEO Instituto Español de Oceanografía / Spanish Institute of Oceanography

IPC Iberian Poleward Current

IPCC Intergovernmental Panel on Climate Change

LADCP Lowered Acoustic Doppler Current Profiler

LDW Lower Deep Water

LSW Labrador Sea Water

MOCHA Meridional Overturning Circulation and Heat Transport Array

MW Mediterranean Water

NAC North Atlantic Current

NAO North Atlantic Oscillation

OCCAM Ocean Circulation and Climate Advanced Modelling

PC Portugal Current

RadProf Radiales Profundas

RAPID Rapid Climate Change

SADCP Ship-mounted Acoustic Doppler Current Profiler

SCOW Scatterometer Climatology of Ocean Winds

SPG Subpolar Gyre

SPGI Subpolar Gyre Index

STG Subtropical Gyre

VACLAN/COVACLAN Variabilidad Climática del Atlántico Noreste // Coordinación y Optimización de VACLAN

WOCE World Ocean Circulation Experiment

“If we knew what it was we were doing,
it would not be called research, would it?”
A.Einstein.

1 General Introduction

The ocean is a crucial component of Earth's climate, playing a key role in the regulation of global energy budget by transporting heat and salt from low to high latitudes and storing large amounts of heat and carbon dioxide. Oceans are assumed to be absorbing large amounts of heat in response to ongoing climate change (*Barnett et al.*, 2005) but, due to the non-linear responses of complex ocean-atmosphere system, this does not imply sustained long-term trends in hydrographic properties at all basins or sites but rather a more heterogeneous response. Moreover, the different time scales of variability require sufficiently long and regularly sampled time series to detect long-term trends (*Wunsch*, 1999). Recent warming over the upper 3000 m of the North Atlantic has been attributed to both long-term climate change (including anthropogenic) and natural multidecadal variability, the latter accounting up to a 60% of the warming since 1970 (*Polyakov et al.*, 2010). Embedded in this positive phase of multidecadal variability characterized by warmer than normal conditions both in the land and sea, 2000-2010 was the warmest decade on record, reaching the highest global average temperatures in 2010 (*Hansen et al.*, 2010). Oscillations on decadal time scales appear naturally in the climate system (*Latif & Barnett*, 1996) and so caution is needed when treating any observed change in water mass properties or ocean circulation as an indicator of climate change (e.g. *Bryden et al.*, 2003). For these reasons oceanographic panels currently urge the establishment of systematic and sustained programs of ocean observation (*Baker et al.*, 2007; *Hughes et al.*, 2012).

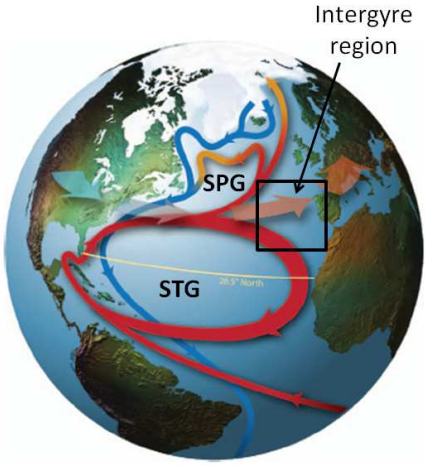

Figure 1.1: Schematic picture of the North Atlantic large scale circulation modified from *Srokosz et al.* (2012), showing the intergyre region between the subpolar (SPG) and subtropical (STG) gyres and the transatlantic hydrographic section 26.5°N.

1.1 The importance of the long-term ocean monitoring programs

There exists a large number of studies dealing with trends and interannual variability of water mass properties, stating widespread warming since at least the second half of the 20th century (e.g. *Solomon et al.*, 2007). However, information about seasonal fluctuations in the ocean interior is less robust and more scarce, due to the lack of subannual monitoring programs, adding a potential source of noise when trying to solve climatic trends. Seasonality in water mass properties and current fields are expected as a response of the yearly heating/cooling cycle and the large-scale response to the wind curl field, and evidence of seasonal variability below the seasonal thermocline has long ago been anticipated theoretically (e.g. *Krauss & Wuebber*, 1982, for the case of the North Atlantic).

The Atlantic Meridional Overturning Circulation (AMOC) plays a key role in the meridional heat transport in the North Atlantic transporting $\sim$ 19 Sv (1 Sv=10^6 m^3s^{-1}) of warm, saline waters northward above $\sim$ 1000m depth and the same amount of cold water southward below 1000 m. The strength of the AMOC was estimated from sparse hy-

drographic observations with insufficient temporal resolution (*Good et al.*, 2013; *Dickson et al.*, 1988; *Nolan et al.*, 2012; *Bryden et al.*, 2005; *Lohmann et al.*, 2009) which could bias the detection of trends. Aiming for the continuous monitor of the temporal evolution of the AMOC, the RAPID (Rapid Climate Change)/MOCHA (Meridional Overturning Circulation and Heat Transport Array) transatlantic currentmeter array along 26.5°N became operative in 2004. Such array deployment has recently revealed that the 8 Sv decline in the AMOC transport observed by *Bryden et al.* (2005) was biased by a seasonal cycle of 6.7 Sv in the AMOC transport (*Kanzow et al.*, 2010). Moreover, 5.2 Sv of such seasonal cycle arise from seasonal density variations of the North Atlantic eastern boundary (*Chidichimo et al.*, 2010). They stated that seasonal geostrophic AMOC anomalies might represent an important and previously underestimated component of meridional transport and storage of heat in the subtropical North Atlantic.

The North Atlantic circulation is also subject to strong interannual, decadal and multidecadal variability. In particular, hydrographic sections in the sub-polar gyre from the coast of the Labrador Sea to Europe show a multi-decadal variability in temperature, while convective events occur on decadal or shorter time scales (*van Aken et al.*, 2011). Such events were shown to homogenize the properties of intermediate layers for significant periods of time, emphasizing the leading role of Labrador Sea convection as a driving mechanism of the variability of intermediate water layers in the North Atlantic. Changes in the subpolar North Atlantic hydrographic properties are tightly related to large-scale atmospheric forcing induced by the North Atlantic Oscillation, NAO (e.g. *Sarafanov*, 2009). However, an overall weak and variable NAO during the first decade of the present century made the relationship less robust (*Hughes et al.*, 2012); the North Atlantic Subpolar Gyre (SPG) index was recently proposed as a further indicator of ocean variability that should be considered in climate change studies (*Häkkinen & Rhines*, 2004; *Hàtún et al.*, 2005).

There are a number of well established monitoring programs in the subpolar regions that have led to long timeseries (*Sarafanov et al.*, 2010; *Hughes et al.*, 2012). However, the temperate mid-latitude areas, except the repetition of the WOCE A5 26.5°N transatlantic section (Fig. 1.1) which has been sampled on regular basis since 2004 (*Cunningham et al.*, 2007), have been observed less frequently. In this work, we exploit a dataset of semiannual occupations of an hydrographic section located west of the Iberian Peninsula (intergyre region, Fig. 1.1) at 43° N, 009–014° W (off Cape Finisterre) to explore the seasonal variability of water masses below the mixed layer in the midlatitude eastern boundary of the North Atlantic. We also use 11-year time series of property variations along this section and another two deep sections located at the southern Bay of Biscay at 8° W (off Cape Ortegal) and 3°47′ W (off Santander), to analyze the interannual thermohaline changes observed during 2003-2013, trying to relate local regional changes to changes observed in other distant regions and interpreting outcomes in the context of

main driving mechanisms of North Atlantic ocean variability. Estimates of water mass transports by directly measured ocean currents are necessary to understand the role that the ocean plays in the world's climate but also, on shorter scales, to infer the connectivity between different marine ecosystems. Direct velocities (LADCP) are measured and geostrophic velocity currents are computed to provide the best representation of circulation patterns in the region. A method based on referencing the geostrophic fields using accurate velocities near the ocean bottom provided by the LADCP bottom-tracking is also introduced following the study carried by *Comas-Rodriguez et al.* (2010) along the transatlantic section 24.5°N.

1.2 Objectives

The main thesis objectives are:

1. To process, to ensemble and to analyze the hydrographic database associated with the VACLAN/COVACLAN projects of the Spanish Institute of Oceanography (IEO) running since 2003, aiming for the standarization of data format and the organization of data by a common structure of folders, making easier to access the information.

2. To provide novel and relevant findings to the scientific community, deepening on the knowledge of the driving mechanisms behind the deep ocean thermohaline properties variability and circulation in the north-west Iberia. The regular repetition of perpendicular to the coast transects on board oceanographic research vessels provides the necessary hydrographical time series for the study of the regional climate variability.

3. To determine the different spatial and temporal scales of variability, as well as the correlation of changes observed in the themohaline properties of water masses (vertically in the water column, temporally during the sampling period 2003-2013 and geographically between different sections).

4. To decompose the isobaric changes observed in temperature and salinity fields on their two natural components of change, following the method developed by *Bindoff & McDougall* (1994): 1) the isopycnal change, related to the intrinsic variation of thermohaline properties without change in density; this term is related to changes in the air-sea fluxes at the formation region or to advection, which means that the sampled water mass is essentially the same (no density change) but with different

properties, and 2) the change by *heave*, due to the shoaling or deepening of isopycnal surfaces in the water column, due to changes in the wind-induced circulation or renewal rates of water masses.

5. To determine the relevance of the seasonal cycle at intermediate depths of the North Atlantic eastern boundary mid-latitudes, extending results from southern latitudes and supporting the importance that the eastern boundary mid-ocean seasonality has in regional and global climate change.

6. To analyze the time series of interannual variability in the study region between 2003-2013, in terms of the North Atlantic large-scale atmospheric forcing, including the deep ocean response to strong shifts in the North Atlantic Oscillation.

7. To establish similarities and differences between the three methods available to estimate the oceanic water mass transports in the region: 1) directly measured velocity fields, 2) indirect velocities calculated from thermohaline properties (geostrophic approximation) and 3) geostrophic fields corrected using near-bottom velocities.

1.3 Thesis organization

The thesis is structured as follows: first, the regional oceanography and main water masses west of the Iberian Peninsula are described in Chapter 2, and the database provided by the series of VACLAN/COVACLAN RadProf oceanographic cruises are introduced. Methods applied for the decomposition of thermohaline changes of water masses, both at seasonal and interannual scales, and the methodology used for the computation of associated transports, both from geostrophy and direct velocity measurements are described in Chapter 3. Results obtained are presented in Chapter 4 and discussed in Chapter 5 through the corresponding subsections. Conclusions are summarized in Chapter 6, both in English and Spanish. Future work is proposed in Chapter 7 and References used throughout the thesis are included at the end of the document.

2

Regional oceanography and data set

2.1 Water masses and circulation in the northwest Iberian Peninsula

The western Iberian margin is a portion of the North Atlantic eastern boundary located at the north-eastern edge of the subtropical gyre. Upper ocean in this region is characterized by a weak anticyclonic basin-scale circulation, exhibiting a mean southward flow of few cms^{-1} (*Mazé et al.*, 1997; *Paillet & Mercier*, 1997) but affected by a wide range of ocean dynamics scales including high frequency shelf-slope dynamics and westward propagating mesoscale activity (*Memery et al.*, 2005). Bathymetry in the region is characterized by a narrow continental shelf ($\sim$ 25 km) and a steep continental slope characterized by the seasonal development of a density driven countercurrent (poleward) known as the Iberian Poleward Current, IPC (e.g. *Frouin et al.*, 1990; *Peliz et al.*, 2005). A seamount is present about 200 km west of the coast of Galicia (the "Galicia Bank"), having a great impact on circulation patterns and marine biodiversity in the region (e.g. *Ruiz-Villarreal et al.*, 2006).

A detailed review of the modal, intermediate and deep water masses of the midlatitude north-east Atlantic Ocean was performed by *van Aken* (2000a,b, 2001) and pathways of such waters masses from their source region towards western Iberia are shown in Fig. 2.1b.

Briefly, these are as follows:

- Eastern North Atlantic Central Water (ENACW) constitutes the upper permanent thermocline of the European and north-west African basins. It is characterized by

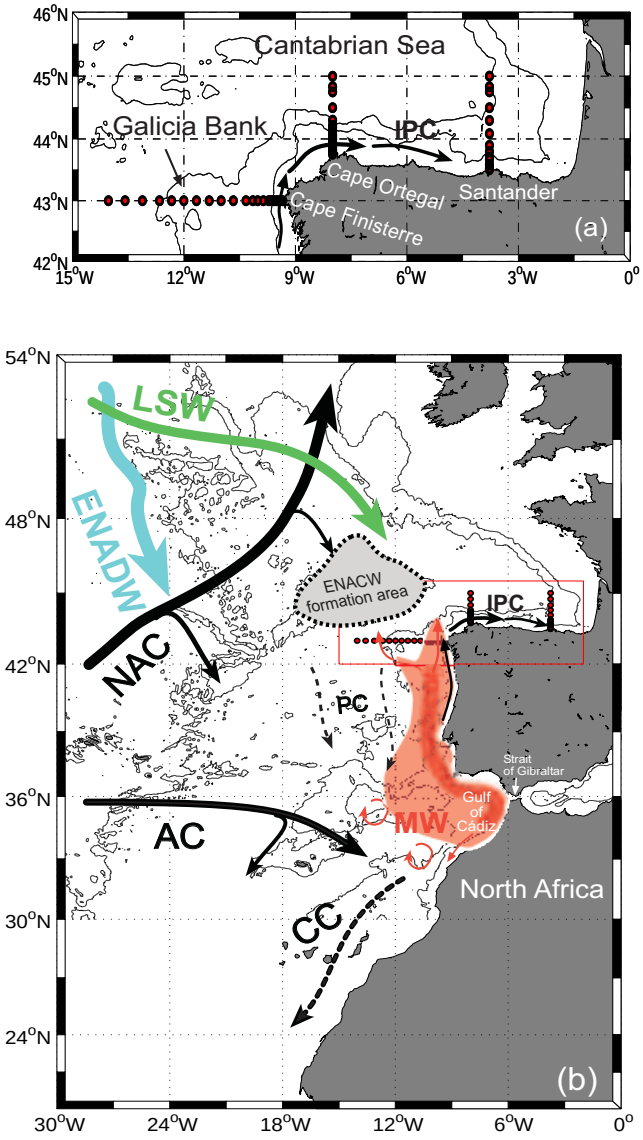

Figure 2.1: **(a)** Zoom of the VACLAN/COVACLAN sampling region including the Finisterre (western Iberia margin), Ortegal (southwestern Bay of Biscay) and Santander (southeastern Bay of Biscay) sections. **(b)** Main circulation patterns of waters in the area. Gyres bounding North Atlantic Current (NAC) and Azores Current (AC) (black bold), southward flowing Portugal Current (PC) and Canary Current (CC) (black dashed). Iberian Poleward Current (IPC) (black). Central water: ENACW formation area is shown as a dashed grey region north of Finisterre, from where it flows southwards with the PC. Intermediate waters: Mediterranean water (MW, red), spreading from the Strait of Gibraltar, flows northwards along the continental slope sometimes showing a detachment contouring the west Galicia Bank, and southward flowing water from the Labrador Sea (LSW, green). Eastern North Atlantic Deep Water (ENADW, blue).

a narrow and nearly straight line in the θ/S with its core located at ~ 350 dbar. ENACW is formed by winter mixing in a wide region from the Azores to the European boundary bounded by the North Atlantic Current (NAC) and the Azores Current (AC) (*Pollard & Pu*, 1985; *Pollard et al.*, 1996). In the western Iberia margin, warmer ENACW of subtropical origin created near the Azores flows eastward and mixes with the colder southward flowing ENACW of subpolar origin (*Fiúza et al.*, 1998). The lower bound of ENACW is characterized by a salinity minimum.

- Mediterranean Water (MW) is formed at the Gulf of Cádiz from the intense mixing of Atlantic central waters and the warm and salty overflow from the Mediterranean Sea through the Strait of Gibraltar. The main core is characterized by a clear salinity maximum spreading from Cape St.Vincent at 37° N as a northward deep boundary current along the European ocean margin, and reaching high latitudes as the Porcupine Bank at 53° N. Along the west Iberian margin, two cores are found: the upper (MW_u) at ~ 750 dbar and the lower (MW_l) at ~ 1250 dbar, becoming indistinguishable north of 42° N. West of Cape Finisterre, an intermediate salinity maximum centered at 1000 dbar is observed between a salinity minimum at about 500 dbar and a minimum connected with the below-lying Labrador Sea Water (LSW) core near 1900 dbar (*Iorga & Lozier*, 1999b; *van Aken*, 2000b).

- Labrador Sea Water (LSW) is the deeper intermediate water mass (i.e. belonging to the permanent thermocline). It is the last stage of the modification of the subpolar gyre mode waters formed in the centre of the cyclonic circulation in the Labrador Sea by deep winter convection, spreading southwards and eastwards in the North Atlantic from its formation area. In the north-east Atlantic, its core is characterized by a deep salinity minimum near 1900 dbar (*Pingree*, 1973).

- Eastern North Atlantic Deep Water (ENADW), found below the intermediate water masses, is formed by a mixture of different polar source water types including a component of Antarctic origin (*van Aken*, 2000a). The term Lower Deep Water (LDW) is used for the bottom waters found deeper than 4000 m.

Table 2.1 summarizes properties of water masses separated by density layers (following the scheme devised by *van Aken* (2000a,b, 2001) with corresponding along-section mean values of pressure, potential temperature and practical salinity.

Table 2.1: Potential density layers defining water masses according to *van Aken* (2000a,b, 2001).Corresponding neutral densities (γ^n, *Jackett & McDougall* (1997)) and depth-averaged values of pressure ($\overline{P}$), potential temperature ($\overline{\theta}$) and salinity ($\overline{S}$) along Finisterre (subscript Fist), Ortegal (Orte) and Santander (Sant)

Water mass	Density ($\mathrm{kg\,m^{-3}}$)	γ_n ($\mathrm{kg\,m^{-3}}$)	$\overline{P}_{\mathrm{Fist}}$	$\overline{\theta}_{\mathrm{Fist}}$	$\overline{S}_{\mathrm{Fist}}$	$\overline{P}_{\mathrm{Orte}}$	$\overline{\theta}_{\mathrm{Orte}}$	$\overline{S}_{\mathrm{Orte}}$	$\overline{P}_{\mathrm{Sant}}$	$\overline{\theta}_{\mathrm{Sant}}$	$\overline{S}_{\mathrm{Sant}}$
ENACW	$27.00 < \sigma_\theta < 27.20$	27.06–27.26	297	12.16	35.70	278	11.92	35.64	265	11.84	35.61
Sal min	$\sigma_\theta \approx 27.2$	27.26	475	11.30	35.61	463	11.22	35.59	457	11.22	35.59
MW	$31.85 < \sigma_1 < 32.25$	27.46–27.79	1002	10.07	35.85	1033	9.41	35.69	1020	9.18	35.63
LSW (core)	$\sigma_2 \approx 36.88$	27.93	1764	4.64	35.13	1786	4.41	35.08	1778	4.57	35.12
ENADW	$41.42 < \sigma_3 < 41.51$	28.02–28.10	3236	2.60	34.94	3230	2.59	34.94	3226	2.59	34.94
LDW (core)	$\sigma_4 \approx 45.83$	28.09	4500	2.08	34.90	4500	2.09	34.90	>4000	2.12	34.90

2.2 The VACLAN/COVACLAN projects

A monitoring programme of ocean properties has been in place since 2003 in the southern Bay of Biscay and northwestern Iberia margin, under the VACLAN/COVACLAN projects (Spanish acronym of "Coordination and optimization of the Northeast Atlantic CLimate VAriability Observing System") of the Spanish Institute of Oceanography. The program aims to maintain a continuous observation programme of climate variability in this region of the North Atlantic eastern boundary. Three deep sections perpendicular to the coast extent to 200 nm off Cape Finisterre (northwestern Iberia, 43°N, $>$ 5000 m), 100 nm off Cape Ortegal (southwestern Bay of Biscay, 8°W, $>$ 4000 m) and 100 nm off Santander (southeastern Bay of Biscay, 3° 47′W, $>$ 4000 m) as it is shown in Fig. 2.1a,b. The sections were sampled twice a year from 2003 to 2010, with data collected to WOCE standards.

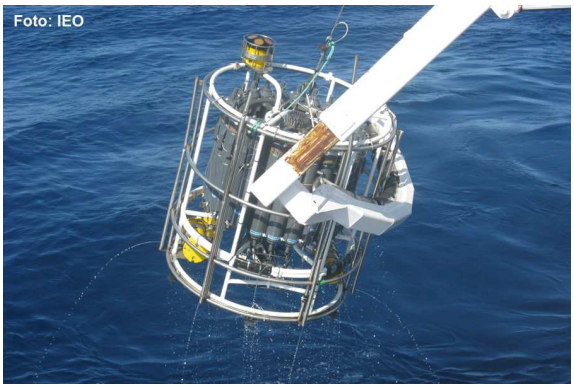

Figure 2.2: Oceanographic rossete leaving the water after the finalization of an hydrographic station.

In 2011 sections were only sampled in summer, and only sampling along the Finisterre section was performed in summer 2012 and 2013. The cruises consist of standard hydrography performed by SBE911+ CTD provided with oximeter, turbidimeter and fluorometer integrated into an oceanographic rosette provided by a set of 24 10l Niskin bottles which collect water from different depths as they are closed automatically from the vessel. A Lowered Acoustic Doppler Current Profiler (LADCP) was incorporated to recover full-depth velocity measurements since September 2004; the LADCP consisted of dual 300 kHz RDI Workhorse (WH) devices one upward looking (slave) and one downward looking (master) placed at the top and bottom of the structure, with a shared pack of batteries (Fig. 2.2). Accurate velocities near the ocean bottom are provided by the bottom-track (BT) mode of the LADCP, and continuous velocity observations were made at the upper 500-750 m of the water column along the ship track using a shipboard ADCP (SADCP) RDI Ocean Surveyor 75 kHz installed on the research vessel's hull since 2008.

The number of sampled stations and the start/end dates of surveys are shown in Table 2.2, where $N_{Fist.}$, $N_{Orte.}$ and $N_{Sant.}$ refers to the number of stations sampled at Finisterre, Ortegal and Santander sections respectively. Note that the Finisterre section was

occupied a total of 18 times during the sampling period, becoming the most repeated and the longest and the deepest sampled transect. Ortegal section was not sampled in February or September 2010 (14 occupations) and Santander section was not sampled in February 2010 (15 occupations).

Table 2.2: VACLAN/COVACLAN series of cruises. "RadProf" is an acronym for the Spanish of "Deep Section". Dates and number of stations sampled at Finisterre (N_{Fist}, 43°N), Ortegal (N_{Orte}, 8°W) and Santander (N_{Sant}, 3° 47′W).

Cruise	dates	N_{Fist}	N_{Orte}	N_{Sant}
RadProf200303	26 March – 17 April, 2003	13	11	11
RadProf200309	10–20 September, 2003	16	8	11
RadProf200402	5–13 February , 2004	18	11	12
RadProf200409	7–13 September , 2004	18	11	11
RadProf200501	27 January – 3 February, 2005	6	10	9
RadProf200508	20 August – 9 September, 2005	20	14	12
RadProf200602	5–13 February, 2006	19	14	12
RadProf200607	12–29 July, 2006	19	13	10
RadProf200702	1–7 February, 2007	21	14	6
RadProf200802	11–19 February, 2008	19	14	12
RadProf200809	3–13 September, 2008	18	14	12
RadProf200902	1–13 February, 2009	15	13	10
RadProf200908	11–21 August, 2009	19	14	12
RadProf201002	9–11 February, 2010	19	–	–
RadProf201009	2–11 September, 2010	19	–	12
RadProf201108	14–24 August, 2011	21	14	12
RadProf201209	12–16 September 2012	23	–	–
RadProf201309	13–17 September 2013	24	–	–

Diagrams of Fig. 2.3, provide a first overview of the year-to-year thermohaline variability in all depths of the Finisterre, Ortegal and Santander water column during the sampling period. Semiannual occupations of the Finisterre section between 2003-2010 are shown in Fig. 2.4a,b and a seasonal pattern emerges at first view from the representation of the θS properties, specially at MW levels (Fig. 2.4c). Indeed, vertical sections of salinity between 2003-2010 (Fig. 2.5)show that the MW vein, which is tight against the slope all year-round, tends to be stronger in summer for most occupations while in wintertime the MW core tends to be broader and displaced offshore, even concentrating in the surroundings of the Galicia Bank.

The study of water masses circulation presented here is based on the hydrography plus LADCP data collected during those seasonal surveys performed in winter (February) and summer (September) 2008 along the Finisterre section (43°N), cruises RadProf200802 and RadProf200809 respectively, as representative of typical winter and summer conditions (see Fig. 2.5); in the first cruise a total of 21 stations were sampled and the LADCP was used in dual mode as planned; in the second cruise (18 sampled stations) bad weather conditions made necessary the replacement of the oceanographic rosette by a smaller one with only one device (master) running in downward looking mode. A mooring line with current-meters at the levels of ENACW, MW and LSW (300, 1000 and 1800 m) was set at 43°N, 11°W (Fig. 2.6a) in 2003 and operated intermittently until 2010. Continuous measurements of the velocity flow at these fixed depths during February and September 2008 will be included in this study . This year, hydrographical conditions in the region were characterized by a shift to cooler and fresher intermediate waters from February to September 2008 as shown by the θ/S diagram of Fig. 2.6b.

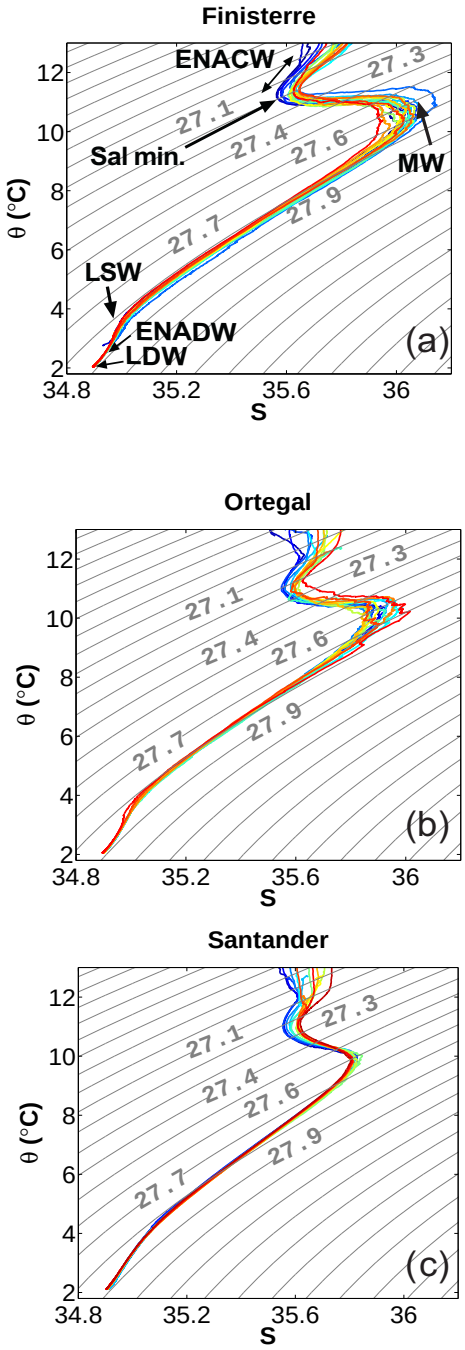

Figure 2.3: θS diagrams of along-section profile averages from cruises performed between 2003 (darkest blue) and 2013 (darkest red) at **(a)**Finisterre, **(b)**Ortegal and **(c)**Santander, overlying γ^n contours in grey.

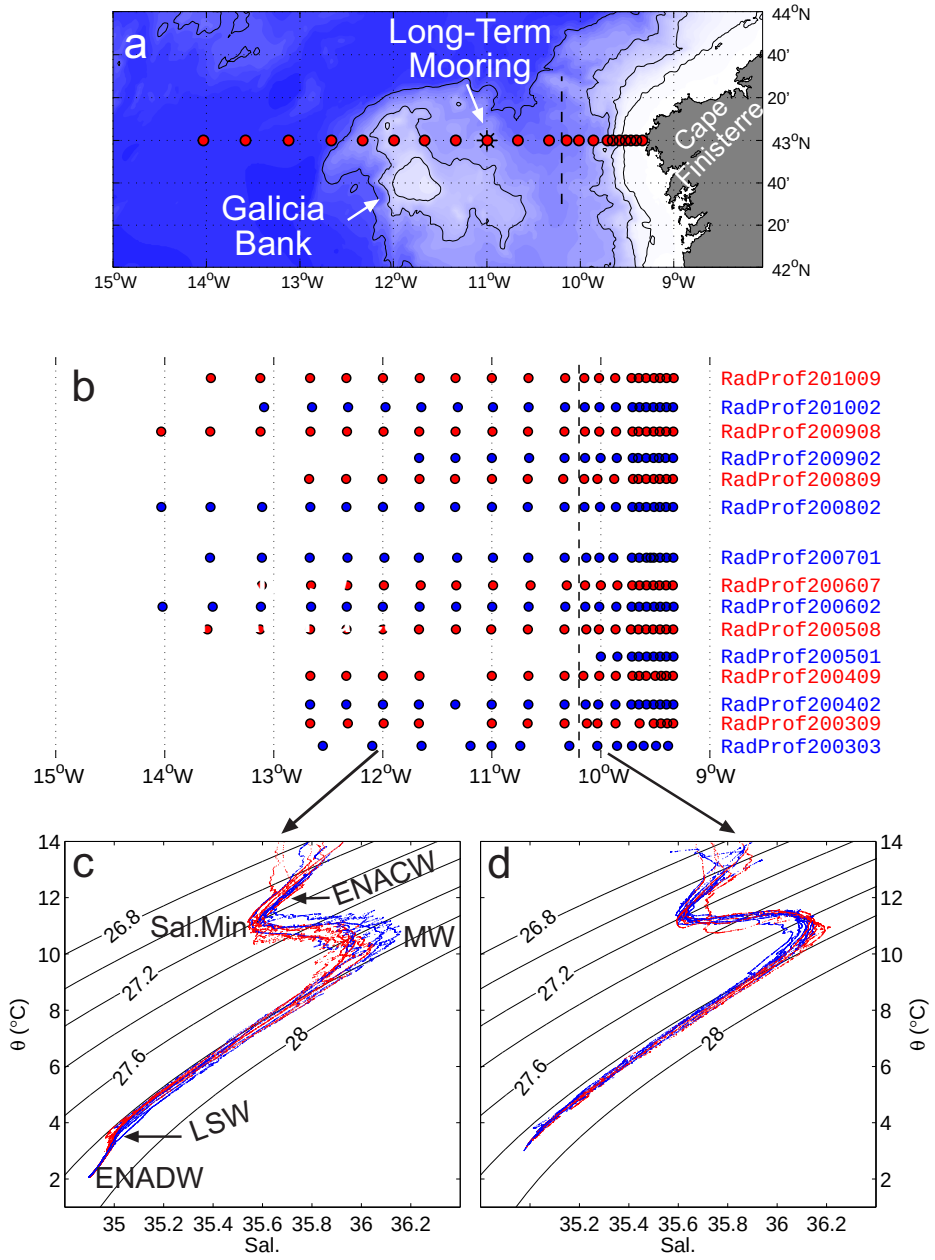

Figure 2.4: **(a)** Zoom of the Finisterre section. **(b)** Graphical representation of the hydrographical database. Dots are plotted at true positions with reference to **(a)**. Blue cruises are for winter and red for summer. **(c)** θS diagram of all profiles at a station 012°40′ W, west of the Galicia Bank (colours keep to represent winter vs summer profiles). **(d)** Same as **(c)** for a slope station 009°43′ W

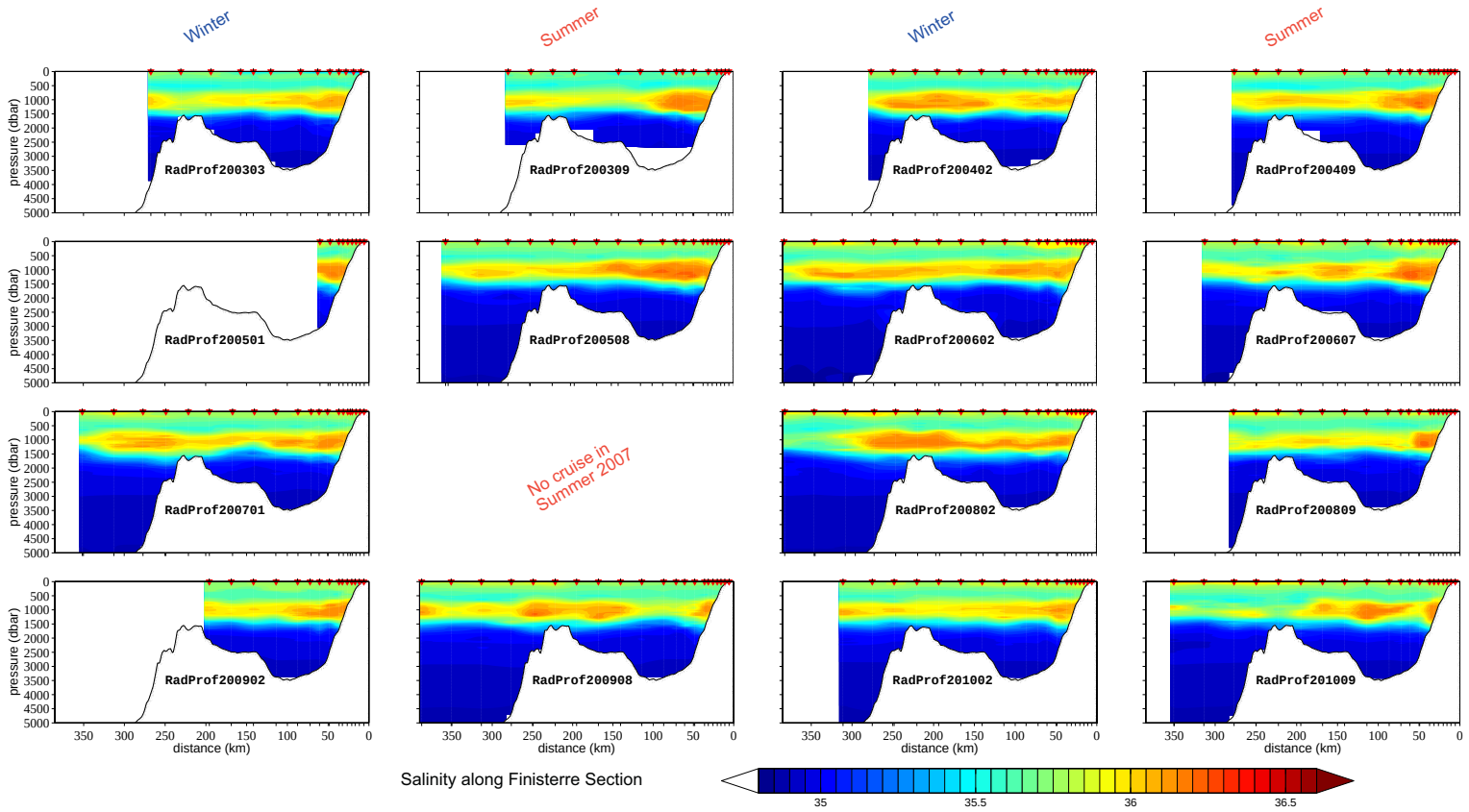

Figure 2.5: Plate showing the salinity field structure for the 15 repetitions of the Finisterre section. Sections are showed in chronological order from left to right, with the first and third columns showing the winter cruises and the second and fourth columns showing the summer cruises, except that of summer 2007.

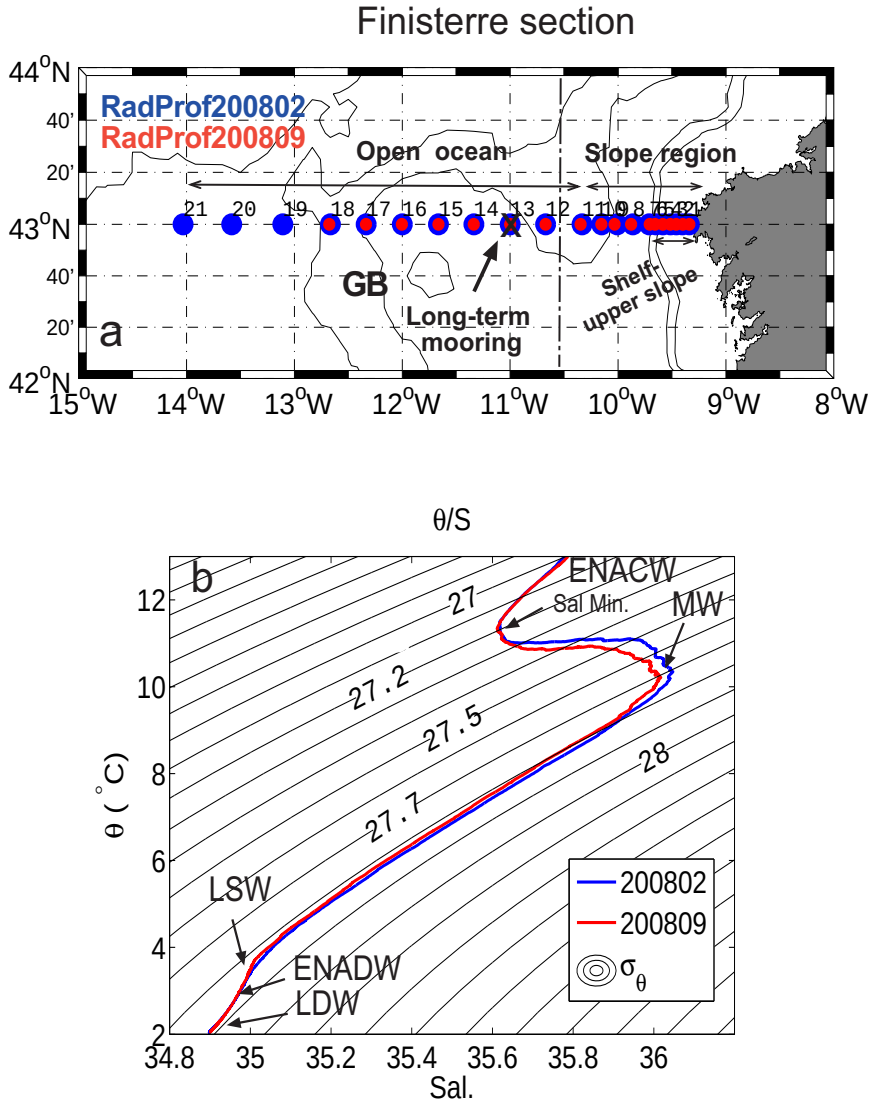

Figure 2.6: a) Map showing location of sampled stations during RadProf200802 (blue) and RadProf200809 (red) along the Finisterre section. The slope region (st.1-11) and the open ocean region (st.11-21/18, respectively). Shelf-upper slope (st.1-7). Long-term mooring placed at 43°N, 11°W (east side of Galicia Bank, GB). b) Section averaged θS properties during both cruises, overlying potential density (σ_θ) contours.

3 Methodology

3.1 Decomposition of hydrographic changes along neutral density surfaces: seasonality and interannual variability.

The first step in order to quantify the seasonality in the different waters masses is to adopt a systematic and objective classification of them. Water masses are distributed as layers with distinct hydrographical properties placed approximately at specific depths. Normally, water masses are labelled by characteristic density levels, while depth is only taken as reference below the permanent thermocline where density gradient is very weak. The most detailed description of the water masses in the midlatitude north-east Atlantic (*van Aken*, 2000a,b, 2001) used isopycnal bounds to tag the main water masses referred to in Sect. 2.1, with the exception of LDW identified with deep water located roughly below 4000 dbar. We have followed these works in order to label the water masses, with the exception of ENACW and the Salinity Minimum, which have been identified focusing on the θ/S diagrams of Fig. 2.4c,d, but using neutral density γ^n (*Jackett & McDougall*, 1997) instead of potential density. Figure 3.1 provides a graphical view of the water masses division. Different behaviour is expected on the slope or further into the basin, and actually a distinct pattern emerges from a first glance of the dataset (see Fig. 2.4c,d). For this reason, the section will be divided into two subsections (see Fig. 2.4a) with the aim of studying the seasonality separately . These are:

1. The *slope*, which extends from the Galicia coast off Cape Finisterre at $\sim 9.3^\circ$ W to the middle of the trough at 10.2° W.
2. The *outer ocean*, which spans from 10.2° W to 14° W, hence including the Galicia Bank.

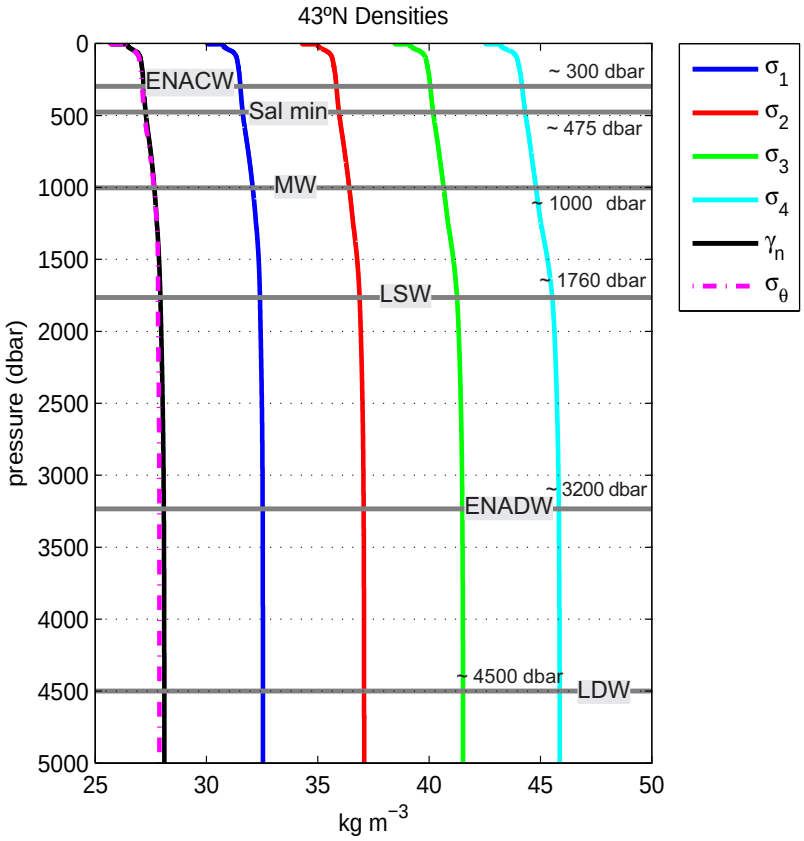

Figure 3.1: Time and zonally averaged potential density relative to the sea surface (σ_θ), 1000 dbar, 2000 dbar, 3000 dbar, 4000 dbar ($\sigma_{1,2,3,4}$) and neutral density (γ^n) as a function of pressure.

In order to analyse water mass changes, it is helpful to consider separately thermohaline changes occurring at fixed density levels (hence causing a true modification of the θS diagram) and vertical displacement of isopycnal levels (a process known as heave). Properties of modal waters formation are set by the balances in atmospheric forcing, so altered heat and freshwater fluxes shaping the mixed layer that is later subducted into the ocean interior will cause subsurface isopycnal changes (warming/freshening). On the other hand, the vertical displacement of density surfaces (which changes the properties at a given depth) can be caused either by changes in the rates of renewal of water masses or by dynamical changes affecting the density field structure. As water masses move further from their sources, the diffusive processes affecting their transformation contribute to blur the specific signatures acquired at the formation stages. *Bindoff & McDougall* (1994) developed a systematic methodology to characterize water mass changes, showing that observed changes along pressure surfaces can be approximately split into

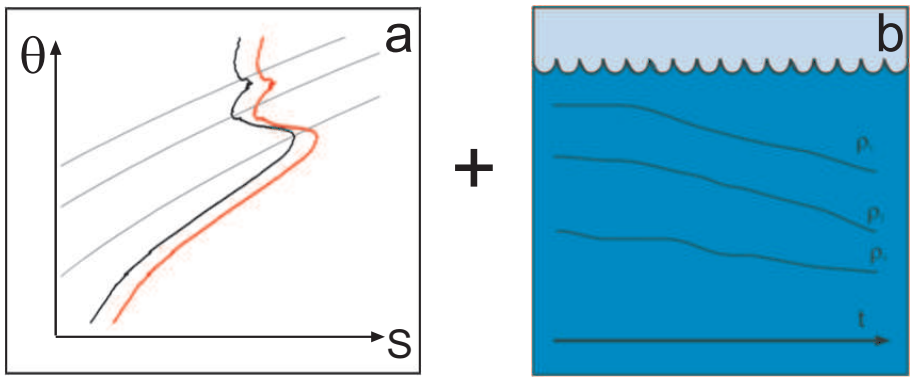

Figure 3.2: Isobaric changes can be decomposed into (a) an isopycnal change causing a modification of the θ/S diagram plus (b) a change by heave due to the variation of the isopycnals pressure with time.

changes of properties along neutral density surfaces and changes due to the displacement of isopycnals through the vertical gradients of properties assumed constant over time. An schematic view of the decomposition of changes is shown in Fig. 3.2.

Isobaric changes can be mathematically expressed as,

$$\left.\frac{\mathrm{d}\theta}{\mathrm{d}t}\right|_p \simeq \left.\frac{\mathrm{d}\theta}{\mathrm{d}t}\right|_n - \left.\frac{\mathrm{d}p}{\mathrm{d}t}\right|_n \frac{\partial\theta}{\partial p} \tag{3.1}$$

$$\left.\frac{\mathrm{d}S}{\mathrm{d}t}\right|_p \simeq \left.\frac{\mathrm{d}S}{\mathrm{d}t}\right|_n - \left.\frac{\mathrm{d}p}{\mathrm{d}t}\right|_n \frac{\partial S}{\partial p}, \tag{3.2}$$

where p and n indicate, respectively, changes at isobars and isopycnals. The left-hand term is thus called the *isobaric change*, the first right-hand term the *isopycnal change* and the second one the *heave term*. The vertical coordinate pressure p is assimilated to the z-axis so Eqs. (3.1) and (3.2) may be written in compact notation as $\theta_z^{'} \simeq \theta_n^{'} - N'\theta_z$ and $S_z^{'} \simeq S_n^{'} - N'S_z$, where N' is the change in height of the neutral surface and the primes indicate temporal change of the scalar quantities. We will apply this methodology in order to characterize the seasonal changes occurring in different water masses in the two regions.

Temporal changes are usually calculated by comparing properties between two cruises, regardless of the time-lag between them and lack of information about variability at shorter timescales. Since we have a true time series of hydrographical sections, we will consider changes referred to an overall average section instead of calculating changes between pairs of cruises. Therefore we will construct the series of anomalies of key prop-

erties (isopynal/isobaric changes and heave) with respect to the overall average section. From these series will be estimated the presence of seasonality and its amplitude.

In order to quantify interannual changes in water properties it is necessary to extract the seasonal cycle. The deseasonalized signal is computed by subtracting each cruise section from the corresponding winter (summer) average field, i.e.

$$\theta_i^{\mathrm{des}} = \theta_i - \overline{\theta}_{\mathrm{winter/summer}}, S_i^{\mathrm{des}} = S_i - \overline{S}_{\mathrm{winter/summer}} \tag{3.3}$$

where i is the number of repeats of a section and subscript "des" refers to the deseasonalized field. Anomalies are calculated at each profile site and then zonally averaged for every cruise i. Next the anomalies are vertically averaged within pressure intervals 0-200, 200-400 and from 400 dbar to the bottom. Then, changes of properties along pressure surfaces are decomposed into changes along neutral density surfaces (isopycnal change) plus changes due to the displacement of isopycnals (heave) following the work of *Bindoff & McDougall* (1994) in the same way as for seasonal changes. We will apply methodology for the decomposition of changes using neutral density surfaces (*Jackett & McDougall*, 1997) every 0.1 $\mathrm{kg\,m^{-3}}$, in the water column between 27-28 $\mathrm{kg\,m^{-3}}$.

An important issue is the magnitude of the high frequency variability along the section. We expect that our series are representative of the slow varying changes in water masses properties at a regional scale. Without a higher sampling rate of the section it is not possible to quantify the bias induced by mesoscale and/or short-term shifts in circulation fields, but some complementary approaches may be considered. First, if the slow-varying background properties dominate over the short-term mesoscale induced changes the series should exhibit autocorrelation. Second, if the series are representative of the regional background hydrographical variability there should be correlation (synchronous variation) between the three different sections at the same levels and across large portions of the water column. Finally, an external estimate of the uncertainty caused by the sampling rate can be evaluated by taking a low-passed version of a higher frequency float-based product. The procedure will be explained in detail in Sect. 4.2.2.

3.2 Ocean velocities and water mass transport estimates

Referencing geostrophic velocities to a level of no motion in the ocean has always been a problematic task; however, the most objective way of estimating this level is by direct measurement of the flow (*Pickart & Lindstrom*, 1994; *Rubio et al.*, 2009). Accordingly, *Oliveira et al.* (2004) suggested that "the best approach to study the circulation in the West

Iberia Coastal Transition Zone is to use direct current measurements in conjunction with the hydrographic sampling". Here, we will compute the transports directly from LADCP record, from the classic geostrophy approach and we will use a hybrid method based on LADCP bottom-tracking to reference geostrophic fields following the study carried by *Comas-Rodriguez et al.* (2010) along the transatlantic section 24.5°N. Bottom tracking provides accurate velocity measurements near the bottom, permiting high-resolution spatial studies that can reveal circulation patterns of deep waters not observable by other way.

3.2.1 Direct currents from LADCP

LADCP data was processed using a re-implementation software of the velocity inversion method originally developed at the Columbia University - Lamont-Doherty Earth Observatory (LDEO) by Martin Visbeck (*Fischer & Visbeck*, 1993) and primarily maintained by Gerd Krahman (IFM/GEOMAR, Kiel)[1]. Near ocean surface velocities provided by the SADCP and near ocean bottom velocities provided by the LADCP bottom-track were included when available as boundary conditions for data processing at every hydrographic station reducing velocity errors (*Visbeck*, 2002). Transport from LADCP measurement was calculated integrating numerically the whole section, i.e. taking the product of meridional velocities $\times$ each area bin, which is the vertical depth bin $\times$ the mid-distance to the two neighbour stations.

Tidal currents need to be removed from LADCP measurements in order to get transports. The Oregon State University (OSU) Tidal Inversion Software (OTIS) was used to predict the tidal barotropic component, calculated using the OSU TOPEX/POSEIDON global tidal model TPXO[2] (*Egbert et al.*, 1994; *Egbert & Erofeeva*, 2002), which fits the Laplace Tidal Equations and the along track averaged data from TOPEX/POSEIDON and Jason satellites by a least-square adjustment. The mid-time of each station was taken for a local barotropic tide prediction (see Fig. 3.3)

Meridional barotropic tidal component was substracted from the corresponding LADCP, constrained by SADCP and BT profiles in order to remove the effects that tides have on-situ measurements. Predicted tide values range from -0.05 to 0.05 ms^{-1}, that means of the order of half the current velocities measured in the region, suggesting tides as an important source of noise when calculating transports in a region of a relatively slow circulation.

[1] See `ftp://ftp.ldeo.columbia.edu/pub/ant/LADCP/UserManuals/how-to.pdf`

[2] See `http://volkov.oce.orst.edu/tides/global.html`

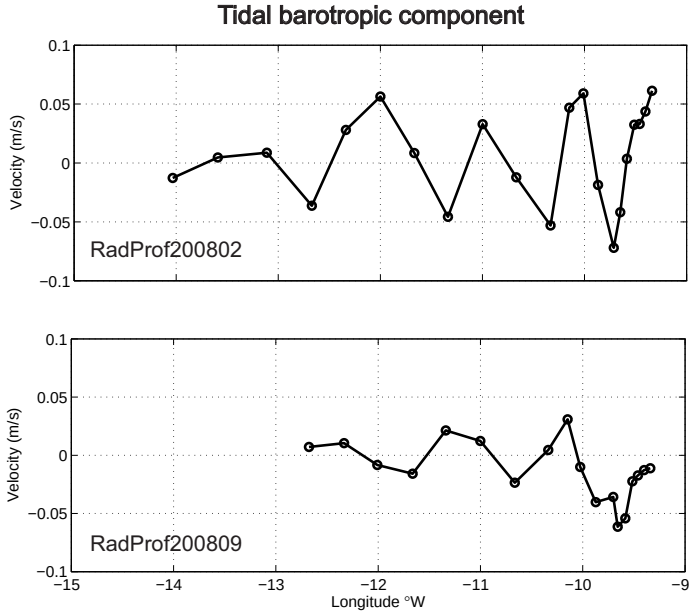

Figure 3.3: Meridional (v) barotropic component of tide predicted by the OTIS model for the Finisterre section during (a) February and (b) September 2008

3.2.2 Geostrophy

CTD measurements were used for computing the geostrophic velocity profiles between station pairs, using the level of no motion at $\gamma_n \sim$28.072 kg m^{-3} ($\sim$3000 m) following the study performed by *Fraile-Nuez et al.* (2008) in the Bay of Biscay. When one or both stations of each station pair is shallower than this level, the deepest common level was used as the no movement reference level (e.g. for station pairs near the slope region, st. pairs 2–1 to 9–8 , and for station pairs surrounding the Galicia Bank, st. pairs 13–12 to 18–17). Table 3.1 shows reference levels used for geostrophic profile calculation between each station pair. Configuration of software is such that geostrophic velocity is set to zero below the deepest common level, that is presumably the deepest sampled level from which we can get reliable information.

Mass transports were calculated across the Finisterre section and separately across the slope region (stns. 1 to 11, from the coast to 10.2 °W) and outer ocean region (stns. 11 to 18, from 10.2°W to 12.7°W) as shown in Fig. 2.6a. The three outermost stations were removed in RadProf200802 in order to have the same geographical coverage than in RadProf200809. The water column was divided into 12 neutral density layers following *Fraile-Nuez et al.* (2008); associated pressure ranges were obtained specifically for our

Table 3.1: Neutral density (γ_n) reference used as the level of no motion for geostrophic calculations between each station pair during RadProf200802 and RadProf200809 cruises.

		$\gamma_n(\mathrm{kg\,m^{-3}})$	
Region	Station pair	RadProf200802	RadProf200809
Open ocean	21–20	28.072	–
	20–19	28.072	–
	19–18	28.072	–
	18–17	28.007	28.024
	17–16	27.915	27.930
	16–15	27.910	27.925
	15–14	27.966	27.974
	14–13	28.012	28.029
	13–12	28.015	28.037
	12–11	28.072	28.072
Slope	11–10	28.072	28.072
	10–9	28.072	28.072
	9–8	28.004	28.026
	8–7	28.012	27.996
	7–6	27.860	27.834
	6–5	27.689	27.725
	5–4	26.976	27.148
	4–3	26.963	27.143
	3–2	26.932	27.100
	2–1	26.857	27.016

data set and shown in Table 3.2. The water layers corresponds to the description provided on Sect. 2.1 from upper ocean layer to Lower Deep Water. Ekman transports were computed across the Finisterre section from climatological wind stress fields of the Scatterometer Climatology of Ocean Winds (SCOW) of the QuikSCAT scatterometer data Oregon State University [3], and added to the Layer 1 mass transport (Table 3.2).

Climatological meridional Ekman transports resulted -0.047 Sv for February and -0.044 Sv for September. That is, two orders of magnitude less than meridional mass transports computed for the 0-500 m layer, as expected. The main contribution to the Ekman transport seasonality in the Finisterre region is provided by its zonal component, enhanced in summer in response to the prevalence of northerly winds (*Álvarez et al.*, 2008).

[3] See `http://cioss.coas.oregonstate.edu/scow/index.html`

Table 3.2: Neutral density (γ_n) layers defining water masses with corresponding pressure ranges (P)

Layer	γ_n kg m^{-3}	Water mass	P (dbar)
1	surface – 27.162	Upper layer	surface– 260
2	27.162 – 27.271	ENACW	260–480
3	27.271 – 27.38	ENACW	480–610
4	27.38 – 27.62	UMW	610–930
5	27.62 – 27.82	MW	930–1360
6	27.82 – 27.922	DMW/LSW	1360–1720
7	27.922 – 27.975	LSW	1720–2050
8	27.975 – 28.008	ENADW	2050–2290
9	28.008 – 28.044	ENADW	2290–2610
10	28.044 – 28.072	ENADW	2610–2970
11	28.072 – 28.0986	ENADW	2970–3780
12	28.0986 – bottom	LDW	3780–bottom

3.2.3 Hybrid approach: Geostrophic velocities corrected by LADCP bottom-tracking

Every geostrophic velocity profile was corrected using bottom track data from the two neighbour stations following the method previously applied by *Cunningham et al.* (2003) at the Drake Passage and *Comas-Rodriguez et al.* (2010) along the 24.5°N transect. The motivation for doing so is that LADCP record at mid-depths in oceanic areas where backscatter signal is weak may be not enough reliable. Differences between geostrophic and bottom-track profiles were obtained at the corresponding depths and averaged for both stations to obtain a final mean. In the case of station pairs where LADCP bottom-track data is only available for one of the two stations, this was taken for correction. An *offset* is thus available for every geostrophic profile providing the corresponding *reference velocity*. Offsets applied for referencing geostrophy are shown in Fig. 3.4. Generally, larger correction will be applied at the slope region (eastward from 10°W), reaching up to ~ 0.15 m/s. As an example of the operation procedure, a comparison of velocity profiles between pairs of LADCPs (including SADCP and BT), the corresponding geostrophic velocity profile initially calculated between them and the final BT referenced geostrophic profile is shown in Fig. 3.5. In order to apply the bottom-track correction to the geostrophic mass transports, we added a *correction term* equivalent to an *offset* velocity as follows: $\sim$ area $\times\rho\times$ Offset, where *area* is the area enclosed by two isoneutral layers and *rho* is the average density within layers. This is equivalent to compute the transports from the corrected velocity fields.

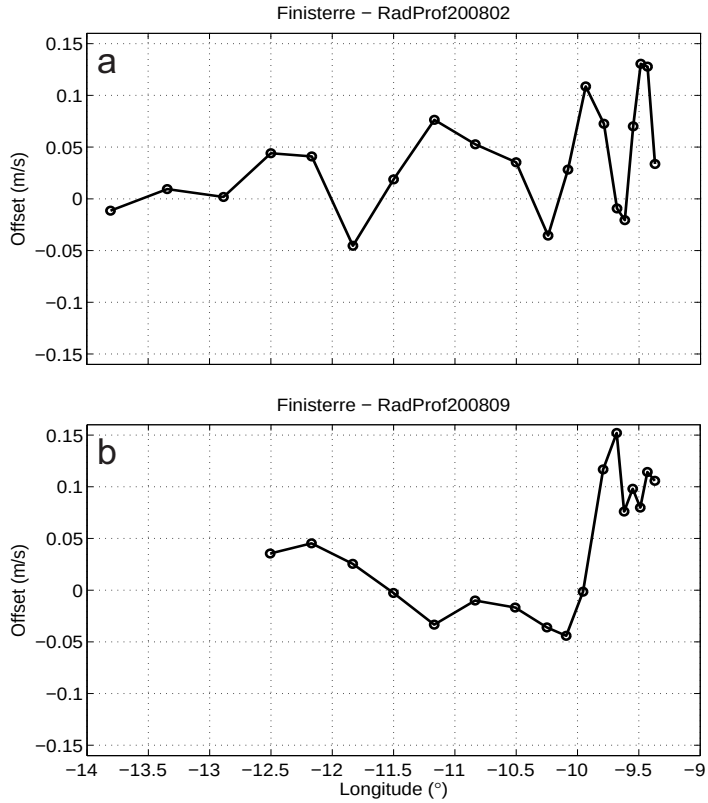

Figure 3.4: Velocity offsets applied for geostrophy correction during a) RadProf200802 and b) RadProf200809.

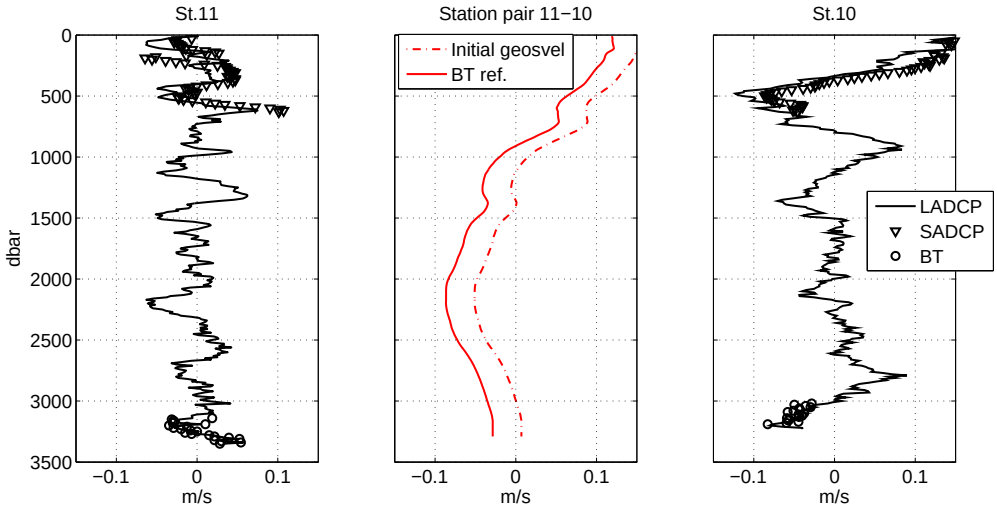

Figure 3.5: Comparison between LADCP velocity profiles of two neighbour stations, initial calculated geostrophic profile between them and the corresponding BT referenced geostrophic profile. Stations are 10 (43°N, 10.15°W) and 11 (43°N, 10.33°W), Radprof200802. Level of no motion was set to γ_n=28.072 ($\sim$3000 dbar). Note that the BT corrected geostrophic profile is constrained by the two neighbour bottom-track, adding a reference velocity of $\sim$0.04 m/s

4 Results

4.1 Seasonality of the deep ocean off the northwest Iberia

Vertical sections of salinity from the cruises series provided a first insight on the presence of a recurrent seasonal pattern in the structure of hydrographic fields (Fig. 2.5), specially evident at the levels of Mediterranean water characterized by the salinity maximum (core c.a. ~ 1000 m). As expected, a saltier MW vein ($S \sim 36.2$) is tight against the slope year-round, but most occupations (though not all) show that this signature of MW on the slope tends to be stronger in summer, while in wintertime the MW core tends to be broader and displaced offshore, even concentrating in the surroundings of the Galicia Bank. Hence, the recurrence of structures in winter and in summer points to the existence of a seasonal cycle at depth. Results about the processes behind this seasonality will be discussed later in Chapter 5, Sect. 5.1.

4.1.1 Quantification, zonal structure and nature of seasonal changes

There are basically two methods for extracting the seasonal cycle from a time series (see for instance *Chelton*, 1982). The first consists of carrying out a harmonic analysis of the data and reconstructing the seasonal cycle from the amplitudes and phases of the annual and higher order constituents (e.g. *Bray*, 1982). The second consists of computing the long-term mean value through the calendar year at the sampling interval of the time series (e.g. *Thomson et al.*, 1985). The latter approach is generally preferred as it filters the slow-varying interannual variability and a seasonal cycle of arbitrary shape is not

forced to accommodate to a reconstruction by few harmonics. On the other hand, this method may incorporate a strong bias if any specific section were strongly anomalous. In the present section we take the summer-average vs the winter-average of properties as the measure of their seasonal amplitude. Actually, our semiannual time series does not provide information to characterize the seasonality signature further. We will apply in Sect. 4.1.2 a simple harmonic analysis to key time series of the record in order to get a statistical measure of the robustness of the seasonality signal.

Figure 4.1 shows the seasonal changes of temperature, salinity, and density along the sections. Note that the anomalies are representing the summer minus winter condition, i.e. positive anomalies (red shades) indicate warmer, saltier or denser water along isobars or deeper isoneutrals during summertime. Here, the pattern previously inferred from Fig. 2.5 is clearly perceptible, with warmer and saltier waters from 1000 to 1750 m tight against the slope in summertime (from coast to about 10° W), versus colder and fresher from 11.5° W to 13.5° W over the Galicia Bank. This implies a warmer and saltier intermediate water broadening and spreading above the Galicia Bank in wintertime. Also clearly identifiable is the seasonal effect on the upper layers with warmer waters down to 100 dbar in summertime except over the shelf, where the effect of summer upwelling is notable. There is also a change in the density field structure with lighter surface waters (down to ~ 100 dbar) in summer than in winter, and denser water below; the near-surface (~ 100 dbar) zero contour separating depths where the sign of the anomaly changes, shoals near the coast suggesting the presence of denser (and cooler) waters that are uplifted from the thermocline during summer upwelling. Changes in the density field (hence in pressure of density surfaces) accounts for the heave component of the isobaric changes in the thermohaline properties, implying changes in the geostrophic flow patterns in the ocean interior, as we will see later.

Right column of Fig. 4.1 shows the summer minus winter mean differences of θ, S, and pressure of γ^n surfaces, providing a graphical view of where properties on isopycnals change and where changes due to heave are of importance. Main results that can be drawn are (i) the strong isopycnal character of changes at the lower bound of Mediterranean waters, tight on the slope and west of the Galicia Bank. (ii) The high seasonal differences on isopycnal pressure levels above isopycnal 27.3 (~ 500 dbar) all along the section, implying an isopycnal shoaling up to 50 dbar in summer with respect to the winter season. Such change is much pronounced on the slope and extends deeper. (iii) An apparent change in the structure of the density field around the Galicia Bank, with the sinking of isopycnals at its eastern flank in summertime at intermediate levels. This readjustment of the density field would imply an enhancement of geostrophic southwards flow in the passage from the Galicia Bank to the shelf during this season. Finally, (iv) there is an enhancement of a recirculation structure associated to the Galicia Bank in summertime.

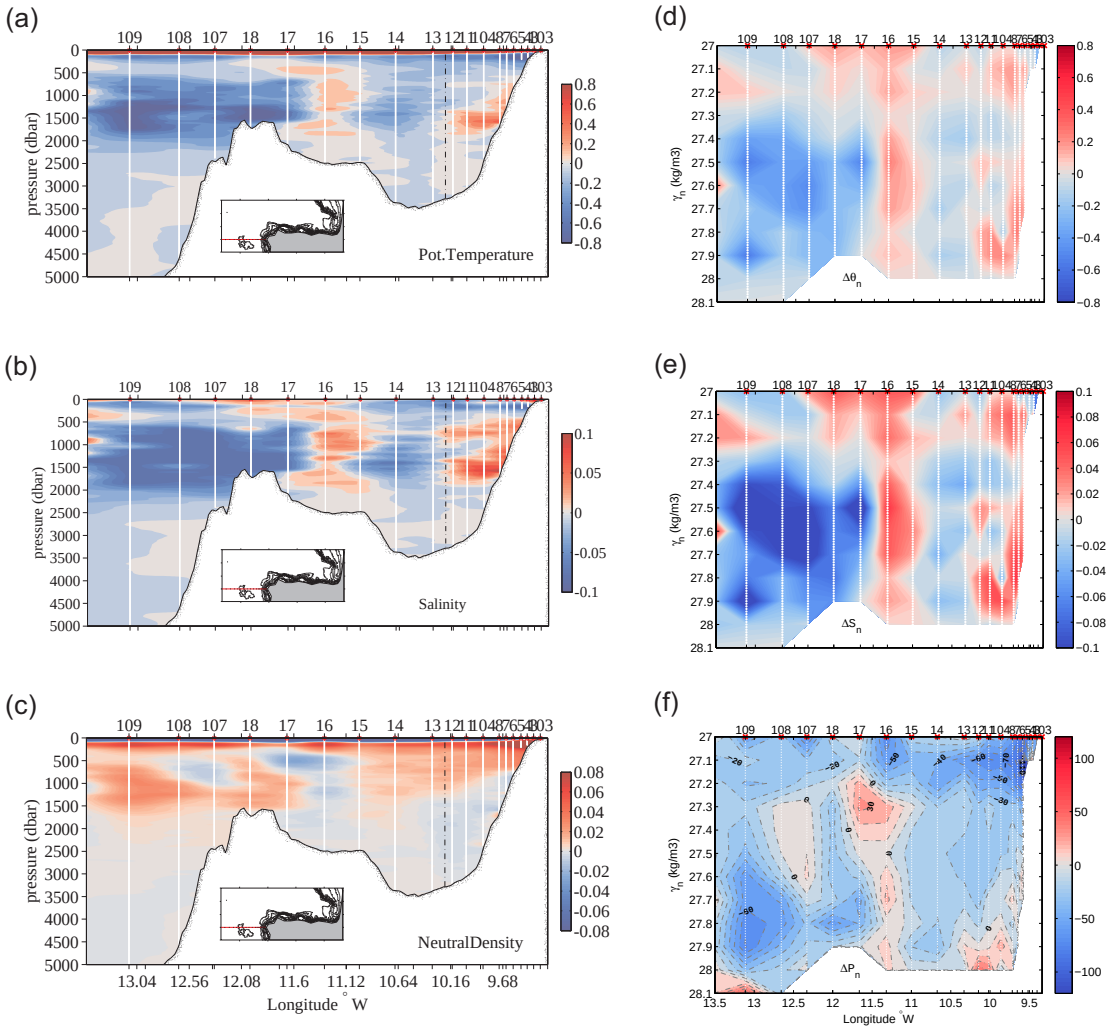

Figure 4.1: Left column: summer–winter differences of **(a)** potential temperature, **(b)** salinity and **(c)** neutral density along isobaric surfaces. Right column: summer–winter differences of **(d)** potential temperature and **(e)** salinity along isoneutral surfaces with associated summer–winter differences of **(f)** isoneutrals pressure.

It is interesting to get overall estimates of the amplitudes of annual cycles at depth. By inspection of Figs. 4.1a, b and even e, it looks rather like there are four distinct regions, one on the slope, one in the channel between the continent and the Galicia Bank, one east of the Bank and one west of it. These four regions appear to be linked to the recirculation system that develops in the surroundings of the Galicia Bank, which seems to yield a differentiated response to the seasonally varying background flows. We could easily apply the methodology of splitting isobaric changes that latter generate Fig. 4.2 to the four regions instead of the two proposed. The reason for keeping only two regions is that some of the subregions are narrow and involve very few stations. For instance, the anomaly at the eastern flank associated with warmer/saltier waters in summertime is confined to stations 15–17. Therefore, we prefer to keep a larger number of stations per region in order to get more reliable results from a statistical point of view, while keeping in mind that there are biases in the thermohaline seasonal signature in the outer and inner regions of the Bank due to its influence on the dynamics. Our approach assumes that, for the purpose of providing an overall view of the hydrographical variability of the outer ocean, the local anomalies caused by the Bank circulation should cancel each other out.

Thus, we consider separately the two regions (slope and outer ocean) and the methodology for splitting the changes, as in Eqs. (3.1) and (3.2), is applied at isopycnal levels from 27 to 28 $\mathrm{kg\,m^{-3}}$. Then, amplitudes of the annual cycle for each of the terms in the decomposition relationship are obtained for every neutral density layer and seasonal anomalies are zonally averaged for each region.

A graphical view of the computation is shown in Fig. 4.2, which provides a continuous profile of seasonal amplitudes, while the numerical values are shown in Table 4.1 as anomalies at the pressure levels of key isopycnals.

The main results of the analysis can be summarized as follows:

- Waters just below the seasonal thermocline cool and freshen in summertime all along the section, with maximum changes at ~ 200 dbar ($\gamma^n \sim 27.1$). At the open ocean, maximum cooling/freshening values exceed $\sim 0.3\,^{\circ}$C and ~ 0.02, and this seasonality decays progressively down to ~ 500 dbar (the salinity minimum at the base of ENACW) where there is no signature at all. The process is driven mainly by heave. On the slope the behaviour is similar but the amplitudes are larger and seasonality extends deeper down the water column. In both areas there is a weaker (than heave) isopycnal warming/salting signature that cannot counteract the much greater cooling/freshening by heave.

- In the density range $\gamma^n \sim 27.3$–27.6 (500–900 dbar; upper MW) we observe cooling/freshening at the outer ocean (0.2 °C and 0.03) and salinification on the slope

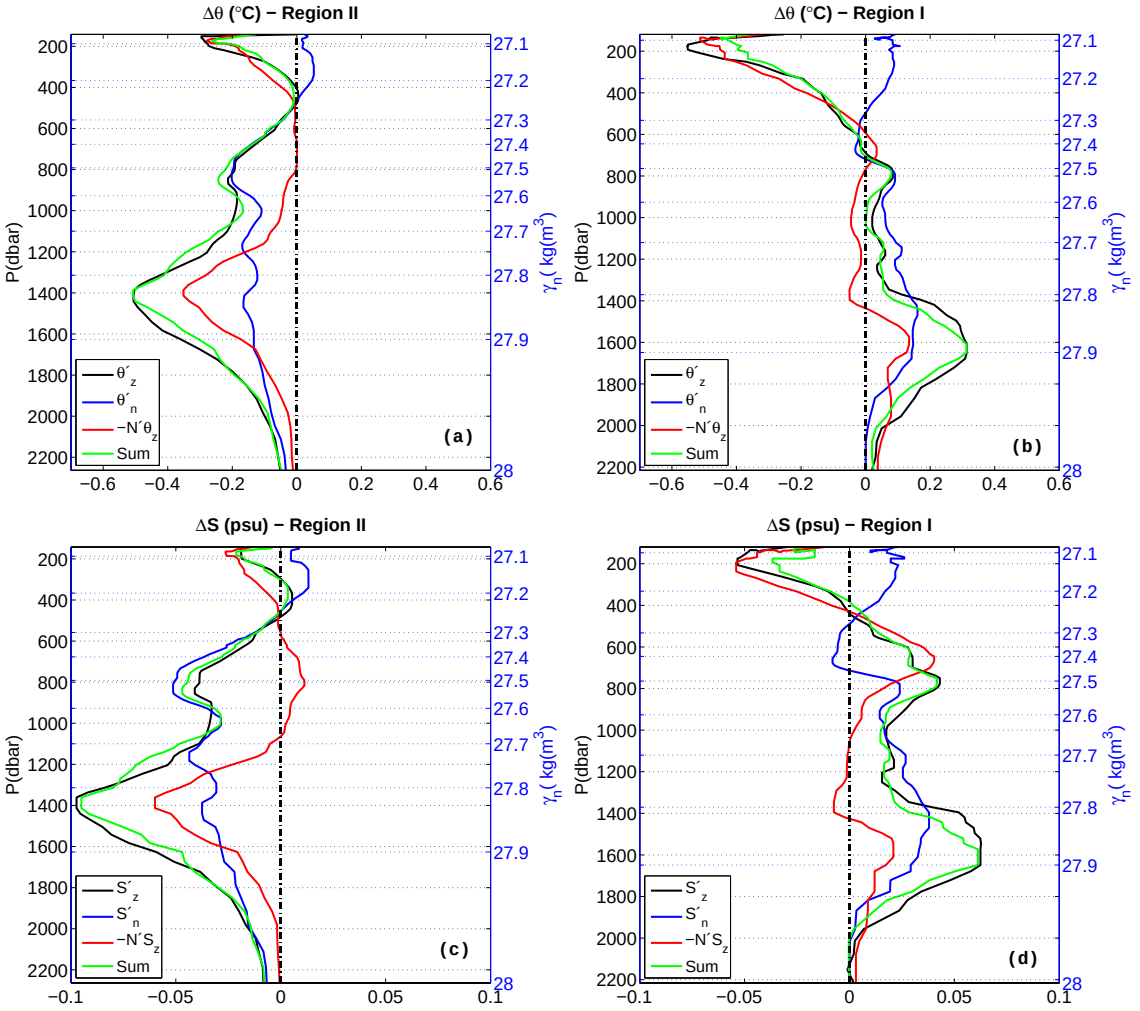

Figure 4.2: Decomposition of θ (top) and S (bottom) isobaric seasonal cycle following Eqs. (3.1) and (3.2). **(a)** and **(c)** are for the open ocean and **(b)** and **(d)** for the slope. Note that the decomposition is only approximate; the difference between the isobaric change (black line) and the sum (green line) of the isopycnal (blue line) and heave (red line) terms indicates the inaccuracy of the decomposition.

Table 4.1: Decomposition of θ and S seasonal changes along isoneutral surfaces (γ^n) as isopycnal plus heave terms in the open ocean and shelf-slope region. Positive (negative) values indicate warmer/saltier (cooler/fresher) conditions in summertime. P_n is the mean pressure of isoneutral γ^n (see Fig. 4.2).

γ^n	P_n (dbar)	θ_z'	θ_n'	N′θ_z	θ_n'-N′θ_z	S_z'	S_n'	N′S_z	S_n'-N′S_z
Open ocean									
27	142	−0.09	0.02	−0.19	−0.16	−0.017	0.007	−0.013	−0.004
27.1	187	−0.27	0.01	−0.15	−0.16	−0.018	0.001	−0.016	−0.016
27.2	367	−0.01	0.04	−0.06	−0.01	0.005	0.010	−0.006	0.004
27.3	558	−0.05	−0.04	−0.01	−0.05	−0.011	−0.012	−0.000	−0.011
27.4	677	−0.13	−0.14	−0.00	−0.14	−0.025	−0.036	0.007	−0.028
27.5	791	−0.19	−0.19	0.00	−0.22	−0.038	−0.050	0.011	−0.044
27.6	927	−0.18	−0.13	−0.04	−0.18	−0.032	−0.035	0.004	−0.031
27.7	1100	−0.21	−0.14	−0.08	−0.25	−0.038	−0.038	−0.005	−0.048
27.8	1314	−0.43	−0.11	−0.29	−0.42	−0.084	−0.029	−0.048	−0.080
27.9	1627	−0.32	−0.12	−0.11	−0.24	−0.059	−0.026	−0.018	−0.045
28	2264	−0.05	−0.03	−0.01	−0.04	−0.008	−0.006	0.000	−0.007
Shelf-slope									
27	119	−0.27	0.09	−0.33	−0.37	−0.029	0.024	−0.011	−0.021
27.1	147	−0.54	0.09	−0.50	−0.39	−0.048	0.026	−0.044	−0.016
27.2	332	−0.17	0.06	−0.24	−0.18	−0.010	0.016	−0.025	−0.009
27.3	533	−0.07	−0.01	−0.03	−0.06	0.011	−0.004	0.021	0.013
27.4	645	−0.01	−0.02	0.03	−0.01	0.029	−0.007	0.040	0.029
27.5	764	0.08	0.08	0.00	0.07	0.043	0.021	0.022	0.044
27.6	926	0.03	0.04	−0.03	0.01	0.023	0.013	0.005	0.017
27.7	1120	0.04	0.09	−0.01	0.06	0.020	0.026	−0.001	0.021
27.8	1371	0.14	0.13	−0.05	0.07	0.039	0.036	−0.009	0.024
27.9	1649	0.31	0.15	0.10	0.31	0.062	0.033	0.017	0.062
28	2215	0.03	0.00	0.03	0.03	0.002	0.000	0.001	0.000

(0.05). Isopycnal change drives the cooling/freshening at the outer ocean and there is a slight salt increase centred at 27.45 (note that as this water layer is characterized by a weak or null thermal gradient – see Fig. 2.4c, d – it is not possible to achieve warming/cooling by heave). The salinity increase on the slope is caused by the strong uprising of isopycnals in this region (i.e. heave).

- The lower layer of MW down to the LSW (range $\gamma^n \sim 27.7$–27.95, 1100–1800 dbar) is the portion of the water column where the seasonal cycle is greatest. At the outer ocean there is strong cooling/freshening up to $0.5\,^{\circ}\mathrm{C}\,/\,0.1$, caused by the combination of isopycnal change and heave, the latter being dominant at 1400 dbar where the amplitude of seasonality peaks. On the contrary the warming and salting on the slope (up to 0.31 °C and 0.062 near 27.9) is strongly dominated by isopycnal change. Maximum values for the outer region may seem higher in Fig. 4.2 than those shown in Table 4.1; the reason is that Fig. 4.2 provides a continuous profile of seasonal amplitudes, while Table 4.1 extracts the values at the pressure levels of key isopycnals.

In summary, there exists a noticeable seasonality signature in the Finisterre section for the whole permanent thermocline, down to c.a. 2000 m. There is a notable asymmetry between the slope region and the outer ocean. ENACW properties oscillates by heave with stronger amplitude on the slope. Upper MW on the slope appears to be upraised in summertime, while at the outer ocean its signature weakens (cools and freshens without significant heave signature). The water layer corresponding to the lower MW exhibits the largest changes, with strong cooling/freshening at the outer ocean and warming/salting on the slope. Overall, it appears that MW during summertime gets tightly attached against the slope and uplifted, reinforcing there its thermohaline signature and losing its presence at the outer ocean. In wintertime the situation reverses, MW seems to detach from the slope and spreads out to the open ocean, even developing a secondary branch at, and west of, the Galician Bank.

4.1.2 Statistical significance

In this section we will check the robustness of the existence of seasonality from a statistical point of view. Testing for seasonality (or whatever periodic variation) in a time series relies in principle on spectral analysis, however, having a very limited number of observations and a signal with strong interannual variability (nonlinear trends) such seasonality testing is not straightforward. As previously noted, a convenient approach is to apply a

simplified harmonic analysis determining the best fit of time series from hydrographical properties to the functional form:

$$\psi(t) = a\cos(\omega t + \phi) = a_1\cos(\omega t) + a_2\sin(\omega t), \tag{4.1}$$

where $\omega = 2\pi f$ is fixed to one year ($f = 1$, which is indeed the shortest solvable scale given the Nyquist frequency of our semiannual series). Then, it can be checked whether the amplitude coefficient is significant by means of a t test. This approach was followed by *Bray* (1980) to determine seasonality of hydrographycal properties at intermediate levels in the Bay of Biscay, which is a very similar problem to ours, though her dataset consisted of 11 points along three years. Prior to attempt any harmonic analysis it is needed to remove the record mean and trends (linear or not) if relevant (e.g *Emery & Thomson*, 2001). This is indeed our case given that, as will be shown next, interannual variability is much larger than the apparent seasonality signal. Therefore, we treat our 8 yr time series of hydrographical properties subtracting firstly a two-degree polynomial (hence removing slowly varying patterns) to compute later the bestfit of Eq. (4.1) of the residual.

Figure 4.3 shows the bestfit of properties (salinity at isobars, pressure of isopycnals and salinity at isopycnals) at levels of selected neutral surfaces $\gamma^n = 27.4$ and $\gamma^n = 27.8$ for the slope region, where we have determined seasonality driven by heave and by isopycnal change respectively (Fig. 4.2). In accord with what is observed in the sections (Fig. 2.5), a see-saw pattern is intermittently present at portions of the time series. After the removal of the trend, the fitting results are significant for heave at 27.4 and for isopycnal change at 27.8. Anomalous years with opposed patterns also arise (e.g. summer 2009 again in agreement with Fig. 2.5). Figure 4.3 provides us an insight of the relative strength of the seasonality with respect to the interannual variability. Values of the estimated amplitude of seasonality represent roughly a 20 % of maximum variations or excursions along the whole time series of properties, interannual variability included (Fig. 4.3 and others not shown). In summary, this analysis reinforces the case for the existence of seasonality superimposed on the interannual variability of hydrographic properties at depth.

4.2 Variations of thermohaline properties at interannual scales

The next step is to deal with the deseasonalized signals representing the interannual changes of water mass properties. Results from the present Section will be discussed later in Chapter 5, Sect. 5.2.

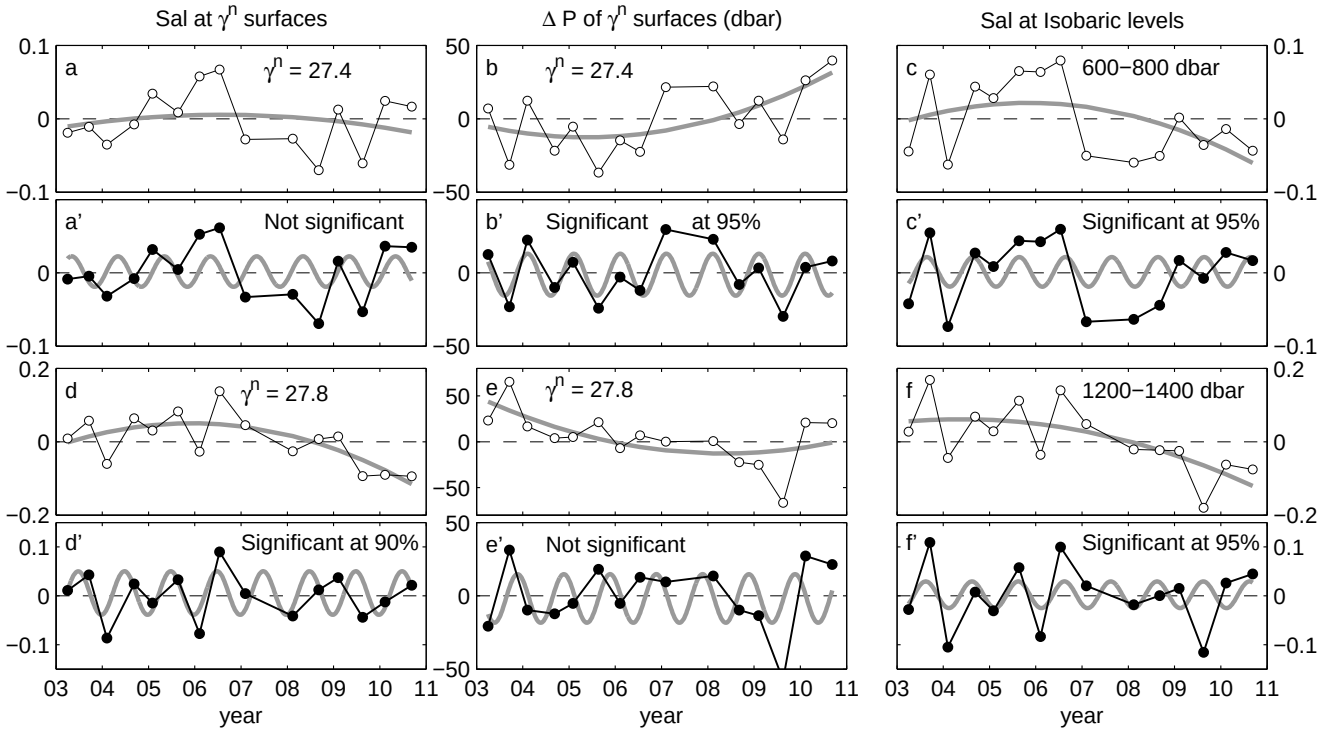

Figure 4.3: Time series of **(a)**, **(d)** salinity anomaly at isopycnal levels $\gamma^n = 27.4$ and 27.8, **(b)**, **(e)** pressure (anomaly) at which these isopycnal levels lie, **(c)**, **(f)** salinity anomaly at isobaric levels 600–800 and 1200–1400 dbar, roughly corresponding to these isopycnals. A two-degree polynomial trend is computed for each series (thick gray). Prime versions of figures correspond to the simple harmonic analysis applied to the residual (time series minus trend, black dots) following Eq. (4.1).

4.2.1 Raw timeseries at isobaric levels. Overall trends

A first insight of the evolution of thermohaline properties of water masses with time is provided by the θ/S diagrams in Fig. 2.3. Note the isopycnal shift of central waters towards a warmer/more saline type at all three sections, seen here as the displacement of the straight line between 27.1 and 27.3 in the θ/S diagram. At deeper water below about $\sigma_\theta \sim 27.4$ the diagrams show no clear changes in properties. Figure 4.4 shows average temperature and salinity timeseries at isobaric levels in order to emphasise interannual changes at the three sections. There are some coherent pattern in changes between the sections and through the water column, as well as notable year to year changes. Linear trends with confidence intervals derived from a T-test at all layers are shown in Fig. 4.5.

Changes in the upper layer (surface to the maximum development of winter mixed layers, 200 dbar) are not well sampled by semiannual sections but the imprint of the cold winters 2005, 2006 and 2009 clearly emerges. The surface salinity is characterized by two periods of smooth increase either side of the cold, fresh winter of 2009. The upper ENACW (200-400 dbar) shows a salinity rise of about 0.5 during 2005 and 2006 and remained pretty stable since then, yielding an overall salt-increase trend of $0.006\,\mathrm{yr}^{-1}$. A 0.30 °C decrease in potential temperature in the 200-400 dbar layer at Finisterre indicates that the strong cooling in winter 2005 was able to penetrate deep in the water column. The effect was transitory since this layer and 400-800 dbar (the Salinity Minimum at the base of ENACW to the upper MW) show a significant warming trend of $0.018 - 0.016\,^\circ\mathrm{C\,yr}^{-1}$ over the time series. Lower thermocline waters (27.5-27.9, 800-2000 dbar including MW and LSW) are characterized by a drop in temperature and salinity in late 2008 and a recovery in 2011. The 1200-1600 dbar layer is the only part of the water column with overall significant negative trends in thermohaline properties. The deep water (28-28.1, $\sim$2000 dbar to $>$ 4000 dbar) showed much weaker interannual variations. A freshening of $>$3600 dbar water (including bottom water) of about 0.004 was observed along the three transects from late 2009 to late 2012. There were coherent variation across most of the water column in 2008 and 2013 (cooling and decreasing salinity) and 2011 (warming and increasing salinity). Next we examine the robustness of the signals described above by considering the effect of the sampling frequency on the results.

4.2.2 Consistency of the record. Correlation, autocorrelation and mesoscale field

A well acknowledged problem when describing the state and the evolution of ocean hydrography from repeated hydrographic sections is to identify the uncertainty induced by

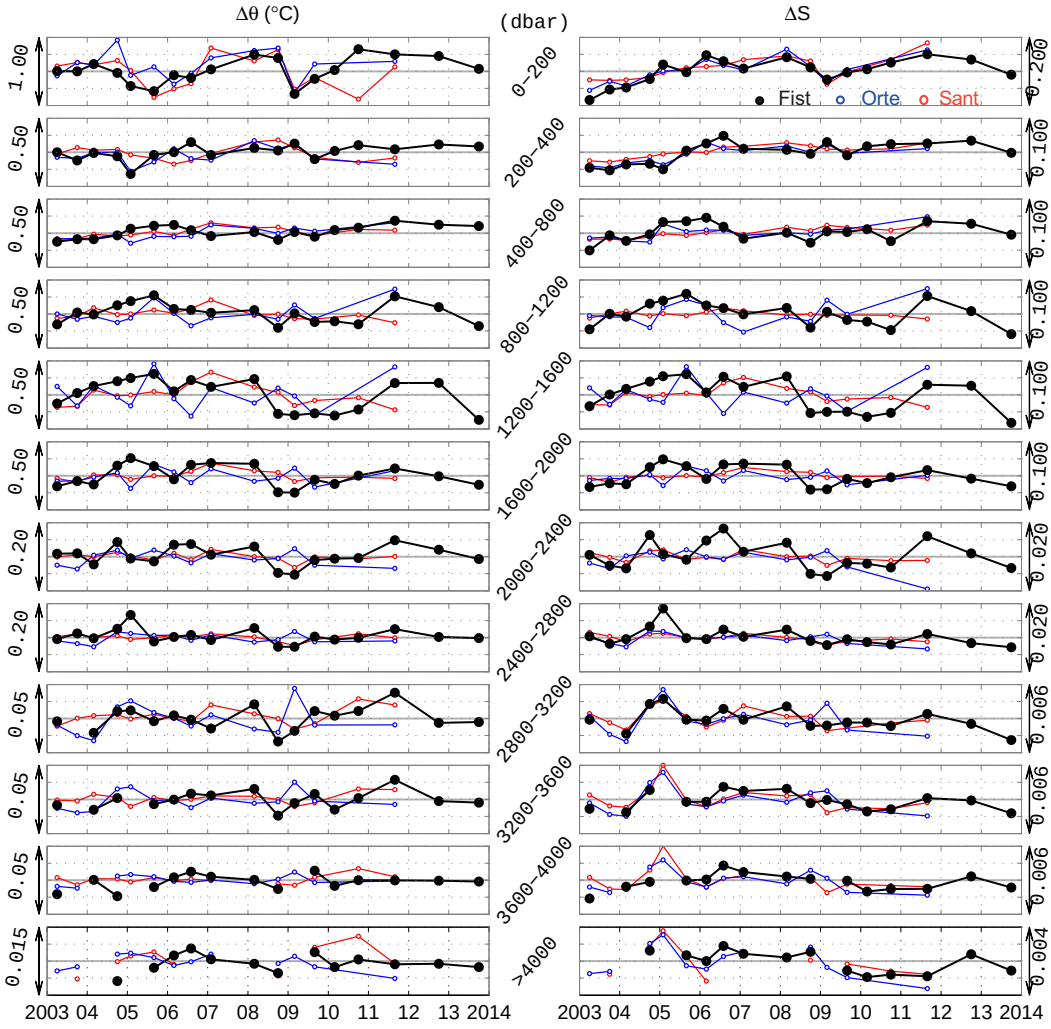

Figure 4.4: Potential temperature (left) and salinity (right) interannual variability at Finisterre (black), Ortegal (blue) and Santander (red) during 2003-2013. Changes were averaged over pressure intervals from surface to 200 dbar and then every 400 dbar down to 4000 dbar. Abyssal water (>4000 dbar) changes were averaged from 4000 dbar to the bottom.

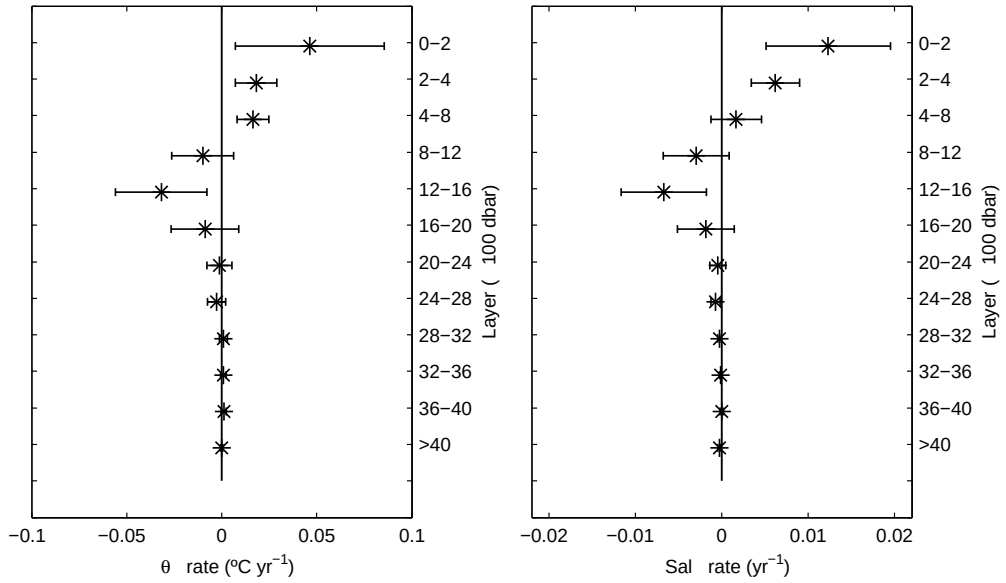

Figure 4.5: Potential temperature (left) and salinity (right) trends for series at Finisterre during 2003-2013 as shown in Fig. 4.4

the mesoscale field. Mesoscale variability in the region exhibit length scales of about 50-100 km diameter and decay scales of $\sim 250\pm100$ days (*Pingree*, 1994) that may be a source of noise for our semiannual time series specially at the slope (*Pingree & Le Cann*, 1992a,b) and MW levels (*Richardson et al.*, 2000). Eddy-like structures are evident in the sections (not shown) and, accordingly, an estimate of correlation scale by a bestfit of salinity fields through an isotropic Gaussian function of the distance between the observations (e.g. *Bretherton et al.*, 1976) yielded a decay scale of $\sim 10-30$ km. Average station spacing is about 25 km (closer in the shelf-break and increasing to 37 km at the outer ocean) so the mesoscale field should be captured by the sampling scheme. In this section we use a statistical approach to infer parts of the water column that may be dominated by mesoscale variability.

If the short-term variability induced by the mesoscale field were greater than or comparable to the large scale interannual variability, we would expect the series to be no different to noise and have no autocorrelation. To detect the presence of autocorrelation in the record (that is, to test the existence of statistically significant temporal coherence of variability), we applied a Durbin-Watson test (e.g *von Storch & Zwiers*, 2001) to the series on isobars (Fig. 4.4). Table 4.2 show the p-values; most surface to 2000 dbar Finisterre and Santander series indicate autocorrelation (above 90% and 95% for most series) which

Table 4.2: p-values from Durbin-Watson test. Test of autocorrelation was applied to series at isobaric levels shown on Fig. 4.4. Zero values indicate p$\leq 10^{-3}$)

	Finisterre		Santander		Ortegal	
P(dbar)	$\Delta\theta(^{\circ})$C	ΔS	$\Delta\theta$	ΔS	$\Delta\theta$	ΔS
0-200	0.04	0.00	0.17	0.00	0.80	0.07
200-400	0.95	0.00	0.00	0.00	0.23	0.01
400-800	0.00	0.02	0.01	0.80	0.93	0.24
800-1200	0.08	0.12	0.09	0.02	0.62	0.12
1200-1600	0.01	0.02	0.00	0.00	0.49	0.83
1600-2000	0.01	0.00	0.01	0.00	0.08	0.26

suggests that series are dominated by the large scale background signal. The Ortegal series fail the autocorrelation tests indicating that these series are more strongly affected by local short-term circulation and the mesoscale field. Deeper layers do neither show autocorrelation but not relevant trends or shifts have occurred at great depths.

If the mesoscale field were dominant in a section we would expect that properties would only correlate vertically at the scale of eddies (within a single 400 dbar layer or two contiguous layers at most). In contrast, if changes were caused by shifts in large-scale advective patterns there may be correlation across a greater pressure range. Correlation coefficients (R) with associated p-values (p) were calculated to test the hypothesis that there is no correlation between the isobaric levels shown in Fig 4.4. Table 4.3 shows correlation coefficients and p-values for potential temperature and salinity anomalies along the Finisterre, Ortegal and Santander sections. The main outcome is that potential temperature and salinity anomalies are highly correlated (from 70% to 90%) across the lower thermocline (from 800 to 2000 dbar) in the three sections (except salinity anomalies at the Ortegal section with only $\sim$60%), suggesting that changes may be more affected by the large-scale. At deep levels below 2400 dbar, correlation of changes is also statistically significant at the 70-90%.

Finally we focus on the correlation of the same water masses at the three sections. No significant correlation may indicate the dominance of the eddy-field, but could also indicate different regional signals of water masses variability. There are significant correlations between all three sections in the surface waters and the upper thermocline (200-400 dbar, especially in salinity , Fig. 4.4). R is as high as 80% between Finisterre and Santander, and more than 90% between Finisterre and Ortegal, significant at the 95% confidence level at 0-200 dbar. This correlation stands also for central waters salinity anomalies, 77% for Finisterre-Santander and 93% Finisterre-Ortegal. For these specific

Table 4.3: Correlation coefficients (R) and p-values for potential temperature and salinity anomalies ($\Delta\theta$, ΔS). Anomalies were averaged every 400 dbar along the Finisterre (subscript Fist.), Ortegal (Orte.) and Santander (Sant.) sections.

	$\Delta\theta$						ΔS					
Pressure layers (dbar)	$R_{Fist.}$	$p_{Fist.}$	$R_{Orte.}$	$p_{Orte.}$	$R_{Sant.}$	$p_{Sant.}$	$R_{Fist.}$	$p_{Fist.}$	$R_{Orte.}$	$p_{Orte.}$	$R_{Sant.}$	$p_{Sant.}$
0–200→200–400	0.36	0.13	0.07	0.80	0.66	0.00	0.69	0.00	0.66	0.01	0.79	0.00
200–400→400–800	0.24	0.33	0.26	0.36	0.12	0.67	0.42	0.08	0.42	0.12	0.84	0.00
400–800→800–1200	0.50	0.03	0.44	0.11	0.48	0.06	0.75	0.00	0.72	0.00	-0.15	0.57
800–1200→1200–1600	0.84	0.00	0.77	0.00	0.90	0.00	0.83	0.00	0.56	0.03	0.75	0.00
1200–1600→1600–2000	0.79	0.00	0.71	0.00	0.89	0.00	0.80	0.00	0.61	0.02	0.86	0.00
1600–2000→2000–2400	0.60	0.00	0.59	0.02	0.45	0.08	0.68	0.00	0.35	0.21	0.33	0.22
2000–2400→2400–2800	0.54	0.02	0.67	0.00	0.73	0.00	0.53	0.02	0.69	0.00	0.89	0.00
2400–2800→2800–3200	0.69	0.00	0.92	0.00	0.61	0.01	0.87	0.00	0.92	0.00	0.83	0.00
2800–3200→3200–3600	0.81	0.00	0.93	0.00	0.84	0.00	0.83	0.00	0.95	0.00	0.90	0.00
3200–3600→3600–4000	0.44	0.10	0.91	0.00	0.71	0.00	0.75	0.00	0.96	0.00	0.98	0.00
3600–4000→ >4000	0.96	0.00	0.67	0.01	0.87	0.00	0.85	0.00	0.96	0.00	0.94	0.00

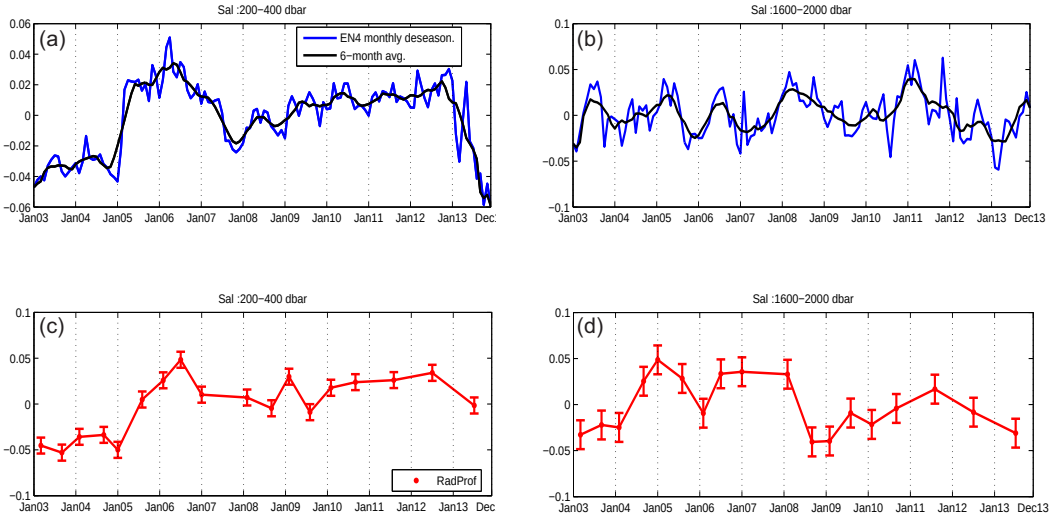

Figure 4.6: Monthly deseasonalized salinity time series from objective analysis (blue line) and 6-month moving average of time series (black line), retrieved from the EN4 UK Met Office product (*Good et al.*, 2013) for the [43°N, 9-15°W] region at a) 200-400 dbar and b) 1600-2000 dbar. Interannual variability observed along the Finisterre section at the same pressure intervals (c) and d)) with estimated error bars calculated from residuals of the blue and black lines.

layers, stats suggest largescale influence; note that this does not contradict the dominance of mesoscale at Ortegal since the autocorrelation test shows large p-values except for salinity anomalies at 0-200 dbar and 200-400 dbar (Table 4.2)

If the timescale of the mesoscale variability is 250±100 days (*Pingree*, 1994) we might expect that 1 or 2 sections per year will undersample that temporal variability, leading to biased results. We can make use of an independent, float-based product with monthly resolution to estimate the uncertainty due to the low frequency sampling. The UK Met Office EN4 product (*Good et al.*, 2013) is constructed as objective analysed fields based on observed subsurface ocean temperature and salinity (mainly from float profilers) on monthly basis. We recovered the grid points along 43°N, 9°-15°W (Finisterre section) for the 2003-2013 period and computed deseasonalized time series of temperature and salinity at the same isobaric levels as our record. The approach is to compare a low-pass filtered version of the time series (representing variability at the time scale we are interested in), to a time series of the same product sub-sampled six-monthly (the rate of our in-situ ocean time series). The standard deviation of the residuals between these two series is taken as representative of the error associated with the semiannual sampling.

The analysis was restricted to the upper 2000 dbar of the water column since there are limited data points below that level (*Good et al.*, 2013). Figure 4.6 shows monthly

Table 4.4: Estimate of short-term variability based on the EN4 product. Estimated short-term variability at the Finisterre section ($\Delta\theta_\varepsilon$, ΔS_ε) compared to the interannual variability exhibited by the section ($\Delta\theta$, ΔS).

ΔP (dbar)	$\Delta\theta_\varepsilon$(°C)	$\Delta\theta$(°C)	ΔS_ε	ΔS
0-200	0.32	1	0.015	0.24
200-400	0.05	0.4	0.008	1.2
400-800	0.04	0.2	0.011	0.1
800-1200	0.1	0.4	0.026	0.1
1200-1600	0.15	0.4	0.032	0.1
1600-2000	0.08	0.4	0.016	0.1

and six-month averaged time series of salinity variations from the EN4 product at two representative levels (a) 200-400 dbar and (b) 1600-2000 dbar.

Salinity variations observed from the sections with estimated error bars are shown for the same pressure intervals in (c) and (d) respectively. Table 4.4 shows a comparison between errors calculated as deviations of the residuals of EN4 time series ($\Delta\theta_\varepsilon$, ΔS_ε) and the size of maximum anomalies observed in the in-situ time series ($\Delta\theta$, ΔS). Estimated errors are an order of magnitude smaller than the background signal supporting also the idea that the large scale variability has been identified above mesoscale noise.

4.2.3 Decomposition of interannual changes: isopycnal vs. heave

Having established that large-scale variations can be detected above mesoscale variability in the time series at Finisterre below the surface layer, we next examine the relative influence of source area fluxes vs circulation changes at that section through the decomposition into heave and isopycnal variations. The θ-S relationship and the approximate depths of the key isoneutrals is given in Fig. 4.7a, and decomposition of the property changes on those isoneutrals is shown on Fig. 4.8. Changes due to heave are the product of vertical gradients of properties (Fig. 4.7a') and the temporal variation of isoneutrals pressure (N', see Fig. 4.7b). Note that the decomposition is only approximate so the difference between the isobaric change (black line) and the sum (green line) of the isopycnal (blue line) and heave (red line) terms accounts for the inaccuracy of the decomposition (Fig. 4.8). Isopycnal changes for salinity and temperature must yield the same functional form (as constrained by density). Changes due to heave differ since they are modulated by their respective reference gradient profiles (Fig. 4.7a') with the main difference of the large salinity inversion in the upper MW levels.

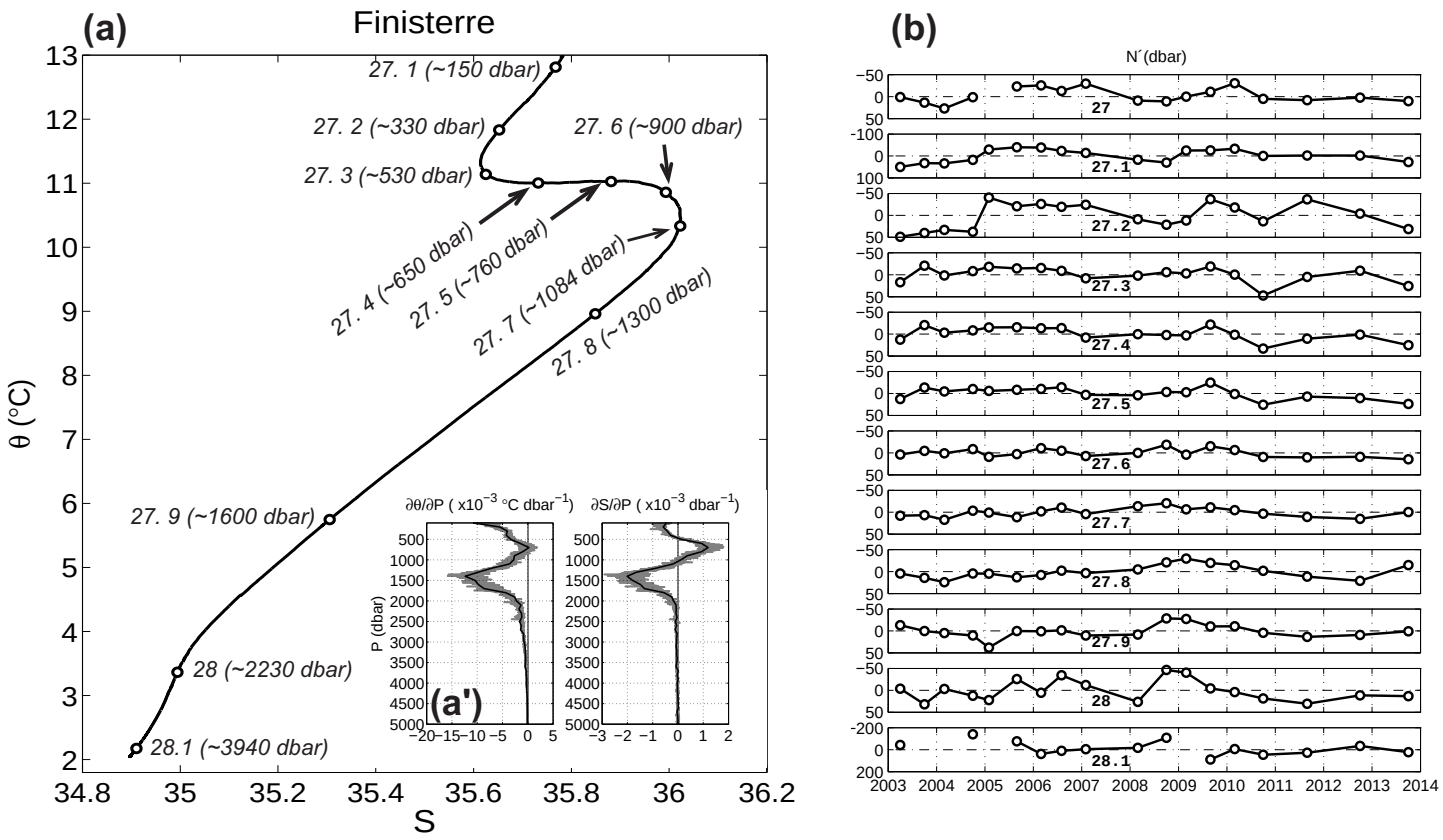

Figure 4.7: **(a)** Location of isoneutrals used for the study (lying at mean pressure in brackets) in the Finisterre along-section/ whole time period θS average. **(a')** Potential temperature and salinity vertical gradients. Black lines represent gradient of properties averaged over time; grey lines show gradients calculated for all profiles sampled during all cruises. **(b)** Interannual variations of isoneutrals pressure in the 2003-2013 period.

A dominance of isopycnal origin in the variability of central waters (27.1 and 27.2) clearly emerges from Fig. 4.8, particularly in the salinity record. The decade is mostly characterized by the rapid warming and salinification after the winter of 2005. Isoneutral 27.2 shoaled by about 100 m in 2005 causing immediate cooling and freshening, but after that there was a process of isopycnal warming/salinification that ended by late 2006, and the water mass has remained stable in this saltier/warmer state since then. The event in 2005 also affected the isoneutral associated with the Salinity Minimum (27.3, $\sim$500-600 dbar). This level had a notable shift in properties after 2011 when the Salinity Minimum was up to 0.15°C warmer and 0.025 saltier than average.

Changes along the isoneutrals of the upper MW to the MW core (27.5-27.7) have an almost exclusively isopycnal origin consisting on warming and salinification since 2003 with maximum in summer 2005 followed by fresher and cooler conditions interrupted at both levels by the abrupt strong warming (0.3-0.4°C) and salinification (0.08-0.1) of isopycnal origin in 2011. Changes on isoneutral 27.9 (LSW) show isopycnal change and heave during the sampling period. Warming/salinification by isopycnal change was observed again from 2003 to 2005, after which warming/salinification by heave was caused by the deepening of isoneutral 27.9 by about 50 dbar (see Fig. 4.7b).

The fresher state around 2009-2011 in the deepest layer is consistent with isopycnal change, however the weak density gradients below the permanent thermocline mean that this conclusion has low certainty. Overall the variations in the deepest water of the Finisterre section are weak and show no clear trends.

During 2008, 2011 and 2013 there were coordinated responses across large parts of the water column so we present the vertical decomposition of changes on Fig. 4.9. In 2008 there was cooling and freshening down to about 2500 dbar (with maximum values at $\sim$1500 dbar) as a combination of isopycnal change and heave. However between the Salinity Minimum and upper MW ($\sim$500-900 dbar, 27.3-27.6) changes had a mainly isopycnal origin. In contrast Figs. 4.9b,e show warming and salinification across the permanent thermocline in 2011, with maximum values at $\sim$1300 dbar (27.8) and with an almost exclusively isopycnal origin from 500 to 2000 dbar (27.3 to $\sim$28). Note that all isoneutrals between 27 and 28.1 deepened in 2011 (Fig. 4.7b). Changes in 2013 showed cooling and freshening of the whole water column (Fig. 4.9c,f), with a maximum at 1300 dbar (27.8, deep MW) through a combination of isopycnal change and heave, the latter associated with the shoaling of isoneutral 27.8 (Fig. 4.7b). The water column down to the Salinity Minimum ($\sim$100-500 dbar, 27-27.3) cooled by isopycnal change and warmed by heave due to the deepening of associated isoneutrals. Changes of water mass properties will be discussed in Chapter 5, Sect. 5.2 in terms of the NAO-induced forcing and main North Atlantic circulation patterns affecting the Finisterre section.

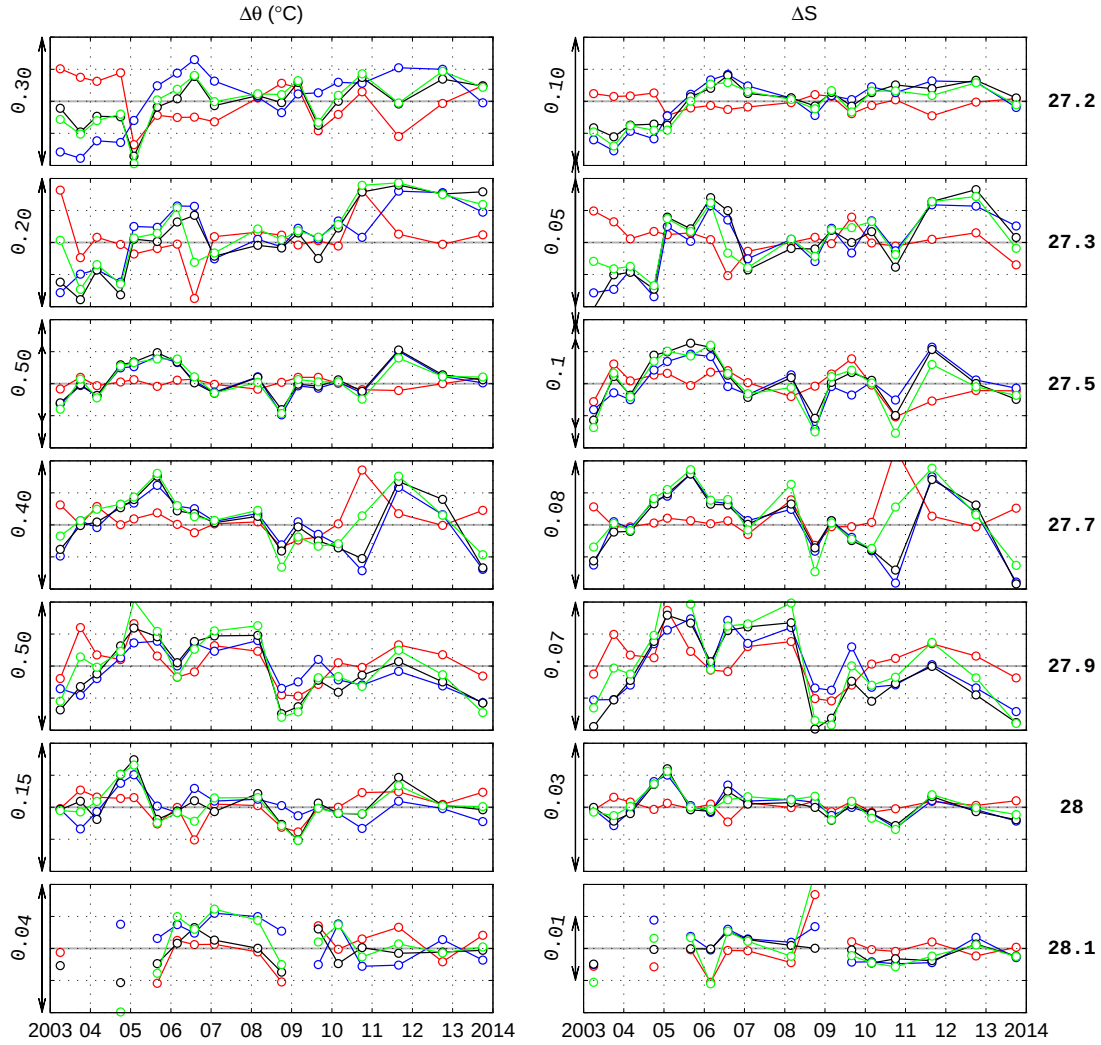

Figure 4.8: Time-series of potential temperature (left) and salinity (right) decomposition of isobaric changes (black, data from Sect. 4.2.1) on isopycnal change (blue) and heave (red) at selected isoneutrals: thermocline waters (ENACW, 27.2), the Salinity Minimum (27.3), Upper MW (27.5), MW core (27.7), Deep Mediterranean - LSW interface (27.9) and deep waters (ENADW, 28; LDW, 28.1). Differences between the black and green (sum of the blue and red) lines represent the inaccuracy of decomposition.

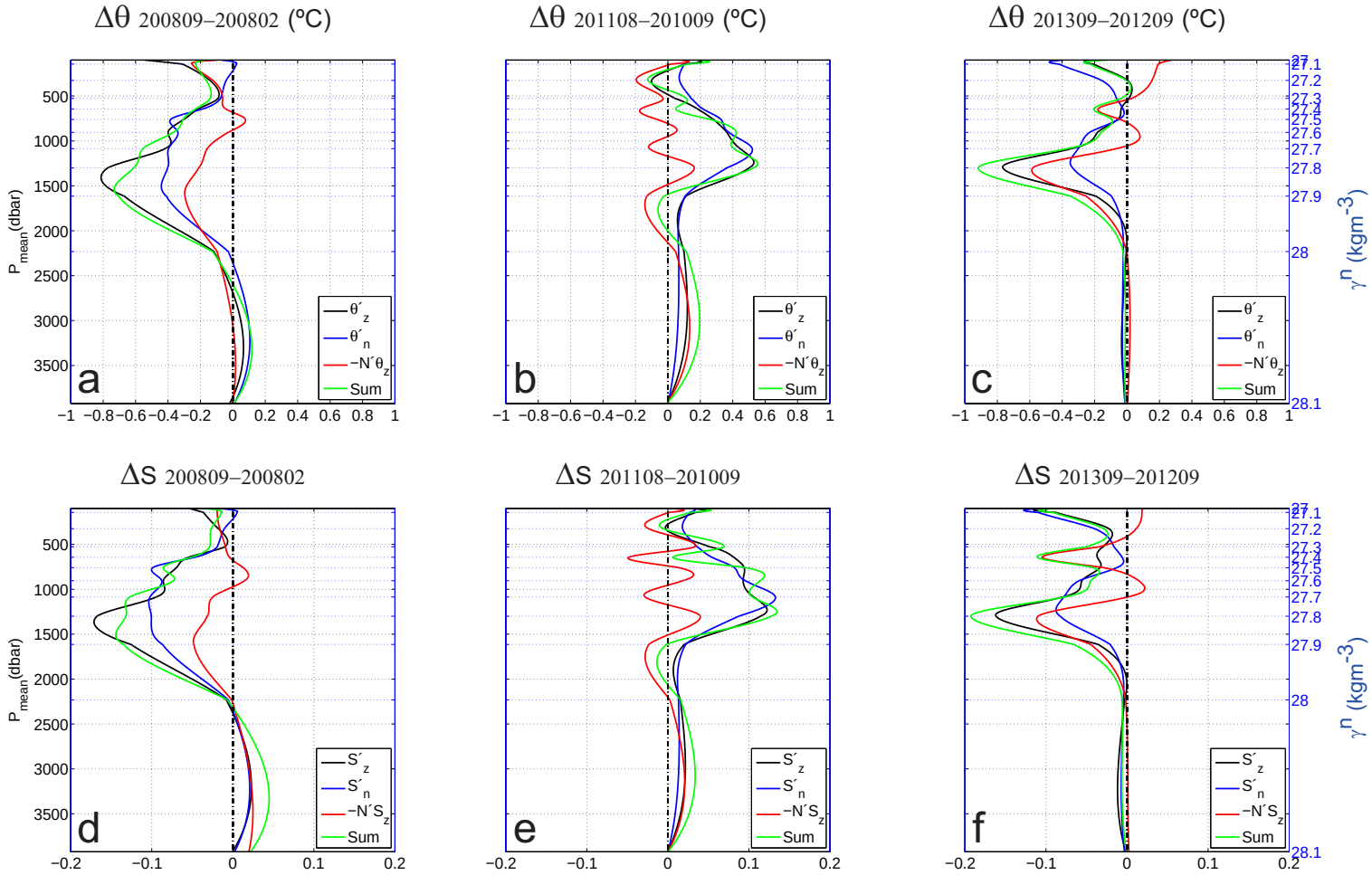

Figure 4.9: Decomposition of the temperature (a,b,c) and salinity (d,e,f) isobaric changes (black) on isopycnal changes (blue) plus changes by heave (red) following *Bindoff & McDougall* (1994). The sum of both (green) accounts for the inaccuracy of the decomposition. Method was applied to changes observed in the water column between 27-28.1 kgm^{-3}, from February 2008 to September 2008 (left), from September 2010 to August 2011 (middle) and from September 2012 to September 2013 (right)

4.3 Currents and water mass transport

In this section we focus on the cruises performed in February and September 2008, as being representative of a typical winter/summer situation. Figure 4.10 show potential temperature (a), salinity (b) and their respective vertical gradients (d,e), neutral density (c) and zonal density gradient (f) during RadProf200802 and RadProf200809. Slightly cooler and fresher thermocline and intermediate waters (from below the mixed layer ∼200 dbar down to 2000 dbar) is observed in summer, not only following the seasonality but also reflecting a drop in properties that affected most of the water column this year, as it was shown in Sect. 4.2.

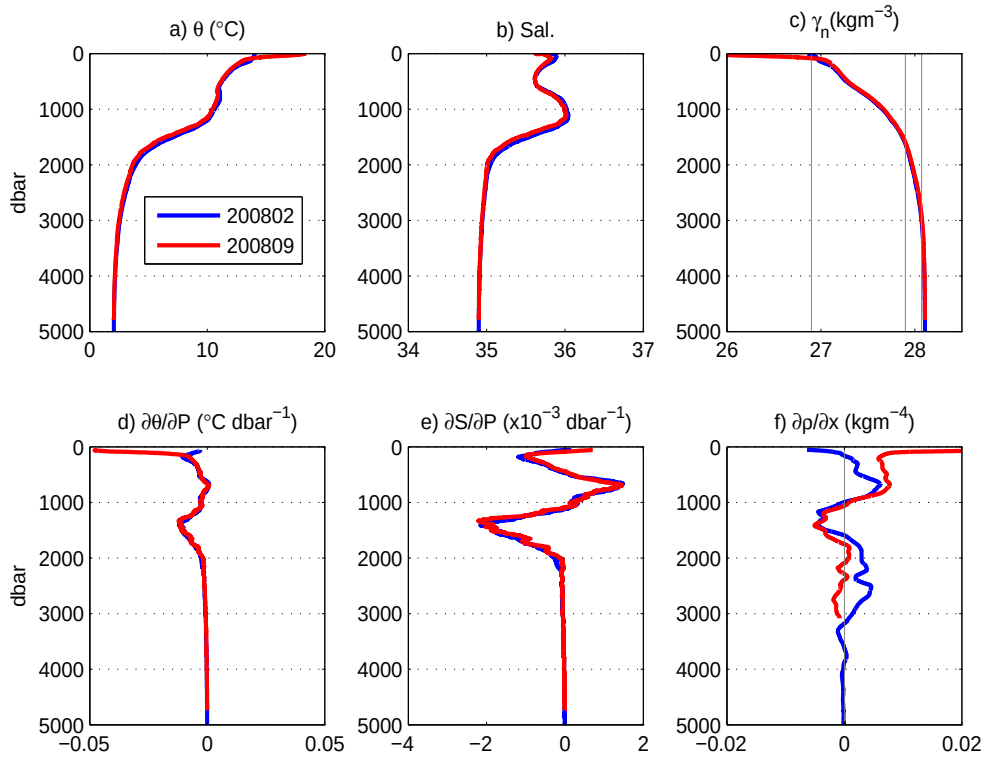

Figure 4.10: Potential temperature (a), salinity (b), neutral density (c), vertical gradient of temperature (d) and salinity (e), and horizontal gradient of density (f) during RadProf200802 (blue) and RadProf200809 (red). Vertical gray lines in c) show pressure of 26.9 (∼100 dbar), 27.9(∼1650 dbar) and 28.072(∼3000 dbar) isoneutrals.

Salinity vertical gradient (Figure 4.10e) is characterized by three marked extremes: two minimum at $\sim$ 200 dbar and 1300 dbar, associated with the interface between upper and thermocline waters and the MW-LSW interface, and a maximum at $\sim$700 dbar defining the ENACW-MW interface. Three crossings by zero define the mixed layer ($\sim$100 dbar), the Salinity Minimum ($\sim$500 dbar) and the salinity maximum associated to MW ($\sim$1100 dbar). Zonal density gradients (Fig. 4.10f) along the zonal section (computed as the overall zonal average) are characterized in general by large values above 3000 dbar, showing two relative maxima at 700 dbar and 1300 dbar, coinciding with those of salinity vertical gradient, a zero crossing at 1000 dbar during both cruises and small or near zero values below 3000 dbar, suggesting this depth as a good reference level for geostrophy calculations. *Daniault et al.* (1994) chose the reference level at 2500 dbar as being the limit for MW influence (relative percentage of Mediterranean salt of 4%).

4.3.1 Directly measured meridional velocities vs geostrophic fields.

Figures 4.11 and 4.12 show the meridional velocity fields from the four approaches previously discussed, i.e. raw LADCP currents as well as the result of removing the modelled barotropic tide and the standard gesotrophic approach together to the LADCP BT-corrected version.

There are strong similarities as well as notable discrepancies between the four different field estimates. Starting with LADCP raw record for the winter cruise RadProf200802 (Fig. 4.11a), it is observed a complex pattern of alternating flows with marked barotropic character (i.e. there is no a clear weakening of currents in the first 3000 m of water column). There is northwards flow at the shelf, southwards at the slope to reverse again at the foot of the slope (the 2500 to 3000 m depth portion, stations 9-10). Then flow is mainly southwards across the valley towards the Galician Bank summit where the flow is again northwards. The northwards flow west of the Galician Bank at mid-depths contrasts to the southwards flow at upper levels. In the standard geostrophic flow (Fig. 4.11b) it is possible to observe roughly the same alternating northwards/southwards bands, although some features are slightly displaced. For example it is present the sequence north-south-north from the shelf to the foot of the slope, but geostrophic field show a much stronger and deeper reaching northward flow in the upper slope. An anticyclonic recirculation above the Galician Bank is evidenced both in LADCP and geostrophy. The detided LADCP (Fig. 4.11c) is similar to the raw field but blurring to some extent the stripped pattern. Finally the correction of geostrophy by LADCP bottom tracking (Fig. 4.11d) strongly changes the velocity field with strong effect at mid-depths, close to the previously taken no-movement reference level, and near the bottom.

In the summer cruise RadProf200809 we also observe similarities and discrepancies between the different meridional velocity estimates. Again the LADCP (Fig. 4.12a and c) suggests a strong barotropic character with southwards flow across the passage and northwards flow at the slope and west of the Galician Bank. The geostrophic field (Fig. 4.12b) indicate recirculation patterns that, while are not absent in the LADCP field, they are strongly exacerbated. For example the return flow between stations 11 and 12 (around 10.5°W, Fig. 4.12b) match a patch of return flow right at station 12 in LADCP (Fig. 4.12c). Also a secondary structure at the Galician Bank consisting of a band of northward flow at depth around station 15 is present both in geostrophy and LADCP. The BT corrected gesotrophy is apparently in this case more similar to the LADCP field but some features as the slope flow seems again strongly exacerbated.

Overall, there is common pattern of northwards flow at the shelf-inner slope, then southwards flow in the passage to the Galician Bank and finally northwards flow again west of the bank. The flow seems less consistent and erratic in wintertime.

4.3.2 Transport estimates

The integration of the meridional velocity fields across the section provide estimates of mass transport with important implications for large-scale circulation. Due to the spatial structure of velocity fields seen on Figs. 4.11 and 4.12 it seems reasonable to split the section in three different regions to compute transports separately (slope, passage and west of Galician Bank). On the other hand, following the methodology explained in Sect. 3.1 we split the section only in two regions (slope and open ocean) to analyse the different hydrographical structures observed in winter and summer (see Fig. 2.6). We will combine both views in the present section. In order to make both cruises comparable the westernmost stations in the winter cruise (west of st. 18) are not considered to estimate transports.

Figure 4.13 provide the vertically integrated transport from detided LADCP and geostrophy (standard and BT-corrected) for the three differentiated regions. These regions are split at stations 7 and 16 as a common framework, although the alternating flow patterns make this choice arguable. The main outcome is that, though the velocity fields were apparently quite similar, integrated transports present notable differences. Shelf-slope poleward flow observed from LADCP seems weaker than from geostrophy, southward flow across the passage is overestimated by geostrophy in winter but subestimated in summer. Also, northward flow west of the Galicia Bank in summer is much stronger as seen by LADCP. As presumed by the meridional velocity fields, transport estimates derived from BT-corrected geostrophy are strongly different from both LADCP or

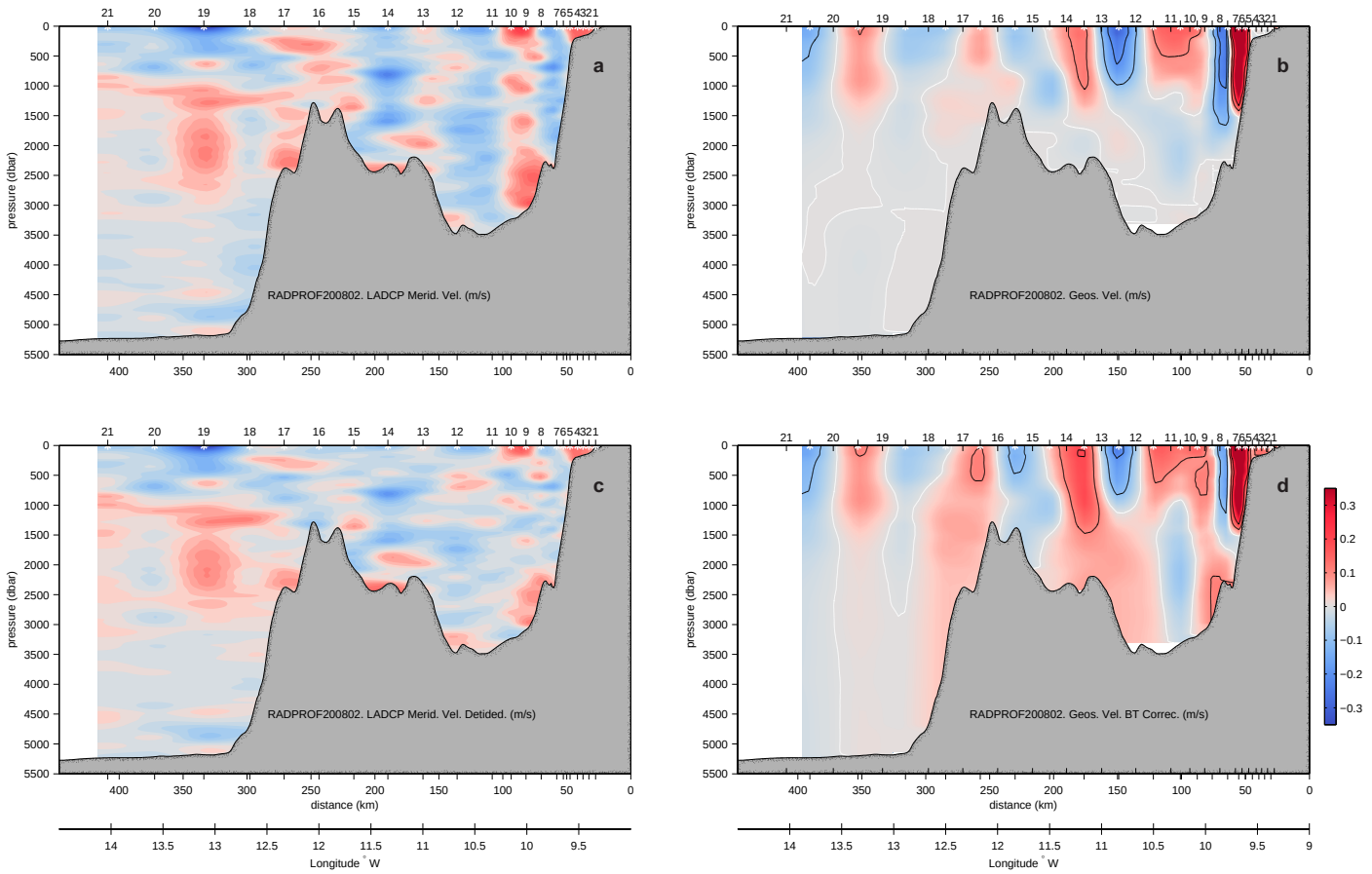

Figure 4.11: Meridional velocity field across the Finisterre section during RadProf200802 from (a) raw LADCP Record, (b) standard geostrophy assuming a reference level of no movement at $\gamma_n \sim 28.072\ \mathrm{kg\,m^{-3}}$, (c) LADCP after removal of modelled barotropic tide and (d) geostrophy corrected by LADCP bottom tracking. Contour lines of geostrophy fields are placed at 0.1 m/s.

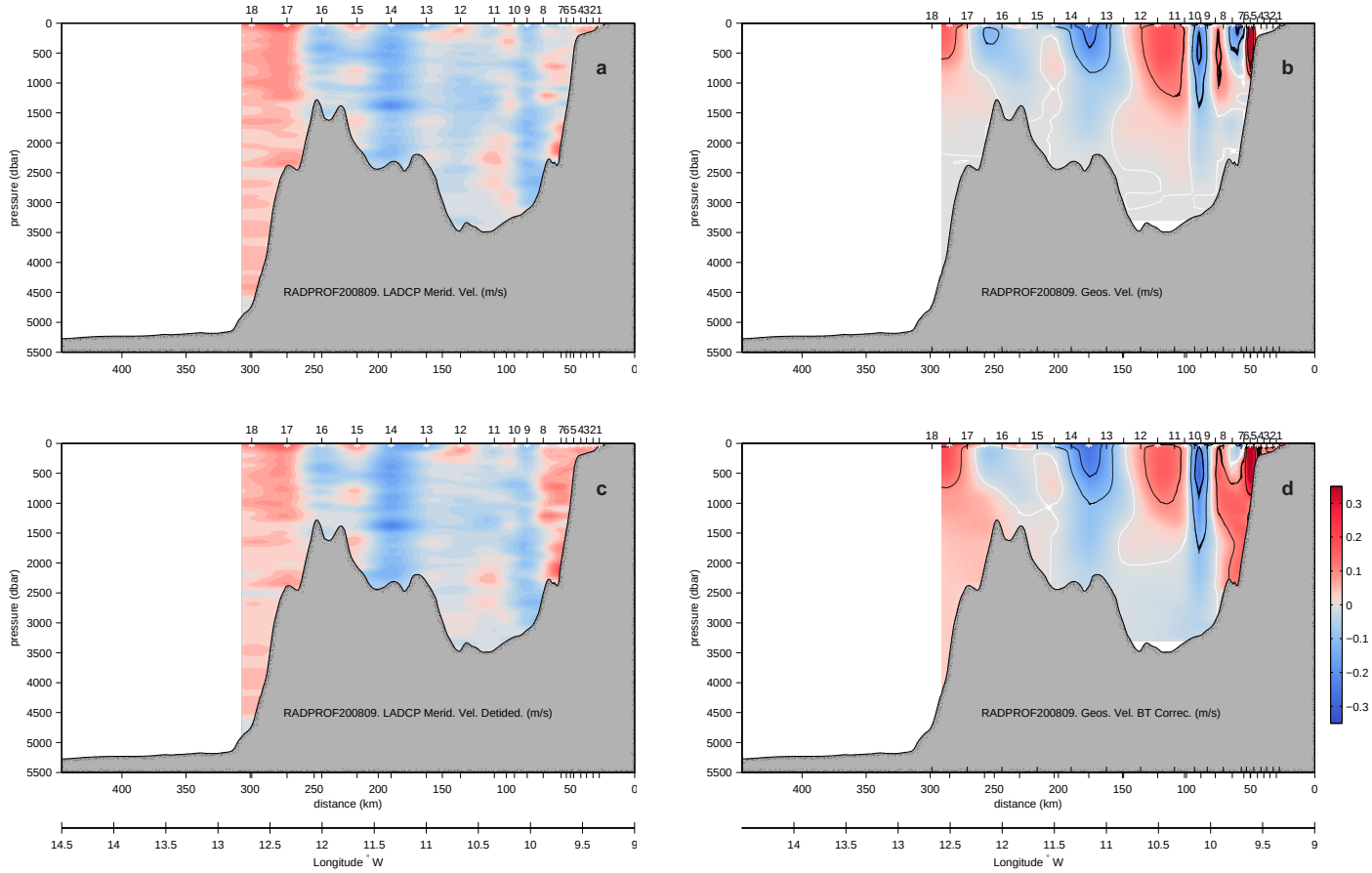

Figure 4.12: Same as Fig. 4.11 for RadProf200809 cruise.

standard geostrophy, even changing completely the sign of the transport for the passage in the winter cruise. We will discuss in Sect. 5.3 the possible sources of difference among the different approaches.

Splitting the section in open ocean and slope region about the mid of the passage (Fig. 4.14) integrates mesoscale features across the section providing a simplified view. Roughly, the shelf-slope transports a northward flow of the order of 1 Sv, a bit more in winter. The open ocean yields southwards flow of 2-3 Sv, stronger in summer.

Since the selection of a no-movement reference levels seems problematic, we will focus on the LADCP record to analyse the vertical structure of the transports (i.e. the flow of the different water masses). Figure 4.15 presents a vertical histogram of transports in the shelf-slope and open ocean for the two cruises.

Interesting features deduced from Fig. 4.15 are:

1. The shelf-slope northward mass transport in winter reaches down to 400 dbar and strengths towards the surface. In summer, on the contrary, flow is more constant across the water column extending down to 1500 dbar.

2. The bulk of the southwards transport across the section is structured as two maxima at the open ocean region, roughly at the interfaces between ENACW and MW and between MW and LSW. The depth of maximum transports appear shallower in the water column during summer ($\sim$600 and $\sim$1400 dbar vs $\sim$800 and $\sim$1600). The level of the core of MW is characterised by no overall net flow.

3. The weakening of southwards transport in winter is partially caused by a counterflow (northwards) at levels in the 2000-3000 m water column that is absent in summer.

As an overall summary, table 4.5 provide cumulative mass transports calculated for pressure intervals of 500 dbar and 3000 dbar to the bottom together with the geostrophic estimates. As stated above, mass transport across the Finisterre section from LADCP measurements showed a larger southward transport in summer (-2.2 Sv) than in winter (-1.3 Sv) with a larger southward mass transport at the open ocean (3 Sv) due to the southward transport of waters down to 2000 dbar and the northward transport of waters deeper than 2000 dbar during summer time. During winter, a more intense northward flow is observed across the slope region (1.3 Sv) in response to the northward transport of upper layers between 0-500 dbar (1 Sv) and deep waters between 2000-3000 dbar both in the slope (1.26 Sv) and open ocean (1.16 Sv). Southward transport (-0.8 Sv) at the slope region between 500-1500 dbar in winter (RadProf200802) and northward transport (1 Sv) in summer (RadProf200809) may indicate the detachment of the MW vein from the slope

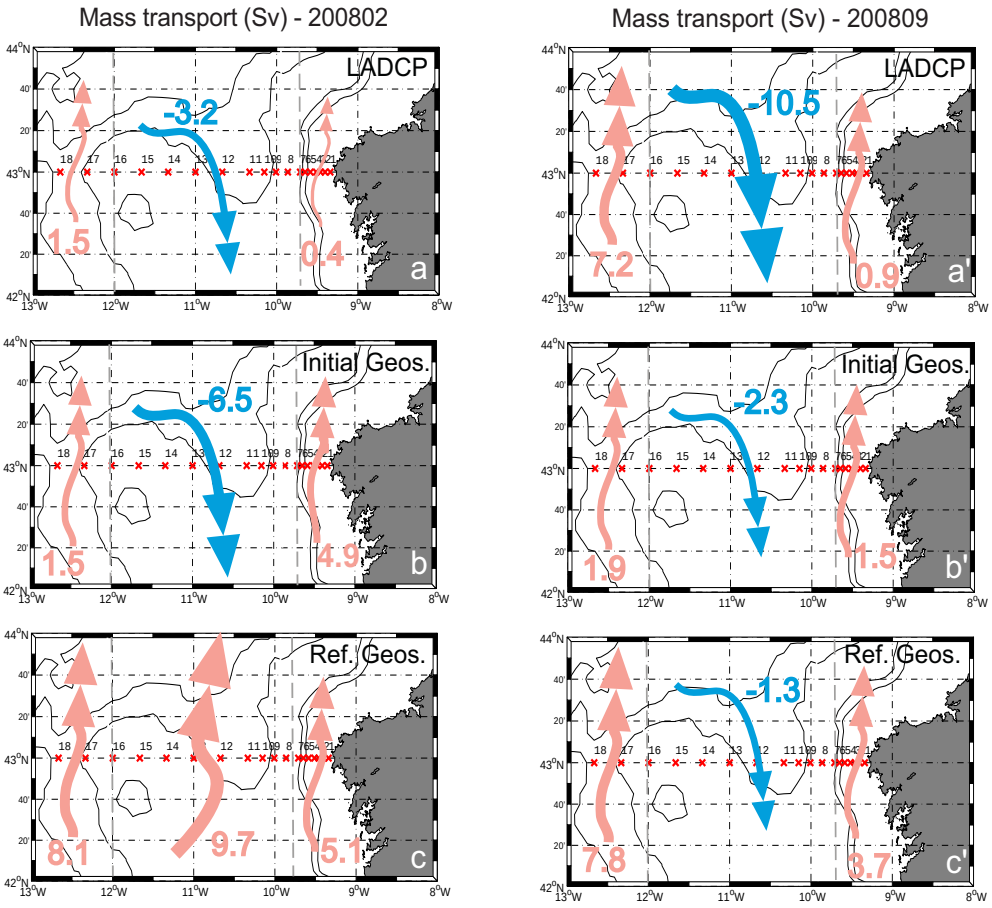

Figure 4.13: Vertically integrated mass transport (Sv) from LADCP measurements (a) standard geostrophy (b) and corrected geostrophy (c) across the Finisterre section during RadProf200802 RadProf200809

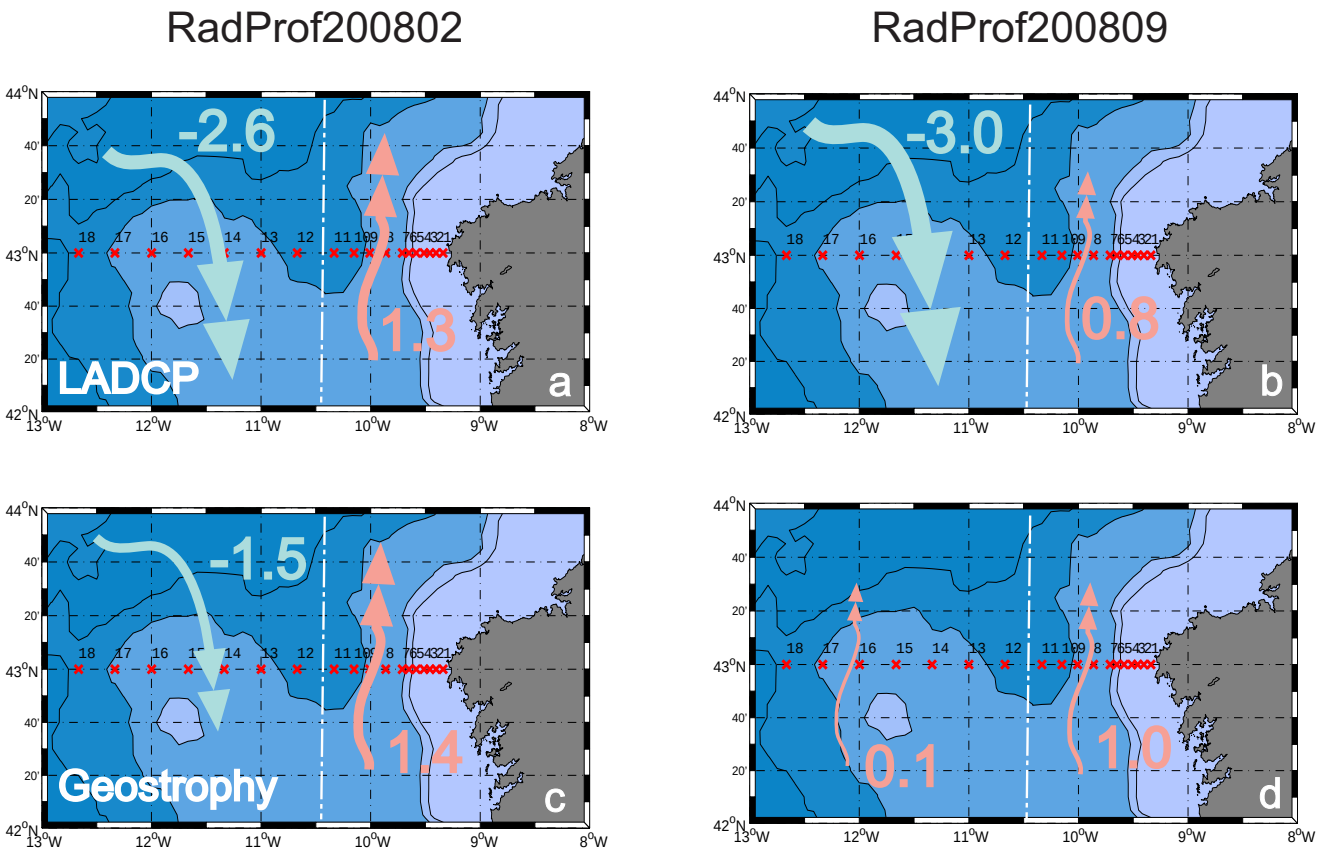

Figure 4.14: Total mass transport across the slope and open ocean regions from LADCP and geostrophy during RadProf200802 (a,c) and RadProf200809 (b,d). Red (blue) arrows indicate northward (southward) transport.

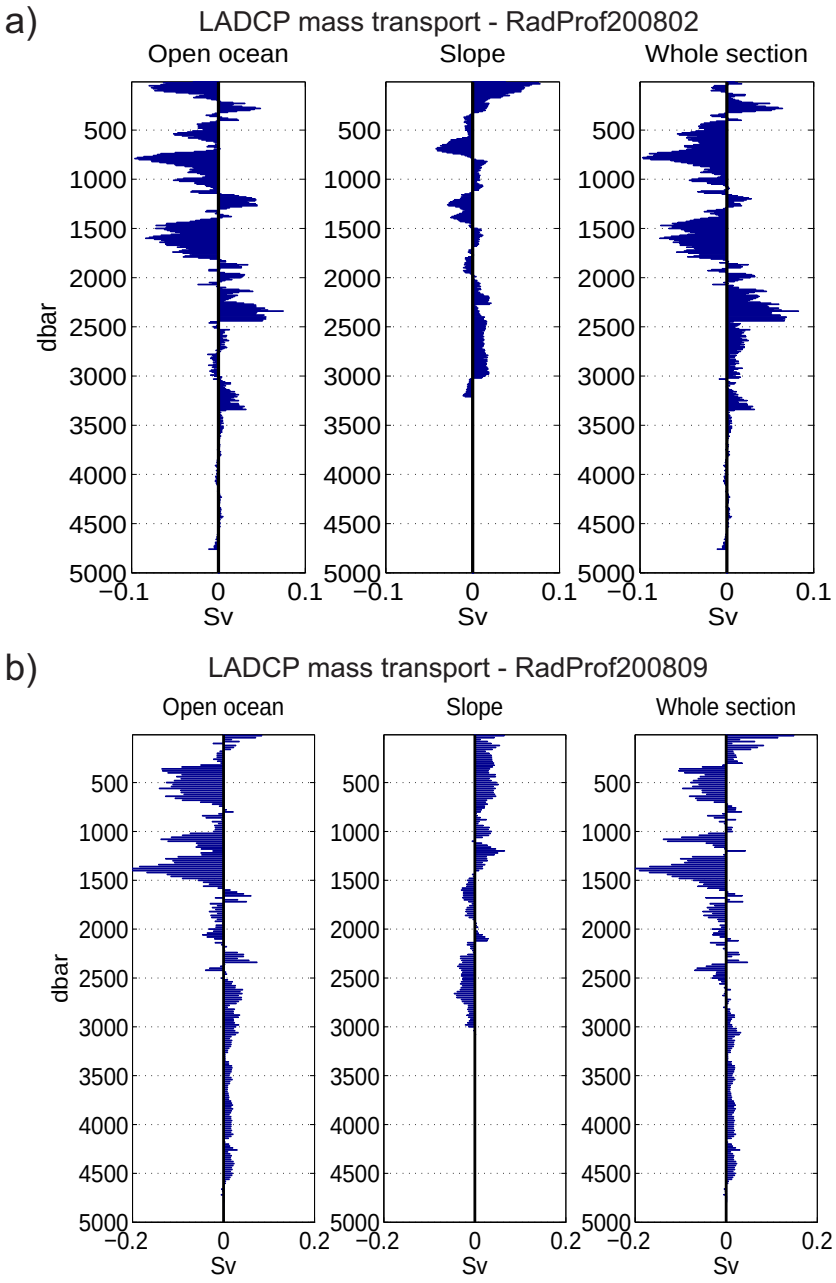

Figure 4.15: Mass transport (Sv) from LADCP measurements across the open ocean region, slope region and the whole Finisterre section during a) RadProf200802 and b) RadProf200809.

Mass transport (Sv)						
		RadProf200802			RadProf200809	
	Open ocean	Slope	Whole Sect.	Open ocean	Slope	Whole Sect.
P (dbar)	Detided LADCP					
0-500	-0.77	1.01	0.23	-0.89	0.95	0.05
500-1000	-1.88	-0.39	-2.27	-1.24	0.67	-0.56
1000-1500	-0.40	-0.44	-0.84	-2.65	0.48	-2.16
1500-2000	-1.31	-0.01	-1.33	-0.20	-0.36	-0.56
2000-3000	1.16	1.26	2.42	0.72	-0.93	-0.20
3000-bottom	0.59	-0.09	0.49	1.20	0.00	1.20
Total	-2.62	1.32	-1.29	-3.06	0.82	-2.24
Water mass	Initial geostrophy					
Upper layer surface – 27.162	-0.69	1.70	1.01	-0.15	0.00	-0.15
ENACW 27.162 – 27.38	-0.58	0.97	0.38	-0.36	0.54	0.18
UMW 27.38 – 27.62	-0.24	0.75	0.50	0.06	0.50	0.57
MW 27.62 – 27.82	-0.04	-0.12	-0.16	0.27	0.48	0.76
DMW 27.82 – 27.922	0.05	-0.85	-0.80	0.12	-0.15	-0.03
LSW 27.922 – 27.975	0.01	-0.62	-0.60	0.09	-0.21	-0.11
ENADW 27.975 – 28.0986	-0.05	-0.42	-0.47	0.05	-0.13	-0.08
Total	-1.55	1.40	-0.15	0.09	1.03	1.13

Table 4.5: Mass transports calculated from detided LADCP and geostrophy

in winter. Geostrophic transports indicate, in agreement with LADCP, that poleward flow at the slope reach deeper levels including MW in summer.

4.3.3 The 43°N, 11°W mooring line

Time series of the Finisterre currentmeter mooring at 43°N, 11°W (station 13 on Figs. 4.11 and 4.12) provide continuous measurements of current velocities at the ENACW (350 dbar), MW (1000 dbar) and LSW (1800 dbar) levels. Though this is only a specific position across the section it provide an independent estimate of the strength and sense of the flow, and hence on the transports. In this sense meridional volume transport can be computed across a slice bounded by stations 12 and 14 ($\sim$ 75 km apart) by linear interpolation of currents at the three levels (Fig. 4.16).

Time series of meridional current meter velocity showed a mainly barotropic circulation at this location during September when the three water masses flow southward. In winter, volume transport is dominated by that of LSW at least until mid-February whereas ENACW transport appear to dominate the southward transport in late September. Averaged transports showed a net southward volume transport of 0.5 Sv during February and 5.4 Sv during September. This much larger southward transport in summer is in agreement to LADCP record. Moreover the northward flow at LSW level around mid-February is well captured by the LADCP record (Fig. 4.11a).

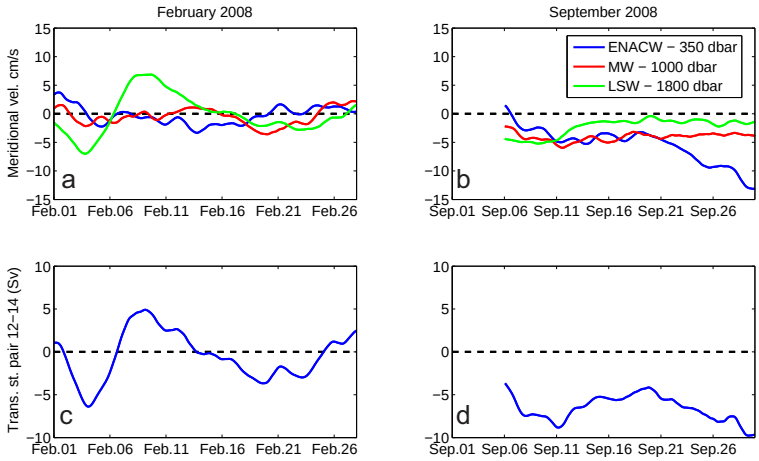

Figure 4.16: Time series of meridional velocity in cm/s from the Finisterre mooring at 43°N, 11°W during a) February 2008 and b) September 2008 with currentmeters at 350 dbar (ENACW, blue), 1000 dbar (MW, red) and 1800 dbar (LSW, green). Depth-integrated meridional transports between stations 12 and 14 ($\sim$ 75 km spaced) during (c)February 2008 and (d) September 2008.

5 Discussion

5.1 The seasonal signature at depth

As introduced in Chapter 2, the 43° N section (Finisterre section, Fig. 2.1a,b) is located in the north-east limb of the North Atlantic subtropical gyre, an area of very weak circulation. Covering ~ 200 nm from the continental shelf to the open ocean and sampling the whole water column, its semiannual monitoring has provided the most detailed view of seasonality at all levels in the area to date.

5.1.1 Origin and processes involved

Changes in the thermohaline properties at the sampling site may be caused by changes in the intrinsic properties of water masses and/or by changes in the circulation patterns (altering the water masses geographical distribution). It is however difficult to disentangle among them as the processes involved in the formation/transformation of water masses are intertwined with those altering the overall dynamics. As the water masses spread further from their sources towards the sampling site, it is more unlikely to discern a signature of shifts remotely imprinted on water properties, and even less any kind of seasonal swing. In the present Sect. we will discuss the observed seasonality signatures in our dataset in the context of the known oceanographic processes that cause seasonality in the North Atlantic eastern boundary.

5.1.1.1 Large scale circulation: the subtropical gyre

Our first-glance overall view indicates a more intense presence of northern origin waters in summertime all along the open ocean region (colder and less saline waters at all depths). Such enhanced advection of subpolar waters during summer suggests large-scale fluctuations of the subtropical gyre (in position and/or strength). *Chidichimo et al.* (2010) and *Kanzow et al.* (2010) studied the seasonality of transports at the subtropics, downstream of our sampling site, by means of time series measured by the RAPID-MOCHA array (26.5° N). They concluded that the major contribution of seasonality to the meridional overturning circulation is precisely the seasonality at the eastern boundary, characterized by a maximum southward transport in spring (between April–May). Other works studying the seasonal variability of the Canary Current indicate in agreement an enhancement of southwards flow in early spring and weakening and even reversal (poleward flows) in late summer–autumn at some levels (*Machin et al.*, 2010; *Mason et al.*, 2011). These changes in the subtropics are connected with seasonal variations in the shape of the subtropical gyre, which has a larger zonal (east–west) and smaller meridional (north–south) extents in summer than in winter (*Stramma & Siedler*, 1988) (see their Fig. 3). Upstream of our sampling site, the North Atlantic Current also appears to suffer seasonality in its transport. Specifically, *Yaremchuk et al.* (2001) studied the circulation of the upper 1000 m in the 40–55° N and 20–40° W region finding among other results that the outflow leaving the eastern side of their study box is maximum around April. Therefore, known seasonality of the subtropical gyre, both upstream (NAC eastwards leakage) and downstream (Canary Current system), points to an enhanced flow in spring and southward displacement of the overall subtropical gyre system in summer. These findings are consistent with the enhanced presence of northern waters in summertime at our sampling site.

The main forcing mechanism capable of altering the circulation of an oceanic basin is the seasonality in the wind stress and wind stress curl, which causes variability in Ekman transports (*Stramma & Isemer*, 1988) and rearrangements of the density field which trigger the generation of Rossby waves that later propagate westwards into the basin (*Krauss & Wuebber*, 1982). Actually, the subtropical gyre of the North Atlantic, particularly its eastern boundary, has been documented to be subject to large-scale seasonal variability in the wind stress curl (*Bakun & Nelson*, 1991, and Fig. 5.1).

Literature provides some clues in order to assess the role of propagating Rossby waves vs. Ekman transport in the observed seasonality at depth in our section, but a firm conclusion is difficult to achieve. *Hirschi et al.* (2007) studied the effect of seasonality in wind forcing on the meridional overturning circulation, stating that southwards of about 36° N the thermal wind contribution (variations of the density field) dominates the seasonal cycle while northwards of this latitude the major contribution is due to Ekman transport.

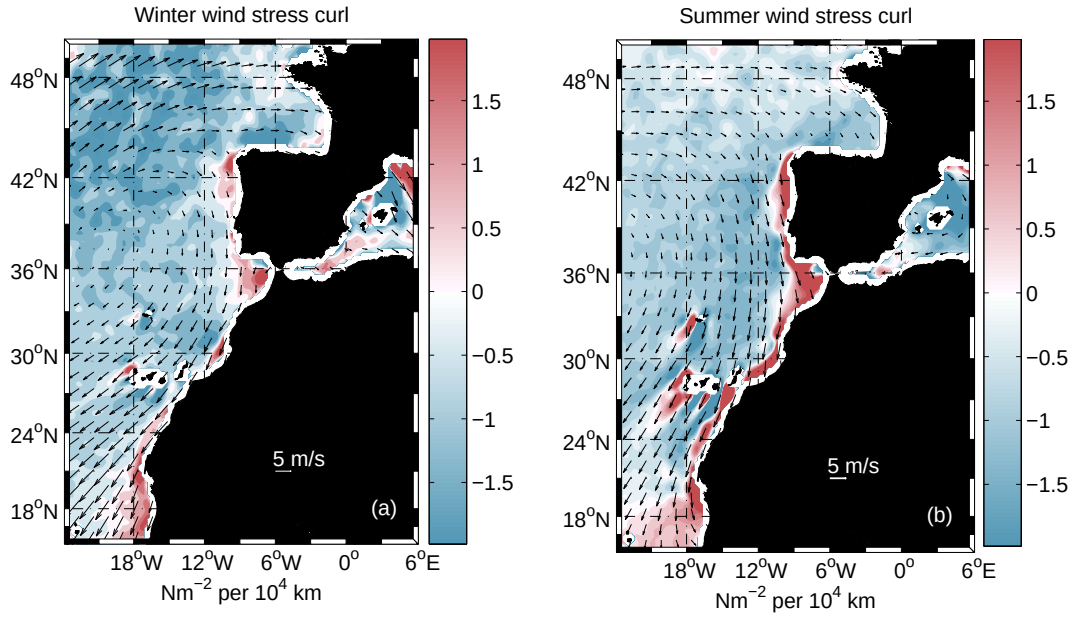

Figure 5.1: **(a)** Winter and **(b)** summer wind stress curl in the North Atlantic. Arrows show the wind velocity field in both seasons

In agreement, *Osychny & Cornillon* (2004) indicate from sea surface height (SSH) signatures that northwards of 41° N there is almost negligible energy at annual or shorter scales, being concentrated at periods longer than 1.5 yr. From these works, propagating Rossby waves at our 43° N section should not be expected to be the main contributor to the seasonality signatures at depth. On the other hand, *Bray* (1982) did attribute observational evidence of seasonal variability below the thermocline in the Bay of Biscay to the westward reflection of a seasonally wind-forced large-scale Rossby wave, and *Friocourt et al.* (2008a) linked seasonal flow reversals of modelled slope currents to annual Rossby waves. As a matter of comparison, Fig. 5.2 provides wind stress curl annual anomalies obtained from the SCOW (Scatterometer Climatology of Ocean Winds) climatology (*Risien & Chelton*, 2008) at (i) the RAPID (Rapid Climate Change) /MOCHA (Meridional Overturning Circulation and Heat Transport Array) region at 26.5° N (where *Kanzow et al.* (2010) show that a wind stress curl forced Rossby wave model successfully accounts for the observed seasonality) and (ii) off Finisterre at 43° N. Wind stress curl anomaly that would trigger Rossby waves is 2–3 times weaker in our region.

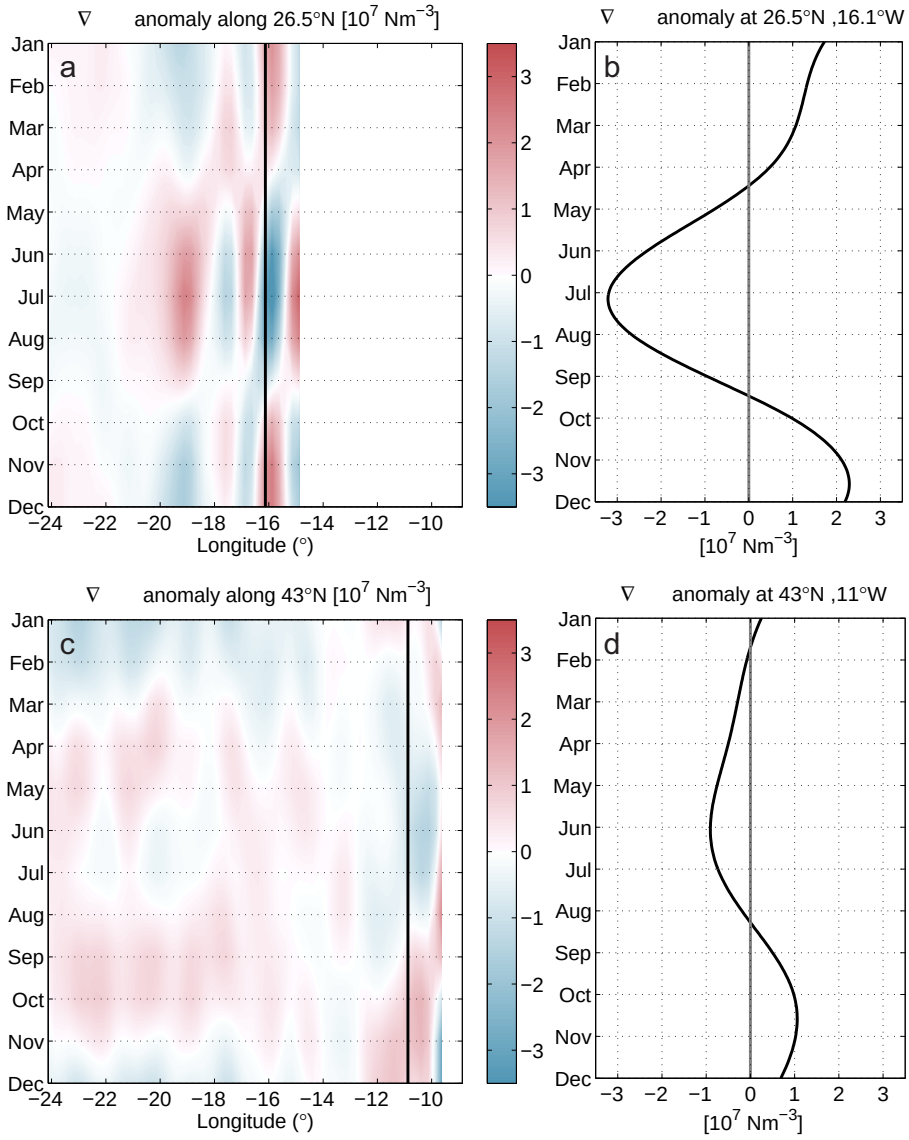

Figure 5.2: Wind stress curl anomaly from SCOW climatology at **(a)** 26.5° N, **(c)** 43° N, and extracted for **(b)** 26.5° N, 16.125° W and **(d)** 43° N, 10.875° W

5.1.1.2 Continental slope dynamics: upwelling, the Iberian Poleward Current and MW spreading

Shelf-slope dynamics at the western Iberian margin are subject to specific processes, some exhibiting strong seasonal character, that interact with the large-scale subtropical gyre seasonality. Northerly winds during the summer months cause widespread upwelling along the shelf (*Wooster et al.*, 1976), while south-westerly winds in wintertime induce onshore Ekman transport. This upwelling/downwelling regime interacts with the slope dynamics characterized by the presence of the Iberian Poleward Current (IPC), a poleward flow driven by the meridional density gradient that carries warmer and saltier waters of southern origin (*Haynes & Barton*, 1990; *Frouin et al.*, 1990; *Pingree & Le Cann*, 1990). The IPC is thought be a permanent feature although it reaches a maximum development in wintertime after the strengthening of the meridional density gradients in late fall and winter (*Peliz et al.*, 2005), aided by downwelling favourable winds, which adds up to a fifth of the total transport (*Frouin et al.*, 1990). On the contrary, during the summer the IPC is not observed at the sea surface and it is thought to be displaced offshore and to persist below the surface (*Peliz et al.*, 2005; *Ruiz-Villarreal et al.*, 2006).

The effect of the upwelling/downwelling cycle on the central waters is reflected in our dataset as enhanced cooling/freshening on the slope in summertime, down to 600 dbar, caused by heave (Fig. 4.2b, d). The minor warming and salt increase at isopycnal levels on the slope in summertime is a striking signature (i.e. the 27.15 isoneutral is saltier and warmer in summertime but it lies much deeper). A rather speculative explanation for the presence of such central waters of southern origin on the slope in summertime may be linked to the presence of the deeper and offshore-displaced IPC pointed out by *Peliz et al.* (2005).

Below central waters, the seasonality at the level of MW appears a robust feature with contrasting character on the slope (more presence in summertime) and at the open ocean (more presence in wintertime). The MW spreading from the Gulf of Cádiz formation area has been widely studied (e.g. *Iorga & Lozier*, 1999a,b; *Bower et al.*, 2002), but information about its seasonality is still scarce and relies on reduced datasets. *Ambar et al.* (1999) reported insights of seasonality of the MW spreading around the Portimao Canyon (off the southern coast of Portugal, 37° N) and off the north-west coast of Portugal at about 41° N, respectively from XBT lines and year-long current meter moorings between July 1993 and May 1994. Their main outcomes were a broader signature of MW in wintertime (i.e. more irregular and extending further offshore) and a cycle in temperature with notable offset: warming phases respectively at Portimao and 41° N from September–January and June–November (in agreement with our findings). *Varela et al.* (2005) also found a more intense MW signature in spring–summer on the slope at 42° N from a year-long weekly hydrostation between May 2000 and April 2001.

The IPC and the upwelling/downwelling cycle interacts with the dynamics of the Mediterranean water spreading at depth, and it has been proposed that poleward flows connect with the levels of MW (e.g. *Torres & Barton*, 2006). *Lafuente et al.* (2008) provided indications of the coupling of MW and the upper slope dynamics while giving further insights of seasonality of the upper branch of the MW off north-western Iberia. From a 4-month record in the upwelling season, of two mooring lines located on the slope slightly northwards of 43° N, they concluded that during the settlement of a wind-induced upwelling the MW behaviour was consistent with a combination of a shoreward and upwards displacement of its core. Such result is in agreement with our observations of salt increase by heave down to 800 dbar on the slope. Moreover, we see that the along-slope vein gets strongly reinforced in summer down to its lower core with the presence of purer Mediterranean water (i.e. warmer and saltier on isopycnals) while the density structure remains. From a historical dataset of current meters, *Huthnance et al.* (2002) inferred flow reversals on the slope at ENACW and MW levels around February–March, an observation that also matches with the loss of presence of MW in winter on the slope.

Daniault et al. (1994) and *Mazé et al.* (1997) provided a larger-scale view of MW spreading along the Iberian margin and outer ocean, finding a bifurcation of the coastal trapped MW tongue south of the Galicia Bank at around 42° N. They proposed an anticyclonic circulation of MW around the Bank to later re-entry in the Iberia Basin, and suggested that the bifurcation may exhibit strong variability, though not necessarily seasonal. Their research was mostly supported by Bord-EST 3 cruise, taking place around May but "at a time when the near-surface winter regime was still dominant". Our results indicate that this pattern indeed corresponds to the typical hydrographical structure during wintertime. The diminished presence of MW in summertime at the outer region (colder and fresher at isopycnal levels) also implies a change in density structure (shoaling of isopycnals around $\gamma^n \sim 27.8$ making waters corresponding to the lower core of MW thinner). The pattern is consistent with the combination of the large-scale summer strengthening of the subtropical gyre and the reinforcement of MW along-slope vein.

5.1.1.3 Water masses formation at sources

5.1.1.3.1 ENACW mode water Circulation and thermohaline properties of the central water east of the mid-Atlantic Ridge between 39° N and 54° N were analysed by *Pollard et al.* (1996) who observed that most of the transport associated with the North Atlantic Current (NAC) west of 20° W flows northwards (20 Sv) but that 10 Sv recirculate anticyclonically towards the west of the Iberian Peninsula, within the region south of the North Atlantic Current. *Mazé et al.* (1997) determined that the eastward flow towards the Iberian Margin at 12.5° W was of the order of 2 Sv from 38° N to 43° N.

The majority of ENACW water is formed by deep winter convection in a region north of 45° N from where it is subducted and advected southwards, being the main ventilation region of mode waters in the North Atlantic. The annual renewal of these mode waters was studied in detail from hydrography data and air–sea flux budgets (e.g. *Paillet & Arhan*, 1996a,b), the region at the Finisterre section being a frontal zone marked by an abrupt meridional shoaling of winter mixed layers (between 40° N and 45° N). *Gaillard et al.* (2005) conducted specific studies west of the Finisterre section (POMME–Multidisciplinary Meso Scale Ocean Program–area) finding a relevant contribution of the mesoscale activity in the net subduction rate of mode waters.

Pérez et al. (2000) described that the thermohaline properties of regional ENACW exhibit strong decadal variability related to large-scale climatic patterns affecting air–sea fluxes variability at the areas of formation. On the contrary, at seasonal timescales *Pérez et al.* (1995) found "a gradual increase of temperature and salinity from spring to late autumn" both at the open ocean and on the shelf without any insights of seasonality of salinity at ENACW isopycnal level. In agreement with their results, we observe colder and fresher waters in summertime due to the uplifting of ENACW isopycnal levels. Such a cycle can be associated, besides the dynamic response to the upwelling cycle, with a greater thickness of the well-mixed new mode waters in spring, just after the end of entrainment phase and during the subduction period (*Marshall et al.*, 1993).

5.1.1.3.2 MW There is even evidence of seasonality of MW right at its origin. Recent observations of the Mediterranean outflow water in the Strait of Gibraltar (*Lafuente et al.*, 2007) showed the existence of a seasonal cycle with warmer and lighter water leaving the Mediterranean Sea in winter, and cooler and denser waters in spring and summer (exhibiting also a maximum in transport) with amplitudes $\Delta T \sim 0.05\,^{\circ}\mathrm{C}$ and $\Delta\sigma \sim 0.015\,\mathrm{kg\,m^{-3}}$. *Fusco et al.* (2008) reported seasonality in the Gulf of Cádiz with a salinity maximum around May–June, apparently in agreement with the maximum outflow around spring. Following the work of *Daniault et al.* (1994), the amount of pure Mediterranean outflow waters present in the MW vein around Finisterre is about a fifth ($\sim 20\,\%$, see their Fig. 14). Therefore seasonality of MW at source cannot be the cause of the actual observed changes but only of a minor fraction.

5.1.2 Results from circulation models

Some modelling exercises within the area have focused on seasonality either at the boundary or offshore, and from surface to mid-depths, providing a non-homogeneous set of outcomes. For example, a large-scale model of MW spreading used by *Filyushkin et al.*

(2008) indicated pronounced seasonality in the transport through the Strait of Gibraltar but did not find a noticeable seasonal signature in salinity distributions of MW across the North Atlantic. A more regional model focused on the western Iberian margin provided by *Coelho et al.* (2002) succeeded in reproducing the general pattern and seasonal variations of upper circulation, including upwelling during the summer, a winter surface poleward current over the shelf and a permanent year-round undercurrent transporting MW along the Portuguese and Spanish slopes. The model was also able to account for notable offshore export of MW at 41–42° N, in agreement with observations, but it did not find a clear difference between winter and summer at MW levels.

Among modelling efforts that suggest notable seasonality at depth, stands the work of *Friocourt et al.* (2007). This study, supported by a regional model including western Iberia and the Bay of Biscay, simulates a strong baroclinic slope current at 42° N with a complex structure having cores at different levels and seasonal flow reversals at all depths. Salinity distribution in the core of MW indicates the presence of two flows: a narrow jet trapped on the slope, and a wider tongue flowing intermittently north-westwards toward the Galicia Bank. The position of the offshore MW tongue varies throughout the year, remaining in the vicinity of the slope from July to October and starting to move offshore around November, while the slope jet weakens and even reverses (i.e. flows equatorward) from November to January. *Friocourt et al.* (2008a) elaborated further on the seasonality of the slope current showing that reversals of the deeper slope currents are at least partly forced by seasonal changes in the flow upstream of the slope-current system. *Slater* (2003) provided, from the large-scale OCCAM (Ocean Circulation and Climate Advanced Modelling) model, a pretty similar outcome showing boundary flow at MW depths directed northward year-round but displacing offshore in winter when a southward flow on the slope develops below 300 m. Both descriptions agree with our results, although we can not infer from our dataset whether the along slope MW vein comes to reverse in winter or simply weakens.

5.1.3 Quantitative comparison with other regions of the north-east Atlantic Ocean

As pointed out in the preceding discussion sections, there are many different dynamical processes that may imprint seasonality on to the deep ocean. However, many of the reviewed works only provide qualitative insights of seasonality or quantitative fluctuations of properties in a limited time frame, and rarely estimates of seasonal amplitude. All the available data about seasonal estimates collected in the reviewed literature have been joined with the seasonal isobaric changes found in our section, both in the slope and outer

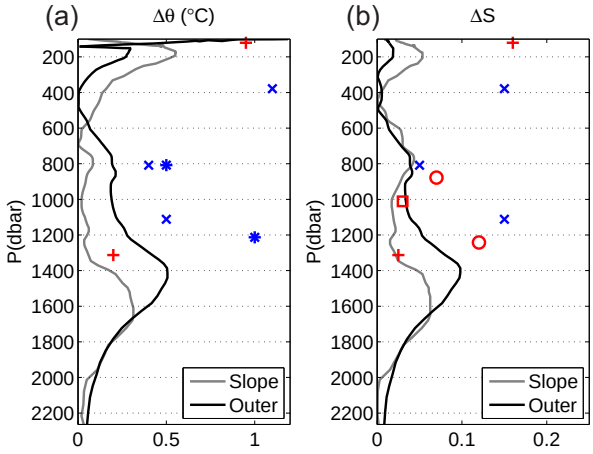

Figure 5.3: **(a)** Potential temperature and **(b)** salinity isobaric changes in the slope (grey line) and outer ocean (black line) superimposed by seasonal anomalies found by *Chidichimo et al.* (2010) (+), *Machin et al.* (2010) (○), *Ambar et al.* (1999) (∗), *Varela et al.* (2005) (×) and *Bray* (1982) (□).

region (black lines in Fig. 4.2) in order to make a quantitative comparison between them (see Fig. 5.3).

Chidichimo et al. (2010) estimated the seasonal amplitude in potential temperature and salinity from the EBH(eastern boundary)–RAPID mooring array (4 yr continuous record) at the subtropical North Atlantic eastern boundary along 26.5° N, finding anomalies of 0.95°C, 0.16 at 120 m and 0.2°C, 0.025 at 1300 dbar. These values are in accord with our temperature seasonal anomalies at the outer upper ocean (see Fig. 5.3a) and temperature and salinity anomalies of intermediate layers in the shelf-slope region (0.14°C and 0.03 along 27.8). A little to the north, seasonality estimated by *Machin et al.* (2010) from the 9 yr continuous record of EBC4 mooring at 28°46′ N, 13°28′ W in the Lanzarote Passage (Canary Basin), was ∼0.07 at 870 m and ∼0.12 at 1230 m in salinity from July–October and from November–December, when maximum salinity was found in both levels. Off the northern coast of Portugal, from a specific mooring at 41° N, 9°44′ W, *Ambar et al.* (1999) also observed a shift from summer to winter of 0.5°C at 800 m and 1°C at 1000 m, between July 1993 and May 1994. In the Galician shelf/slope, a shift was also observed from summer to winter in a year-long series, from May 2000 to April 2001, of weekly hydrographical profiles at fixed location 42.13° N, 9.5° W by *Varela et al.* (2005): they found seasonal shifts in temperature and salinity of about 1.1°C and 0.15 at $ENACW_{sp}$ levels (300–450 m), 0.4°C and 0.05 at the upper MW (∼ 800 m) and 0.5°C and 0.15 in the lower MW (∼ 1100 m) . In these cases, seasonal estimates are, in general, higher than those encountered in our section. *Bray* (1982) also estimated a

seasonal amplitude of 0.03 in salinity at ~ 1000 m, from a series of 11 cruises over 3 yr in the Bay of Biscay area (2–20°W, 42–52°N), in concordance with our results (~ 0.02–0.03 along 27.6–27.7 between 900–1100 dbar). Note that red points in Fig. 5.3 represent observations spanning several years (from 3 to 9 yr), while those in blue are based on 1 yr sampling. We would like to highlight here the importance of establishing continuous and long time series of ocean properties in order to get a statistically significant seasonal cycle.

5.1.4 Capability of Argo floats to resolve seasonality in Finisterre

It is interesting to determine whether the spatio-temporal coverage of the Argo fleet is enough to resolve the seasonal signature as our in situ dataset does. We used the data viewer interface provided by the Argo website [1] to retrieve the winter (January/February/-March) and summer (June/July/August) salinity maps averaged for the Mediterranean water influence levels (1000–1250 dbar) in the region 30–50°N, 0–20°W (Fig 5.4).

It appears difficult to evidence a recurrent seasonal pattern from such horizontal sections. The inspection of the available profiles (figures not shown) that support each of these interpolated field evidences that there may be large areas without profiles, specially the slope region, which is strongly undersampled (currents are stronger at these areas so floats are quickly advected). Nevertheless, we have computed the summer minus winter anomaly map (Fig. 5.5). The overall general view indicates less MW content in the open ocean of western Iberia in summertime (out to 16° W), which is consistent with our results from the section, and a higher MW content patch at the northwestern corner, which could be interpreted in a very speculative manner as a signature of enhanced northwards MW slope flow in summertime. However, the patchy character of the fields raises suspicions on its representativeness and the increase of MW in summertime west of 16°W seems quite odd.

Fig. 5.6 provides the time series from interpolated fields at some locations in the eastern boundary along 42.5° N. Though there are periods when there appears to be a seasonally oscillating behavior, the time series yields much less clear signs of seasonality than the time series derived from the hydrographical section do. In summary, we do not feel that we can draw firm conclusions about seasonality of the western Iberian margin hydrography from the Argo buoys, especially at the slope. Their coverage is not enough to capture the seasonal changes in the whole water column; the continuous repetition of the hydrographical section is becoming worthwhile for the study of the regional deep oceanography in the western Iberia at seasonal timescales.

[1] `http://www.argo.ucsd.edu/index.html`

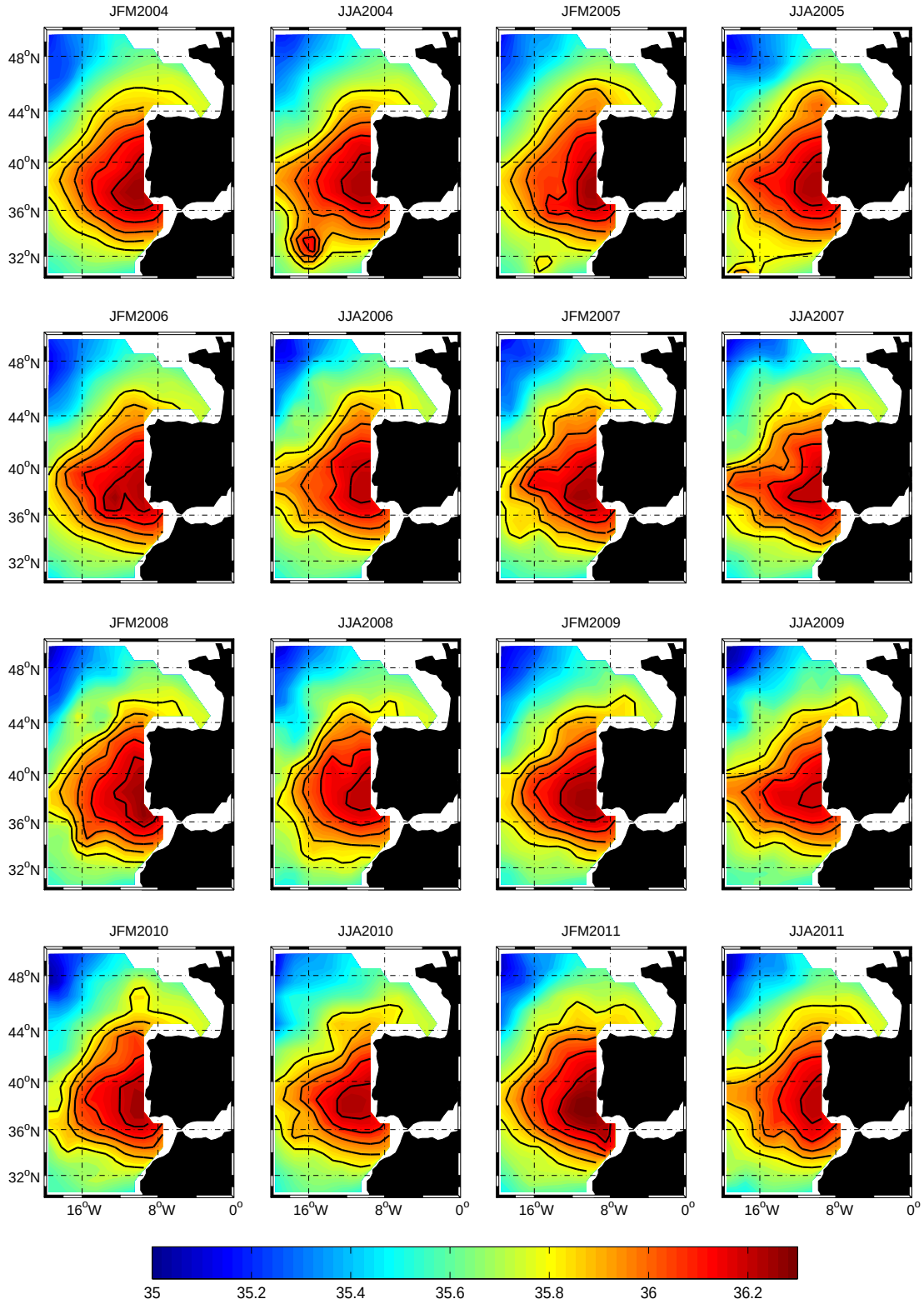

Figure 5.4: Winter (JFM) and summer (JJA) salinity fields at 1000–1250 dbar level from Argo floats for the period 2004–2011. Black contours are plotted from 35.8 to 36.2 every 0.1.

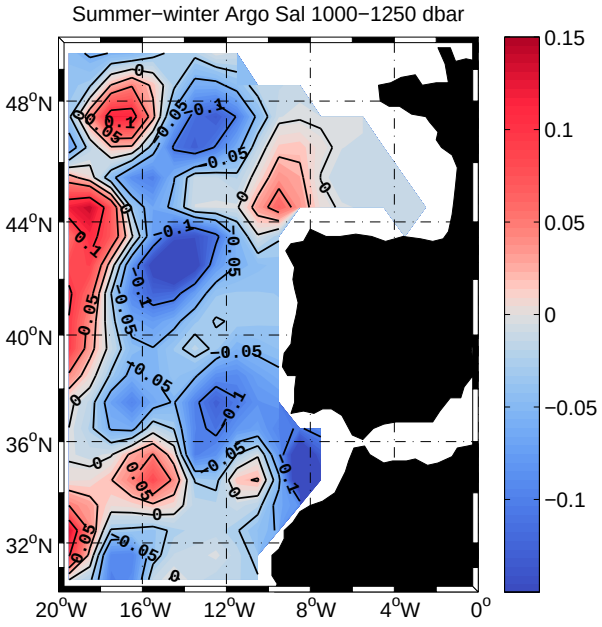

Figure 5.5: Summer (JJA)–winter (JFM) average salinity field at 1000-1250 dbar level from Argo floats for the period 2004–2011

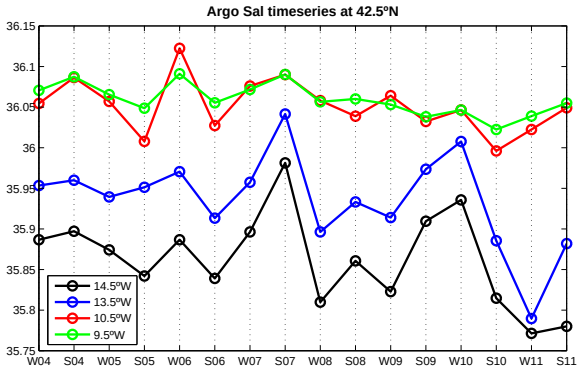

Figure 5.6: Time series of the salinity field along the 42.5° N section from the interpolated field at 1000–1250 dbar level from Argo floats for the period 2004–2011, at different locations in the slope (9.5° W and 10.5° W) and the outer ocean region west of the Galicia Bank (13.5° W and 14.5° W)

5.2 North Atlantic forcing driving interannual changes

The monitoring programme along the Finisterre section has provided a detailed view of interannual variability during the 2003-2013 period. The variability is the result of a complex combination of changes in large scale advective patterns, the intrinsic properties of water masses at their formation areas and local processes. The coherent response during specific years across large parts of the water column suggests an influence of the large-scale circulation pattern. In this section we discuss the causes of the observed coherent variability in relationship with the present understanding of North Atlantic circulation.

5.2.1 Climatic indexes and large-scale circulation of the North Atlantic

The North Atlantic Oscillation (NAO) is a leading pattern of weather and climate variability over the Northern Hemisphere strongly affecting the ocean through changes in heat content, gyre dynamics and deep water formation (*Hurrell & Deser*, 2010). During a negative phase of the NAO, the Labrador Current is enhanced bringing more fresh water into the subtropics, and the northward penetration of Mediterranean Water in the eastern North Atlantic also increases, there is southward displacement of the Subpolar Front in the western North Atlantic basin and the advection of more warm/salty subtropical water towards the northeastern North Atlantic (*Eden & Willebrand*, 2001; *Núñez Riboni et al.*, 2012). A high positive NAO phase is associated with the strengthening and eastward expansion of the Subpolar Gyre (SPG) bringing cooler, fresher conditions to the eastern region (*Sarafanov*, 2009). Figure 5.7 shows an scheme of North Atlantic circulation changes during positive and negative NAO phases.

Strong and rapid shifts in the winter NAO index may cause similar effects in the North Atlantic Ocean circulation as a long period of sustained NAO index (*Chaudhuri et al.*, 2011). For example, the circulation of the North Atlantic subpolar gyre appears to have weakened in response to a large shift in the NAO from a period of very high to a very low index in winter 1996 (*Häkkinen & Rhines*, 2004).

The data presented here indicate that the temperature and salinity in the North Atlantic eastern boundary is responsive to extreme states of the NAO. In 2010, a low winter NAO index was followed by a large increase of temperature and salinity of almost the whole water column in 2011. Years with a high positive winter NAO index, such as 2007-2008 (high positive) and 2012 (very high positive) were followed by water mass property changes of the opposite sense; cooling/freshening across much of the water column. Note that changes associated with high positive NAO events were due to heave and isopycnal

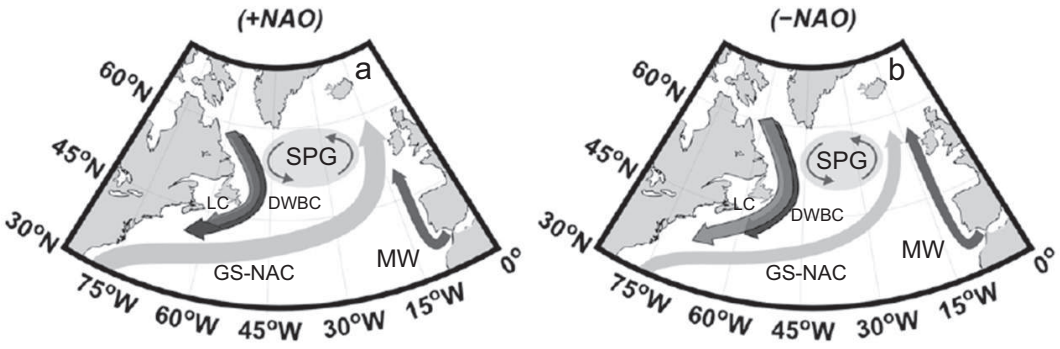

Figure 5.7: Schematic changes of the North Atlantic basin circulation during (a) positive and (b) negative NAO phases modified from *Chaudhuri et al.* (2011). LC: Labrador Current (upper 1000 m); DWBC: Deep Western Boundary Current ($>$ 1000 m); GS-NAC: Gulf Stream-North Atlantic Current; SPG: Subpolar Gyre; MW: Mediterranean Water (500-1500 m). Thick (thin) lines mean enhanced (diminished) associated transport.

change (sinking of isopycnals) while changes after the high negative NAO only involve isopycnal change (Fig. 4.9). We do not know at this stage whether this may be a typical behaviour of large negative/positive NAO years.

It has been shown that the strength and extent of the subpolar gyre can have a profound influence on the water mass properties of the subpolar gyre (*Hàtún et al.*, 2005; *Häkkinen & Rhines*, 2009). An index of the strength of the gyre circulation has been developed and shown to be only indirectly related to the NAO index (*Häkkinen et al.*, 2011a,b, 2013). The subpolar gyre index is reproduced with the NAO winter index in Fig. 5.8 for the period 1993-2012. There is no clear relationship between the SPG index and variations in water mass properties at interannual scales in our mid-latitude section.

In summary, the time series presented here reflect a local oceanic response induced by the NAO. The influence is characterized by the presence of more cool/fresh water from the northwestern North Atlantic one year after a high positive NAO index year, and more intrusion of subtropical waters from the south one year after a strong negative NAO index year. The results provide more evidence of the role of the NAO in driving rapid changes in the deep ocean as well as in surface waters.

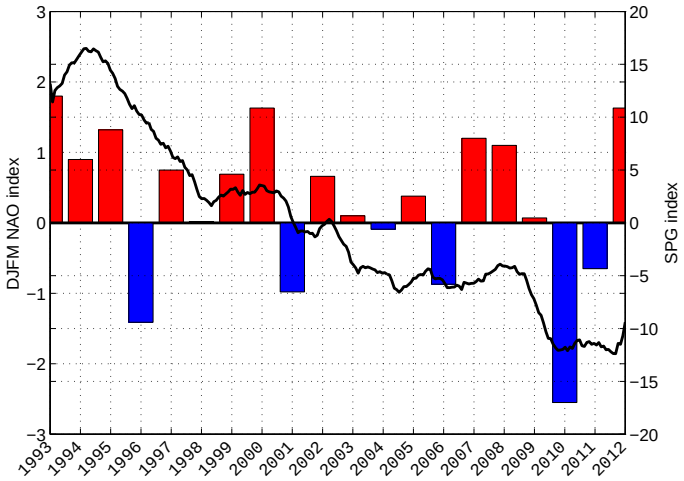

Figure 5.8: Winter(December-March) Hurrell NAO index with bars (red:positive NAO years; blue: negative NAO years), obtained as the first principal component of the winter SLP from `climatedataguide.ucar.edu/climate-data/hurrell-north-atlantic-oscillation-nao-index-pc-based` (*Hurrell & NCAR Staff*, 2014). SPG index obtained as the first principal component of SSH (*Häkkinen et al.*, 2013).

5.2.2 Changes in the main water masses

Besides causing changes in advective patterns (and not unconnected with these), large scale atmospheric variability conditions the formation of different water masses from modal to deep waters at their source areas. Next we discuss the variability observed in each water mass.

5.2.2.1 ENACW

During the winter of 2005, the ENACW layers of the Finisterre section cooled by about 0.5°C in the upper 200 dbar and about 0.3°C in the layer 200-400 dbar. A more saline mode water was the outcome of this process, seen as isopycnal warming in the neutral levels 27.2 and 27.3, and a shoaling of isoneutral 27.2. This same pattern of change has been documented in the Bay of Biscay where it was attributed to the heat loss and the low net precipitation-minus-evaporation of the cold, dry winter affecting a wide region including the Western Mediterranean Sea (*Somavilla et al.*, 2009). The implication is that the winter 2005 atmospheric conditions profoundly affected a wide area of upper ocean

from the western Bay of Biscay to the eastern margin. The results are consistent with previous work that shows that the main driver for ENACW salinity variations is the local precipitation minus evaporation (P-E) balance (directly affected by the NAO), and that properties acquired by the ENACW every winter remains at least one year after the water mass formation (*Pérez et al.*, 2000). For the deeper layers of the ENACW (the Salinity Minimum) the influences on the water mass properties are more complex because these layers can mix with warm saline Mediterranean Water and the slightly lighter Subarctic Intermediate Water (SAIW) (*Pollard et al.*, 1996). The results from the Finisterre section suggest that the deep ENACW was affected by the cold winter of 2005 (no change in layer thickness but significant isopycnal change), but it is possible that the conditions were also influenced by the incursion of Subarctic Intermediate Water carried by a stronger North Atlantic Current flowing northeastward at lower depths (*Häkkinen & Rhines*, 2009).

5.2.2.2 MW-LSW levels

The Finisterre section is located on the northern edge of the subtropical gyre across the theoretical pathway of MW (Fig. 2.1). The results at MW core (800-1200 dbar) show density compensated changes consisting of warming/salinification to 2005, cooling/freshening to late 2010, and sharp changes in 2011 and 2013. We have suggested that these changes in properties, particularly after strong NAO years, may be an advective response. Note that interpreting isopycnal changes at MW levels as having advective origin may appear counter-intuitive but reflects the fact that we are dealing with a water mass characterized by large lateral gradients. Also note that right at the core of MW there can not be property changes by heave since the vertical gradients of temperature and salinity vanish.

These changes are consistent with the proposed response of the SPG to the NAO discussed in the literature. Periods of increasing and positive NAO index induces an expanding SPG and cooling and freshening of northern subpolar intermediate waters, but warmer and more saline MW in the eastern subtropical gyre since the spreading of the MW towards northern latitudes is blocked (*Lozier & Stewart*, 2008; *Lozier & Sindlinger*, 2009; *Chaudhuri et al.*, 2011). This was the case for several decades up to the mid-1990s. After the mid-1990s the intermediate waters of northern North Atlantic warmed and became more saline as the SPG contracted and more subtropical water entered the region (*Sarafanov et al.*, 2009). Our results are consistent with this view, with the warming/salinification observed to 2005 being likely a response to the contracting SPG (and more spreading of MW), and the subsequent cooling and freshening possibly a response to new positive phases of the NAO (and blocking of MW).

The most significant change in the properties of the LSW was seen in autumn 2008 as a drop in temperature and salinity that lasted to 2011. A similar change was seen in the Rockall Trough (which lies to the north) in 2006-2009 and is thought to indicate the arrival of a particular vintage of LSW formed in winter 2000 (*Nolan et al.*, 2012). It is possible, but not certain, that the 2008 event at the Finisterre section indicates the arrival of the LSW_{2000} there. It has long been known that the largest changes to LSW properties are those induced by changes in air-sea fluxes during winter convection at source, sometimes as a direct response to the NAO (*Pickart et al.*, 2003; *Flatau et al.*, 2003). The range of property variations are so large that the variability of LSW at source may leave an imprint on the water mass far from the origin, and a range of travel times from the source to the eastern basins has been estimated based on matching Labrador Sea conditions with local changes (*Read & Gould*, 1992; *Cunningham & Haine*, 1995; *Pickart et al.*, 2003; *Yashayaev et al.*, 2007). Our results suggest that such remote imprints in LSW properties may reach even further that previously assumed.

5.2.2.3 Deep waters

The variations in the deepest water of the Finisterre section are weak and show no clear trends (see Fig. 4.4). Though there is evidence in the literature of changes in deep waters of the North Atlantic, during the time span of our timeseries the deep ocean in the Atlantic Iberian basin has remained stable. Examples of observed changes include decadal density-compensated temperature anomalies formed in the subpolar gyre and then propagated equatorwards (*Mauritzen et al.*, 2012); and rapid freshening of the deep North Atlantic over past decades (*Dickson et al.*, 2002; *Curry et al.*, 2003; *Solomon et al.*, 2007; *Atkinson et al.*, 2012). *Atkinson et al.* (2012) found a decreasing southward transport in the 3000-4700 m layer (LNADW) along 25°N, coincident with a density compensated cooling and freshening of the Denmark Strait Overflow Water in the Deep Western Boundary Current at that latitude.

5.3 On the north-west Iberia deep ocean circulation

5.3.1 Direct velocities vs geostrophy: Similarities and discrepancies

The exercise of estimating velocity fields from different approaches highlights the difficulties inherent to measure the instantaneous flow across an oceanographic section characterised by relatively strong mesoscale activity and weak background overall currents.

The general presence of an intense eddy field in the ocean makes circulation measurements very noisy and calculation of transports very sensitive to the begin and end points of measurements (*Wunsch*, 2008). Since mesoscale structures can change during the time spent on the sampling of an hydrographic section, a synoptic view of the ocean may be lost as mesoscale structures evolve between the begin and end dates (*Vargas-Yáñez et al.*, 2005). According to this mesoscale variability, the Finisterre section, which takes 3-4 days to be completed, evidenced a system of alternating southward/northward currents, jets and recirculations, making difficult the computation of reliable transports across the section.

Moreover, each methodological approach have advantages and caveats. Geostrophic calculations have provided the bulk of our present knowledge on ocean circulation but the they do not take into account the ageostrophic component of the flow and are very dependent of a correct choice of the no movement reference level, an idealization that is not always appropriate. On the other hand LADCP profiles may be strongly biased by local high frequency currents as inertial and the tide. Moreover these techniques are still under development and errors caused by the movement of the profiler are still matter of concern.

There are several studies dealing with comparisons of geostrophy fields and directly measured current velocities, *Hinrichsen & Lehmann* (1995) studied the mesoscale mass distribution and flow associated to the MW from CTD and ADCP measurements in the southern Iberia Basin off Portugal coast and the Gulf of Cádiz, showing a good agreement between geostrophic and direct measured velocities, except near the coast where strong ageostrophic velocities are expected. *Lherminier et al.* (2007) calculated absolute transports across the Greenland-Portugal Ovide section during 2002 and 1997 using an inverse model constrained by direct ADCP measurements obtaining that direct current measurements differ significantly from geostrophy when the circulation is barotropic, a result that seems to match with our observations at Finisterre. In the Agulhas Current the velocity and vorticity study carried by *Beal & Bryden* (1999) showed an unchanged density structure of the current, that is, the baroclinic part of circulation provided by geostrophy appeared well captured by LADCP, while the barotropic part of circulation seemed to be the main source of the intensity flow variability. Besides, LADCP and mooring measurements revealed an equatorward Agulhas Undercurrent not observed before. These authors attributed differences between LADCP and geostrophic velocities to the geostrophic method, and they used the LADCP to improve reference levels and overall geostrophic transports estimates, including improvement of deep water transport estimates. *Quaresma & Pichon* (2013) suggested that internal tides, which cause isoneutral rapid displacements up to tens of dbar, may be also a source of discrepancy between geostrophy and ADCP velocities. They worked on a barotropic tidal model along the western Iberia margin,

showing M2 barotropic current velocities up to 10 cm/s near the slope and Galicia Bank region that cause associated sea surface amplitudes up to 1 m in the region (see their Fig. 8 and 10). Moreover, they found internal tide generation "hotspots" around Cape Finisterre (at the slope region near the edge of the submarine canyon of Mugia) and the southeastern side of the Galicia Bank (see their Fig. 17).

The results shown in Sect. 4.3 indicate that despite an overall agreement in the current structure fields there are also notable discrepancies. The first one is the very strong slope current inferred from geostrophy (up to 0.5 m/s in the winter cruise) that is not reflected at all in the LADCP record. It is not clear what is the cause of such discrepancy though it is acknowledged that applying geostrophy right at a steep slope is problematic due to the necessity of making assumptions about the geopotential anomaly at the seafloor. Also, in order to resolve the structure, the stations are very close (as much as 5 km) and this is also an issue when computing geostrophic fields. The second large discrepancy arises from the absence of a no movement level across the passage as seen by the LADCP. This circumstance suggest that the LADCP may be, despite its inherent problems, more appropriate to estimate transports in this section. The cruise RadProf200809 in particular was made under a strong dominant southwards background flow all across the passage but geostrophy indicates alternating flows. Our interpretation is that these mesoscale structures are being advected by the mostly barotropic overall flow, thus undetected in geostrophy.

Finally, there exists large differences between the standard and bottom-tracked velocity referenced geostrophic fields. While at some stations the corrected velocity field resembles better the LADCP record, there are several profiles where the correction have shifted all the profile by an unfeasible large offset. The most striking case is that of the RadProf200802 cruise where near-bottom northwards countercurrent across most of the passage caused the corrected gesotrophic flow to became widespread northwards. The method is clearly not suitable for a complex topographical area as the one in Finisterre section. Probably the swings in near-bottom currents caused by the internal tide are a source of problems. Regarding the comparison of raw LADCP and the barotropic tide removed version it seems that the overall structure of the fields stand.

5.3.2 Finisterre section circulation. Consistency with previous knowledge.

As part of an eastern boundary current system, the Coastal Transition Zone off the Iberian Peninsula is characterized by complex dynamics similar to that of the California Current system in the North Pacific (*Lynn & Simpson*, 1987; *Haynes et al.*, 1993). The large-scale

circulation in the North Atlantic eastern basin is dominated by the North Atlantic Current (48°-53°N) and the Azores Current (34°Ű35°N), defining an inter-gyre region characterized by a weak and southward circulation (*Pollard & Pu*, 1985; *van Aken*, 2001). The Finisterre section is embedded in the southward flowing region known as the Portugal Current (*Arhan et al.*, 1994) favoured by northerly winds typical of upwelling systems, and a marked, narrow (∼25-40 km) and weak (∼20 cm s^{-1}) poleward undercurrent flowing at ∼300-500 m along the continental slope: the Iberian Poleward Current (IPC), which brings warm and salty subtropical waters northwards along the continental slope of the western Iberian Peninsula during winter (*Frouin et al.*, 1990; *Peliz et al.*, 2003).

Circulation in the western Iberia margin, although mainly seasonal, is superimposed by short-term fluctuations hosting a wide spectrum of mesoscale structures such as eddies, meanders, jets, counter-currents and upwelling filaments affecting the water mass interchange between the shelf-slope and open ocean in time scales less than one month (*Haynes et al.*, 1993; *Huthnance*, 1995; *Huthnance et al.*, 2002; *Peliz et al.*, 2002; *Huthnance et al.*, 2009).

The two occupations of the section in winter and summer under typical seasonal hydrographical configurations provide and overall view of a slope flow of the order of 1 Sv, apparently stronger in winter, and a southward flow of 2-3 Sv in the open ocean, stronger in summer. In the present section we will discuss these results within the context of present knowledge of circulation in the region.

5.3.2.1 Overall transport across the section

Regarding the bulk transport across the section some field-based studies and modelling exercises are available. The structure of the velocity field across the section, with southern flow across the passage and northwards flow at the slope and again west of the Galician Bank, confirms previous findings by *Daniault et al.* (1994). An inverse model of general circulation in the eastern North Atlantic applied by *Paillet & Mercier* (1997) found most of the NAC recirculating northward but some branches flowing southward later connecting with the Azores Current in the south. One of this branches flows southward along the western Iberia margin carrying 2 Sv in the 0-800 m layer in a typical late winter situation (March). This result agrees with the 2.5 Sv southward mass transport down to 1000 m from detided LADCP in February (see Table 4.5). *Penduff et al.* (2001) also applied a regional primitive equation model forced by seasonal and monthly surface fluxes finding that the southward recirculating branches of NAC bring 11.2 Sv toward the subtropical gyre across the intergyre region though their scale is much broader than the extension covered by our repeated survey. *Lherminier et al.* (2007) also covers a section west of the

Iberian Peninsula slightly south of Finisterre as the easternmost leg of the OVIDE section and their results are also in agreement with our estimates.

5.3.2.2 The shelf-upper slope. The Iberian Poleward Current.

Several studies have focused on the slope poleward flow characteristic of the western Iberia margin, succeeding on reproduce observed seasonality driven by the summer upwelling, the winter surface poleward current and the offshore exports both at IPC levels and the permanent MW undercurrent along the Portuguese and Spanish slopes (*Coelho et al.*, 2002; *Friocourt et al.*, 2007, 2008b,a). *Santos et al.* (2002) found from a numerical model study of the European margin that the slope current, intensified in autumn, is confined to the upper slope and outer shelf extending down to 1500-2000 m, according to our results. In the other hand, *Mazé et al.* (1997) pointed to the contrast between a variable meridional flow at upper levels of the eastern boundary in opposition to the more persistent southward regime in the open ocean, something that may also be concluded from our study.

As it was noted above, the poleward flow over the continental shelf was present both during winter and summer 2008, both from LADCP and corrected geostrophy (Figs. 4.11 and 4.12). According to *Coelho et al.* (2002) the poleward transport in the Iberian shelf-slope region is present all year round, decreasing from winter to summer. *Peliz et al.* (2002) found from a survey carried off the northern coast of Portugal, a circulation system with zonal variability characterized by a coastal northward counter current coexisting with upwelling southward jets, the slope poleward flow and the large-scale southward flow. These authors suggest that this coastal counter-flow is the response to the offshore drift of the upwelling current influenced by the Western Iberian Buoyant Plume. *Lherminier et al.* (2007) found a northward transport of 2.1 ± 0.4 Sv associated to the Eastern Boundary Current of the Iberian shelf and slope during summer 2002, not too different to our results. Our results roughly agree with the magnitude of the slope current as well as the summer/winter behaviour, with stronger shelf flow in winter and offshore deeper flow in summer. The deeper-reaching slope poleward flow during summer and the deeper-reaching southward flow down to intermediate depths at the outer ocean in winter, are consistent with the attachment to the slope of the MW vein during summer and spreading over the Galicia Bank in winter (enhancement of the southward flow due to recirculation) previously suggested Sect. 4.1.

The slope flow is expected to respond to the concurrent upwelling/downwelling conditions so Figure. 5.9 provides the upwelling index (seaward transport per km parallel to coastline) in 2008 respect to the climatological record. The index showed not abnormal values, negative during February and positive during September.

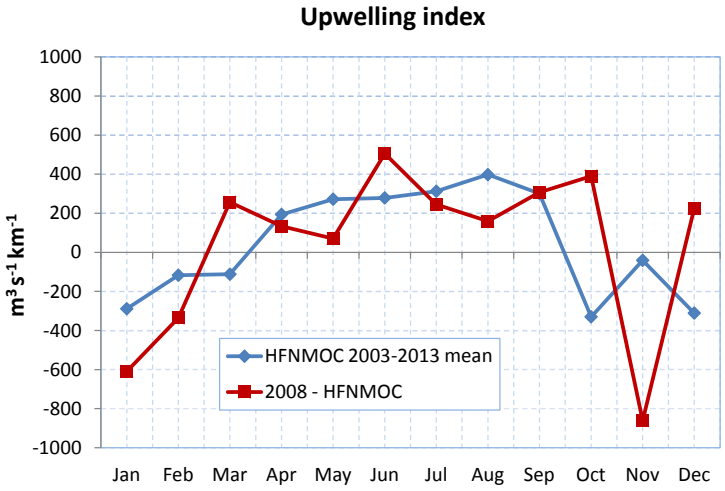

Figure 5.9: Monthly time series of upwelling index at 43°00'N, 011°00' W, retrieved from the Spanish Institute of Oceanography visor tool of upwelling index `www.indicedeafloramiento.ieo.es`

5.3.2.3 Recirculation around the Galicia Bank.

The Galician Bank is a large seamount and hence it is expected that it would condition the local circulation, generation retention cells and recirculation structures (e.g. *Lavelle et al.*, 2010). *Mazé et al.* (1997) decomposed the flow associated to the MW into three longitudinal regions characterized by a northward transport of 7.6 Sv west of the Galicia Bank, part of which recirculates anticyclonically around the seamount, a southward transport of 3.8 Sv between the east part of the Galicia Bank and 10°30'W, and a northward flow of 2 Sv between this longitude and the continental slope. They also found that Central Water (ENACW) showed a zonal distribution similar to that of the underlying MW, suggesting that the southward flow east of the Galicia Bank is a recirculation of a part of the northward ENACW flow in the west. The coupling between ENACW and MW was also reported by these authors who confirmed the existence of a poleward slope flow at both water levels through 43°N of 4.7 Sv. They also observed the warm and salty surface water displaced 200 km offshore with a corresponding high salinity anomaly at MW levels (900m) indicating that part of the MW core may be also displaced offshore.

Our records support a permanent anticyclonic recirculation around the Galicia Bank, but exhibiting stronger transports in summer. Such outcome is in good agreement with that obtained by *Mazé et al.* (1997) in direction, and comparable in magnitude despite they worked with a different cruise (May 1989) and it is expected strong variability. Regarding to the seasonality of recirculation around the Galicia Bank, we can only put forward the

enhancement of the flows in the summer cruise, that may be triggered by the enhancement of the southwards flow during this period of the year as it is reflected by the weaker signature of MW in the open ocean.

6

Conclusions/Conclusiones

The VACLAN/COVACLAN monitoring program running since 2003 off the northwestern Iberia and southern Bay of Biscay, has provided the most detailed view of the seasonal and interannual variability of the deep ocean in the area to date. Hydrographical properties of a zonal section $\sim$200 nm off Cape Finisterre (43° N, 009–014° W) have been sampled for the period 2003–2010 by means of two cruises per year (summer/winter). The sampling has revealed that there exists a noticeable seasonal signature in this part of the eastern boundary of the North Atlantic down to 2000 dbar. The magnitude of seasonality is roughly 20 % of the interannual variability observed for the overall period, reaching values up to 0.5 °C, 0.04 in salinity just below the maximum extent of winter mixing (c.a. 200 dbar), and 0.4 °C and 0.08 in salinity at around 1400 dbar, within the lower bounds of Mediterranean water.

The spatial structure of the seasonality shows a strong contrast between the near-slope area and the outer ocean. The most remarkable and novel finding is the behaviour of the Mediterranean Water vein that gets attached and reinforced along the slope in summer and spreads offshore in wintertime. The observed pattern confirms, from a much larger dataset, some dynamical aspects regarding the Iberian margin seasonality and MW spreading that had been previously inferred from quite reduced datasets. Among them we can highlight the shoreward and upwards displacement of slope MW as a response to the seasonal upwelling and the appearance of a secondary branch of MW around the Galicia Bank, a feature that appears to be typical of the winter regime. The results have been discussed in terms of the seasonality of large-scale and continental slope processes and a brief review of modelling efforts regarding seasonality at the area has been made, showing that key features, reproduced by some of them as the winter flow reversal at

MW levels on the slope, are consistent with our observations. The time series of in situ data provided here become a valuable tool for evaluating circulation models at regional or oceanic scales. The seasonality in the area must be taken into account when analysing specific hydrographical observations or long-term series.

This study has provided a detailed view of interannual changes in the last decade in the mid-latitude transitional intergyre region, complementing well the established monitoring programs in the subpolar and subtropical regions. The time series exhibited statistically significant autocorrelation, correlation across large portions of the water column, and geographical correlation mostly between Finisterre and Santander sections, suggesting that the sampling scheme is adequate to resolve background variability over mesoscale activity. The most comprehensive results are provided by the Finisterre section which is the deepest, longest and most often repeated. This section has been shown to be representative of changes in the North Atlantic eastern boundary, showing a primarily isopycnal origin for termohaline properties changes. Statistically significant trends over the time series were found in the ENACW, dominated by a change to a saltier/warmer state after the extreme winter forcing of 2005. A significant long-term trend was also observed at the transition level between MW and LSW, dominated by the change to colder/fresher conditions towards the end of the series, from 2008 to 2010. Variability below the 2000 dbar is very small, oscillating around the limits of what is measurable.

The water mass properties of the section are strongly influenced by the state of the NAO, most obviously as a rapid and local response to the high positive NAO in winters 2007-2008 and 2012 (inducing cooling and freshening), and the extremely negative NAO index in winter 2010 (inducing warm and saline intermediate conditions). The results are consistent with present knowledge about North Atlantic circulation and its response to atmospheric circulation.

The present work supports the importance of the maintenance of continuous monitoring programs of the deep ocean variability, through the periodic repetition of hydrographic sections, as a valuable tool for analyzing deep ocean changes on interannual to decadal scales, including unpredictable strong shifts essential to predict future local or global climate change. The results derived from this monitoring program are expected to contribute to future revisions and further developments in long-term Spanish climate monitoring strategy.

Geostrophic current velocities were computed from CTD measurements along the Finisterre deep section ($>$ 5000 m, $\sim$ 200 nm off Cape Finisterre), during winter and summer 2008, choosing a level of no motion at γ^n = 28.072kg m^{-3} ($\sim$3000 m) or the deepest common level at shallower stations near the slope or the Galicia Bank seamount. Geostrophic fields showed an alternating system of northward and southward currents

evidencing mesoscale structures not observable by direct measurements from LADCP, which showed a more barotropic circulation according to a fixed currentmeter mooring at 43°N, 11°W. As a consequence, the geostrophic field seem to underestimate mass transport across the Finisterre section by one order of magnitude during winter, even reversing the flow during summer. LADCP measurements revealed a more intense southward mass transport in summer (2.2 Sv) than in winter 2008 (1.30 Sv) across the Finisterre section. Findings also include a poleward flow extending from the shelf and slope down to 1500 dbar during summer, and a permanent anticyclonic recirculation of the water column around the Galicia Bank. Results are consistent with the spreading of the MW vein over the Galicia Bank in winter (posterior recirculation) and the constraint of its core against the slope in summer. This study revealed the importance that systematic measurements of current velocities have on determining the real ocean circulation patterns in this region, both as a tool to obtain a direct measurement of currents, and as an useful method to improve regional circulation models in a region characterized by a wide range of dynamics and variability scales.

El programa de monitorización VACLAN/COVACLAN llevado a cabo desde el año 2003 en la región del noroeste de la Península Ibérica y sur del Golfo de Vizcaya ha proporcionado la visión más detellada de la variabilidad estacional e interanual del océano profundo en el área hasta la fecha.

Se han muestreado las propiedades hidrográficas de una sección zonal ~ 200 millas náuticas al oeste de Cabo Finisterre (43° N, 009–014° O) a través de la realización de campañas semianuales de invierno/verano durante el periodo 2003-2010. Dicho muestreo ha revelado la existencia de una señal estacional notable en esta porción del contorno oriental del Atlántico Norte hasta los 2000 dbar. La magnitud de la estacionalidad es aproximadamente un 20 % de la variabilidad interanual observada durante todo el periodo, alcanzando valores de 0.5 °C y 0.04 en salinidad justo por debajo de la profundidad máxima de la capa de mezcla invernal (200 dbar) y 0.4 °C y 0.08 en salinidad en torno a los 1400 dbar, en el límite inferior del agua mediterránea.

La estacionalidad muestra una estructura zonal con un fuerte contraste entre la región más cercana al talud continental y el océano abierto. El hallazgo más novedoso es el comportamiento de la vena de agua mediterránea, la cual aparece ceñida y reforzada a lo largo del talud en verano, propagándose hacia fuera de la costa en invierno. Este patrón observado confirma algunos aspectos dinámicos relacionados con la estacionalidad en el margen Ibérico y la propagación del agua mediterránea, inferidos previamente con bases de datos más reducidas. Entre ellos podemos destacar el desplazamiento hacia la costa y hacia arriba en la columna de agua de la vena de agua mediterránea en el talud en respuesta al afloramiento estacional, y la aparición de una rama secundaria alrededor del banco de Galicia, característica que parece ser típica del régimen de invierno. Los resultados se discutieron en términos de la estacionalidad de larga escala y los procesos de talud continental, y se ha realizado un repaso a los esfuerzos de modelización de la estacionalidad en el área de estudio, mostrando que las principales características reproducidas por algunos de ellos en el talud (como la inversión invernal a niveles del agua mediterránea), son consistentes con nuestras observaciones. La series temporales de datos in-situ se convierten por lo tanto en una herramienta de valor para la evaluación de los modelos de circulación a escalas regionales y oceánicas. La estacionalidad en el área debe ser tenida en cuenta a la hora de analizar observaciones hidrográfcias específicas o series temporales a largo plazo.

Este programa de monitorización ha proporcionado una visión detallada de los cambios interanuales durante la última década en la región de transición entre los dos grandes giros (latitudes medias del Atlántico Noreste), complementando los ya bien establecidos programas de monitorización en las regiones subpolares y subtropicales. Las series temporales exhiben autocorrelación, correlación a lo largo de grandes porciones de la columna de agua y correlación geográfica estadísticamente significativa principalmente

entre la sección de Finisterre y Santander, sugiriendo que el esquema de muestreo establecido resulta adecuado para resolver la variabilidad sobre la actividad de mesoscala.

Los resultados más completos los proporciona la sección de Finisterre, la más profunda, larga y repetida, siendo representativa de los cambios en el contorno oriental del Atlántico Norte. Las series temporales hidrográficas muestran principalmente cambios isopicnos de las propiedades termohalinas. Las tendencias encontradas son estadísticamente significativas en las aguas centrales, dominadas por un cambio hacia un estado más salino y cálido posterior al forzamiento atmosférico extremo del invierno de 2005. El nivel de transición entre el agua mediterránea y el agua del mar de Labrador mostró una tendencia caracterizada por un cambio hacia condiciones más frias y menos salinas entre de 2008 y 2010. La variabilidad observada por debajo de los 2000 dbar es muy pequeña, oscilando en los límites de lo que es medible.

Las propiedades de las masas de agua en la sección están fuertemente influenciadas por el estado de la NAO, respondiendo de manera local y rápida al fuerte índice NAO positivo de los inviernos 2007-2008 y 2012 (induciendo enfriamiento y disminución de la salinidad), y el extremadamente negativo índice NAO en el invierno de 2010 (induciendo condiciones más cálidas y salinas de las aguas intermedias). Los resultados son consistentes con el conocimiento actual de la circulación del Atlántico Norte y su respuesta al forzamiento atmosférico.

Este estudio pone de manifiesto la importancia que tiene el mantenimiento de los programas de monitorización continuada de la variabilidad del océano profundo a través de la repetición periódica de secciones hidrográficas, estableciéndose como una herramienta esencial para el análisis de los cambios del océano profundo en escalas interanuales a decadales, incluyendo fuertes cambios impredecibles y esenciales para la predicción de futuros cambios en el clima local y global. Se espera que los resultados derivados de este programa de monitorización contribuyan a futuras revisiones y a un mayor desarrollo de la estrategia de monitorización a largo plazo del clima en España.

Finalmente se computaron las velocidades geostróficas de las corrientes a partir de las medidas de CTD realizadas a lo largo de la sección de Finisterre durante el invierno (febrero) y verano (septiembre) de 2008, eligiendo un nivel de referencia en $\gamma^n = 28.072$ $\mathrm{kg\,m^{-3}}$ ($\sim$3000 m) o el nivel común más profundo para las estaciones más someras en las proximidades del talud continental o el Banco de Galicia. Los campos geostróficos se caracterizan por la alternancia de corrientes hacia el norte y hacia el sur evidenciando estructuras de mesoscala no observadas por las medidas directas de LADCP, las cuales muestran una circulación más barotrópica de acuerdo a las medidas de un fondeo fijo de correntómetros situado en 43°N, 11°O. Como consecuencia, el campo geostrófico parece subestimar el transporte de masa a través de la sección de Finisterre en un orden de magnitud en invierno, incluso invirtiéndose el flujo durante el verano.

Las medidas de LADCP revelaron un transporte de masa hacia el sur más intenso en verano (2.2 Sv) que en invierno (1.30 Sv) a través de la sección de Finisterre. Los resultados muestran un flujo hacia el norte extendiéndose en la plataforma y el talud hasta los 1500 dbar durante el verano, y una recirculación anticiclónica permanente de la columna de agua alrededor del banco de Galicia. Los resultados son consistentes con la propagación de la vena de agua mediterránea sobre el banco de Galicia en invierno (y posterior recirculación) y la restricción de su core contra el talud en verano.

Este estudio revela también la importancia que tiene la medida sistemática de la velocidad de las corrientes a la hora de determinar los patrones de circulación real del océano en la región, tanto para la obtención de medidas directas como para servir de herramienta en la mejora de los modelos de circulación regional, en una región caracterizada por un amplio rango de escalas de variabilidad y dinámica oceánica.

7 Future work

- The maintenance of the annual sampling of the deep ocean hydrography and circulation along the Finisterre section through the series of oceanographic cruises *RadProf* is suggested as being essential to provide a systematic and continuous temporal register of the water mass properties changes in this region of the Iberian margin.
- A new design of the monitoring program may include the westward extension of the Finisterre section towards the central North Atlantic in order to further study of the Mediterranean Water spreading in the North Atlantic Ocean. Moreover, given that the observed changes at the deepest levels are very small, it would be possible to limit the regular sampling down to 2000 m depth (where main changes are observed), repeating the whole section down to the ocean bottom (more than 5000 m) every 2-3 years.
- Besides, it would be interesting the implementation of the hydrographic sampling with measurements provided by gliders, combining the repetition of the section on board research vessels with the deployment of such state-of-the-art autonomous vehicles.
- Part of the future work should include the time series of oceanic transports both from geostrophy and direct LADCP measurements for the whole time period 2003-2013, comparing results obtained from the three proposed methods as a function of cruise conditions and available data.
- It is also necessary the development of internal tide regional models in order to account for the tidal baroclinic component.

Bibliography

Álvarez, I., M. Gomez-Gesteira, M. deCastro, and E. M. Novoa (2008), Ekman transport along the Galician coast (NW, Spain) calculated from QuikSCAT winds, *J. Mar. Sys.*, *72*(1-4), 101 – 115, doi: 10.1016/j.jmarsys.2007.01.013.

Ambar, I., L. Armi, A. Bower, & T. Ferreira, Some aspects of time variability of the Mediterranean Water off south Portugal, *Deep-Sea Research. I*, *46*, 1109–1136, 1999, doi: 10.1016/S0967-0637(99)00006-0.

Arhan, M., A. Colin De Verdiére, & L. Mémery, The Eastern Boundary of the Subtropical North Atlantic, *J. Phys. Oceanogr.*, *24*, 1295–1316, 1994, doi:10.1175/1520-0485(1994)024<1295:TEBOTS>2.0.CO;2.

Atkinson, C. P., H. L. Bryden, S. A. Cunningham, & B. A. King, Atlantic transport variability at 25°N in six hydrographic sections, *Ocean Sci.*, *8*, 497–523, 2012, doi:10.5194/os-8-497-2012.

Baker, D. J., R. W. Schmitt, & C. Wunsch, Endowments and New Institutions for Long-Term Observations, *Oceanography*, *20*, 10–14, 2007, doi:10.5670/oceanog.2007.19.

Bakun, A., & C. S. Nelson, The Seasonal Cycle of Wind-Stress Curl in Subtropical Eastern Boundary Current Regions, *J. Phys. Oceanogr.*, *21*, 1815–1834, 1991, doi:10.1175/1520-0485(1991)021.

Barnett, T. P., D. W. Pierce, K. M. AchutaRao, P. J. Gleckler, B. D. Santer, J. M. Gregory,

& W. M. Washington, Penetration of human-induced warming into the world's oceans, *Science*, *309*, 284–287, 2005, doi:10.1126/science.1112418.

Beal, L. M., & H. L. Bryden, The velocity and vorticity structure of the Agulhas Current at 32°S, *J. Geophys. Res. Oceans*, *104*, 5151–5176, 1999, doi:10.1029/1998JC900056.

Belkin, I. M., Propagation of the "Great Salinity Anomaly" of the 1990s around the northern North Atlantic, *Geophys. Res. Lett.*, *31*, L08306, 2004, doi:10.1029/2003GL019334.

Belkin, I. M., S. Levitus, J. Antonov, & S. A. Malmberg, "Great Salinity Anomalies" in the North Atlantic, *Prog. Oceanogr.*, *41*, 1–68, 1998, doi:10.1016/S0079-6611(98)00015-9.

Bindoff, N. L., & W. R. Hobbs, Oceanography: Deep ocean freshening, *Nature Climate Change*, *3*, 864–865, 2013, doi:10.1038/nclimate2014.

Bindoff, N. L., & T. J. McDougall, Diagnosing climate change and ocean ventilation using hydrographic data, *J. Phys. Oceanogr.*, *24*, 1137–1152, 1994, doi:10.1175/1520-0485(1994)024.

Bower, A. S., N. Serra, & I. Ambar, Structure of the Mediterranean Undercurrent and Mediterranean Water spreading around the southwestern Iberian Peninsula, *J. Geophys. Res.*, *107*, 3160, 2002, doi:10.1029/2001JC001007.

Bray, N. A., Seasonal variability in the intermediate waters of the Eastern North Atlantic, Ph.D. thesis, Woods Hole Oceanographic Institution, 1980.

Bray, N. A., Seasonal variability in the Intermediate Waters of the eastern North Atlantic, *J. Phys. Oceanogr.*, *12*, 972–983, 1982, doi:10.1175/1520-0485(1982)012<0972:SVITIW>2.0.CO;2.

Bretherton, F. P., R. E. Davis, & C. B. Fandrys, A technique for objective analysis and design of oceanographic experiments applied to MODE-73, *Deep-Sea Res.*, *23*, 559–582, 1976, doi:10.1016/0011-7471(76)90001-2.

Bryden, H. L., E. L. McDonagh, & B. A. King, Changes in ocean water mass properties: Oscillations or trends?, *Science*, *300*, 2086–2088, 2003, doi:10.1126/science.1083980.

Bryden, H. L., H. R. Longworth, & S. A. Cunningham, Slowing of the Atlantic Meridional Overturning Circulation at 25°N, *Nature*, *438*, 655–657, 2005, doi:10.1038/nature04385.

Chaudhuri, A. H., A. Gangopadhyay, & J. J. Bisagni, Contrasting Response of the Eastern and Western North Atlantic Circulation to an Episodic Climate Event, *J. Phys. Oceanogr.*, *41*, 1630–1638, 2011, doi:10.1175/2011JPO4512.1.

Chelton, D. B., Statistical Reliability and the Seasonal Cycle - Comments on Bottom Pressure Measurements Across the Antarctic Circumpolar Current and Their Relation to the Wind, *Deep-Sea Res.*, *29*, 1381–1388, 1982, doi:10.1016/0198-0149(82)90016-4.

Chidichimo, M., T. Kanzow, S. Cunningham, W. Johns, & J. Marotzke, The contribution of eastern-boundary density variations to the Atlantic Meridional Overturning Circulation at 26.5°N, *Ocean Sci.*, *6*, 475–490, 2010, doi:10.5194/os-6-475-2010.

Coelho, H. S., R. J. J. Neves, M. White, P. C. Leitao, & A. J. Santos, A model for ocean circulation on the Iberian coast, *J. Mar. Sys.*, *32*, 153–179, 2002, doi:10.1016/S0924-7963(02)00032-5.

Comas-Rodriguez, I., A. Hernandez-Guerra, & E. L. McDonagh, Referencing geostrophic velocities using ADCP data at 24.5°N (North Atlantic), *Sci. Mar.*, *74*, 331–338, 2010, doi: 10.3989/scimar.2010.74n2331.

Cunningham, S. A., & T. W. N. Haine, Labrador Sea-Water in the Eastern North-Atlantic .2. Mixing Dynamics and the Advective-Diffusive Balance, *J. Phys. Oceanogr.*, *25*, 666–678, 1995, doi:10.1175/1520-0485(1995)025<0666:LSWITE>2.0.CO;2.

Cunningham, S. A., S. G. Alderson, B. A. King, & M. A. Brandon, Transport and variability of the Antarctic Circumpolar Current in Drake Passage, *J. Geophys. Res. Oceans*, *108*, 2003, doi:10.1029/2001JC001147.

Cunningham, S. A., T. Kanzow, D. Rayner, M. O. Baringer, W. E. Johns, J. Marotzke, H. R. Longworth, E. M. Grant, J. J. M. Hirschi, L. M. Beal, C. S. Meinen, & H. L. Bryden, Temporal variability of the Atlantic meridional overturning circulation at 26.5°N, *Science*, *317*, 935–938, 2007, doi:10.1126/science.1141304.

Curry, R., B. Dickson, & I. Yashayaev, A change in the freshwater balance of the Atlantic Ocean over the past four decades, *Nature*, *426*, 826–829, 2003, doi:10.1038/nature02206.

Daniault, J. P., J. P. Mazé, & M. Arhan, Circulation and mixing of Mediterranean Water west of the Iberian Peninsula, *Deep-Sea Res. I*, *41*, 1685–1714, 1994, doi:10.1016/0967-0637(94)90068-X.

Dickson, B., I. Yashayaev, J. Meincke, B. Turrell, S. Dye, & J. Holfort, Rapid freshening of the deep North Atlantic Ocean over the past four decades, *Nature*, *416*, 832–837, 2002, doi10.1038/416832a.

Dickson, R. R., J. Meincke, S.-A. Malmberg, & A. J. Lee, "The Great Salinity Anomalyt't' in the Northern North Atlantic 1968–1982, *Prog. Oceanogr.*, *20*, 103 – 151, 1988, doi:10.1016/0079-6611(88)90049-3.

Eden, C., & J. Willebrand, Mechanism of interannual to decadal variability of the North Atlantic circulation, *J. Clim.*, *14*, 2266–2280, 2001, doi:10.1175/1520-0442(2001)014<2266:MOITDV>2.0.CO;2.

Egbert, G. D., & S. Y. Erofeeva, Efficient Inverse Modeling of Barotropic Ocean Tides, *J. Atmos. Oceanic. Technol.*, *19*, 183–204, 2002, doi:10.1175/1520-0426(2002)019<0183:EIMOBO>2.0.CO;2.

Egbert, G. D., A. F. Bennett, & M. G. G. Foreman, TOPEX/POSEIDON tides estimated using a global inverse model, *J. Geophys. Res. Oceans*, *99*, 24821–24852, 1994, doi:10.1029/94JC01894.

Emery, W. J., & R. E. Thomson, *Data Analysis Methods in Physical Oceanography*, Elsevier, 2001.

Filyushkin, B. N., S. N. Moshonkin, & N. G. Kozhelupova, Seasonal evolution of the Mediterranean Water propagation in the North Atlantic, *Oceanology*, *48*, 771–779, 2008, doi:10.1134/S0001437008060027.

Fischer, J., & M. Visbeck, Deep Velocity Profiling with Self-contained ADCPs, *J. Atmos. Ocean. Tech.*, *10*, 764–773, 1993, doi:10.1175/1520-0426(1993)0102.0.CO;2 .

Fiúza, A. F. G., M. Hamann, I. Ambar, G. D. del Río, N. González, & J. M. Cabanas, Water masses and their circulation off western Iberia during May 1993, *Deep-Sea Res. I*, *45*, 1127–1160, 1998, doi:10.1016/S0967-0637(98)00008-9.

Flatau, M. K., L. Talley, & P. P. Niiler, The North Atlantic Oscillation, Surface Current Velocities, and SST Changes in the Subpolar North Atlantic, *J. Clim.*, *16*, 2355–2369, 2003, doi10.1175/2787.1.

Fraile-Nuez, E., F. Plaza, A. Hernandez-Guerra, M. Vargas-Yanez, & A. Lavin, Mass transport in the Bay of Biscay from an inverse box model, *J. Geophys. Res.*, *113*, 2008, doi:10.1029/2007JC004490.

Friocourt, Y., B. Levier, S. Speich, B. Blanke, & S. S. Drijfhout, A regional numerical ocean model of the circulation in the Bay of Biscay, *J. Geophys. Res.*, *112*, 2007, doi:10.1029/2006JC003935.

Friocourt, Y., B. Blanke, S. Drijfhout, & S. Speich, On the Dynamics of the Slope Current System along the West European Margin. Part II: Analytical Calculations and Numerical Simulations with Seasonal Forcing, *J. Phys. Oceanogr.*, *38*, 2619–2638, 2008a, doi:10.1175/2008JPO3745.1.

Friocourt, Y., S. Drijfhout, & B. Blanke, On the Dynamics of the Slope Current System along the West European Margin. Part I: Analytical Calculations and Numerical Simulations with Steady-State Forcing, *J. Phys. Oceanogr.*, *38*, 2597–2618, 2008b, doi:10.1175/2008JPO3744.1.

Frouin, R., A. F. G. Fiúza, I. Ambar, & T. J. Boyd, Observations of a poleward surface current off the coasts of Portugal and Spain during winter, *J. Geophys. Res.*, *95*, 679–691, 1990, doi:10.1029/JC095iC01p00679.

Fusco, G., V. Artale, Y. Cotroneo, & G. Sannino, Thermohaline variability of Mediterranean Water in the Gulf of Cádiz, 1948-1999, *Deep-Sea Res. I*, *55*, 1624–1638, 2008, doi:10.1016/j.dsr.2008.07.009.

Gaillard, F., H. Mercier, & C. Kermabon, A synthesis of the POMME physical data set: One year monitoring of the upper layer, *J. Geophys. Res.*, *110*, 2005, doi:10.1029/2004JC002764.

Ganachaud, A., Large-scale mass transports, water mass formation, and diffusivities estimated from World Ocean Circulation Experiment (WOCE) hydrographic data, *J. Geophys. Res. Oceans*, *108*, 2003, doi:10.1029/2002JC001565.

Garcia-Lafuente, J., J. Garrido, G. del Rio, F. Aldeanueva, D. Marcote, & A. Roman, Low-frequency variability of the Mediterranean undercurrent off Galicia, northwestern Iberian Peninsula, *J. Mar. Sys.*, *74*, 351–363, 2008, doi:10.1016/j.jmarsys.2008.02.007.

Garcia-Lafuente, J. G., A. S. Roman, G. D. del Rio, G. Sannino, & J. C. S. Garrido, Recent observations of seasonal variability of the Mediterranean outflow in the Strait of Gibraltar, *J. Geophys. Res.*, *112*, 2007, doi:10.1029/2006JC003992.

Good, S. A., M. J. Martin, & N. A. Rayner, EN4: Quality controlled ocean temperature and salinity profiles and monthly objective analyses with uncertainty estimates, *J. Geophys. Res. Oceans*, *118*, 6704–6716, 2013, doi:10.1002/2013JC009067.

Hakkinen, S., & P. Rhines, Shifting surface currents in the northern North Atlantic Ocean, *J. Geophys. Res*, *114*, 2009, doi:10.1029/2008JC004883.

Hakkinen, S., & P. B. Rhines, Decline of subpolar North Atlantic circulation during the 1990s, *Science*, *304*, 555–559, 2004, doi:10.1126/science.1094917.

Häkkinen, S., P. B. Rhines, & D. L. Worthen, Warm and saline events embedded in the meridional circulation of the northern North Atlantic, *J. Geophys. Res. Oceans*, *116*, 2011a, doi:10.1029/2010JC006275.

Häkkinen, S., P. B. Rhines, & D. L. Worthen, Atmospheric Blocking and Atlantic Multidecadal Ocean Variability, *Science*, *334*, 655–659, 2011b, doi:10.1126/science.1205683.

Häkkinen, S., P. B. Rhines, & D. L. Worthen, Northern North Atlantic sea surface height and ocean heat content variability, *J. Geophys. Res. Oceans*, *118*, 3670–3678, 2013, doi:10.1002/jgrc.20268.

Hansen, J., R. Ruedy, M. Sato, & K. Lo, Global surface temperature change, *Rev. Geophys.*, *48*, 2010, doi:10.1029/2010RG000345.

Hàtún, H., A. B. Sando, H. Drange, B. Hansen, & H. Valdimarsson, Influence of the Atlantic subpolar gyre on the thermohaline circulation, *Science*, *309*, 1841–1844, 2005, doi:10.1126/science.1114777.

Haynes, R., & E. D. Barton, A poleward flow along the Atlantic coast of the Iberian Peninsula, *J. Geophys. Res.*, *95*, 11425–11441, 1990, doi:10.1029/JC095iC07p11425.

Haynes, R., E. D. Barton, & I. Pilling, Development, persistence, and variability of upwelling filaments off the Atlantic coast of the Iberian Peninsula, *J. Geophys. Res. Oceans*, *98*, 22681–22692, 1993, doi:10.1029/93JC02016.

Hendry, R., Environmental Conditions in the Labrador Sea in 2008, *Tech. Rep. 09/27*, Northwest Atlantic Fisheries Organization (NAFO), 2008.

Hinrichsen, H.-H., & A. Lehmann, A Comparison of Geostrophic Velocities and Profiling ADCP Measurements in the Iberian Basin, *J. Atmos. Oceanic Technol.*, *12*, 901Ű–914, 1995, doi:10.1175/1520-0426(1995)012<0901:ACOGVA>2.0.CO;2.

Hirschi, J. J. M., P. D. Killworth, & J. R. Blundell, Subannual, seasonal, and interannual variability of the North Atlantic Meridional Overturning Circulation, *J. Phys. Oceanogr.*, *37*, 1246–1265, 2007, doi:10.1175/JPO3049.1.

Hughes, S. L., N. P. Holliday, F. Gaillard, & the ICES Working Group on Oceanic Hydrography, Variability in the ICES/NAFO region between 1950 and 2009: observations from the ICES Report on Ocean Climate, *ICES Journal of Marine Science*, *69*, 706–719, 2012, doi:10.1093/icesjms/fss044.

Hurrell, J., & NCAR Staff, The Climate Data Guide: Hurrell North Atlantic Oscillation (NAO) Index (PC-based), 2014.

Hurrell, J. W., & C. Deser, North Atlantic climate variability: The role of the North Atlantic Oscillation, *J. Mar. Sys.*, *79*, 231–244, 2010, doi:10.1016/j.jmarsys.2008.11.026.

Huthnance, J. M., Circulation, exchange and water masses at the ocean margin: the role of physical processes at the shelf edge, *Prog. Oceanogr.*, *35*, 353–431, 1995, doi:10.1016/0079-6611(95)00012-6.

Huthnance, J. M., H. M. van Aken, M. White, E. D. Barton, B. Le Cann, E. F. Coelho, E. A. Fanjul, P. Miller, & J. Vitorino, Ocean margin exchange - water flux estimates, *J. Mar. Sys.*, *32*, 107–137, 2002, doi:10.1016/S0924-7963(02)00034-9.

Huthnance, J. M., J. T. Holt, & S. L. Wakelin, Deep ocean exchange with west-European shelf seas, *Ocean Sci.*, *5*, 621–634, 2009, doi:10.5194/os-5-621-2009.

Iorga, M. C., & M. S. Lozier, Signatures of the Mediterranean outflow from a North Atlantic climatology 1. Salinity and density fields, *J. Geophys. Res.*, *104*, 25985–26009, 1999a, doi:10.1029/1999JC900115.

Iorga, M. C., & M. S. Lozier, Signatures of the Mediterranean outflow from a North Atlantic climatology 2. Diagnostic velocity fields, *J. Geophys. Res.*, *104*, 26011–26029, 1999b, doi:10.1029/1999JC900204.

Jackett, D. R., & T. J. McDougall, A neutral density variable for the World's Oceans, *J. Phys. Oceanogr.*, *27*, 237–263, 1997, doi:10.1175/1520-0485(1997)027<0237:ANDVFT>2.0.CO;2.

Kanzow, T., S. A. Cunningham, W. E. Johns, J. J. M. Hirschi, J. Marotzke, M. O. Baringer, C. S. Meinen, M. P. Chidichimo, C. Atkinson, L. M. Beal, H. L. Bryden, & J. Collins, Seasonal Variability of the Atlantic Meridional Overturning Circulation at 26.5°N, *J. Clim.*, *23*, 5678–5698, 2010, doi:10.1175/2010JCLI3389.1.

Krauss, W., & C. Wuebber, Response of the North-Atlantic to Annual Wind Variations Along the Eastern Coast, *Deep-Sea Res. A*, *29*, 851–868, 1982, doi:10.1016/0198-0149(82)90050-4.

Kwon, Y.-O., & S. C. Riser, North Atlantic Subtropical Mode Water: A history of ocean-atmosphere interaction, *Geophys. Res. Lett.*, *31*, 2004, doi:10.1029/2004GL021116.

Latif, M., & T. P. Barnett, Decadal climate variability over the North Pacific and North America: Dynamics and predictability, *J. Clim.*, *9*, 2407–2423, 1996, doi:10.1175/1520-0442(1996)009<2407:DCVOTN>2.0.CO;2.

Lavelle, J.W., & C. Mohn , Motion, commotion, and biophysical connections at deep ocean seamounts, *Oceanogr.*, *23(1)*, 90–103, 2010, doi:10.5670/oceanog.2010.64.

Levitus, S., J. Antonov, & T. Boyer, Warming of the world ocean, 1955-2003, *Geophys. Res. Lett.*, *32*, L02604, 2005, doi:10.1029/2004GL021592.

Lherminier, P., H. Mercier, C. Gourcuff, M. Alvarez, S. Bacon, & C. Kermabon, Transports across the 2002 Greenland-Portugal Ovide section and comparison with 1997, *J. Geophys. Res. Oceans*, *112*, C07003, 2007, doi:10.1029/2006JC003716.

Lohmann, K., H. Drange, & M. Bentsen, A possible mechanism for the strong weakening of the North Atlantic subpolar gyre in the mid-1990s, *Geophysical Research Letters*, *36*, n/a–n/a, 2009, doi:10.1029/2009GL039166.

Lozier, M. S., & L. Sindlinger, On the Source of Mediterranean Overflow Water Property Changes, *J. Phys. Oceanogr.*, *39*, 1800–1817, 2009, doi:10.1175/2009JPO4109.1.

Lozier, M. S., & N. M. Stewart, On the temporally varying northward penetration of Mediterranean Overflow Water and eastward penetration of Labrador Sea water, *J. Phys. Oceanogr.*, *38*, 2097–2103, 2008, doi:10.1175/2008JPO3908.1.

Lumpkin, R., K. G. Speer, & K. P. Koltermann, Transport across 48°N in the Atlantic Ocean, *J. Phys. Oceanogr.*, *38*, 2008.

Lynn, R. J., & J. J. Simpson, The California Current system: The seasonal variability of its physical characteristics, *Journal of Geophysical Research: Oceans*, *92*, 12947–12966, 1987, doi:10.1029/JC092iC12p12947.

Machin, F., J. L. Pelegri, E. Fraile-Nuez, P. Velez-Belchi, F. Lopez-Laatzen, & A. Hernandez-Guerra, Seasonal Flow Reversals of Intermediate Waters in the Canary Current System East of the Canary Islands, *J. Phys. Oceanogr.*, *40*, 1902–1909, 2010, doi:10.1175/2010JPO4320.1.

Marshall, J. C., A. J. G. Nurser, & R. G. Williams, Inferring the Subduction Rate and Period Over the North-Atlantic, *J. Phys. Oceanogr.*, *23*, 1315–1329, 1993, doi:10.1175/1520-0485(1993)023<1315:ITSRAP>2.0.CO;2.

Mason, E., F. Colas, J. Molemaker, A. F. Shchepetkin, C. Troupin, J. C. McWilliams, & P. Sangra, Seasonal variability of the Canary Current: A numerical study, *J. Geophys. Res.*, *116*, 2011, doi:10.1029/2010JC006665.

Mauritzen, C., A. Melsom, & R. Sutton, Importance of density-compensated temperature change for deep North Atlantic Ocean heat uptake, *Nat. Geosci.*, *5*, 905–910, 2012, doi:10.1038/ngeo1639.

Mazé, J. P., M. Arhan, & H. Mercier, Volume budget of the eastern boundary layer off the Iberian Peninsula, *Deep-Sea Res. I*, *44*, 1543–1574, 1997, doi:10.1016/S0967-0637(97)00038-1.

Memery, L., G. Reverdin, J. Paillet, & A. Oschlies, Introduction to the POMME special section: Thermocline ventilation and biogeochemical tracer distribution in the north-east Atlantic Ocean and impact of mesoscale dynamics, *J. Geophys. Res.*, *110*, 2005, doi:10.1029/2005JC002976.

Nolan, G., K. Lyons, S. Fennell, G. Westbrook, T. M. Grath, & A. Berry, Annex 9: Regional report - Ireland area (area 4b), in *ICES 2012 Report of the Working Group on Oceanic Hydrography (WGOH)*, CM 2012/SSGEF:03, pp. 59–68, ICES Headquarters, Copenhagen, Denmark, 2012.

Núñez Riboni, I., M. Bersch, H. Haak, J. H. Jungclaus, & K. Lohmann, A multi-decadal meridional displacement of the Subpolar Front in the Newfoundland Basin, *Ocean Sci.*, *8*, 91–102, 2012, doi:10.5194/os-8-91-2012.

Oliveira, P. B., A. Peliz, J. Dubert, T. L. Rosa, & A. M. P. Santos, Winter geostrophic currents and eddies in the western Iberia coastal transition zone, *Deep-Sea Res. Pt. I*, *51*, 367–381, 2004, doi:10.1016/j.dsr.2003.10.016.

Osychny, V., & P. Cornillon, Properties of Rossby waves in the North Atlantic estimated from satellite data, *J. Phys. Oceanogr.*, *34*, 61–76, 2004, doi:10.1175/1520-0485(2004)034<0061:PORWIT>2.0.CO;2.

Paillet, J., & M. Arhan, Oceanic ventilation in the eastern North Atlantic, *J. Phys. Oceanogr.*, *26*, 2036–2052, 1996a,doi:10.1175/1520-0485(1996)026<2036:OVITEN>2.0.CO;2.

Paillet, J., & M. Arhan, Shallow pycnoclines and mode water subduction in the eastern North Atlantic, *J. Phys. Oceanogr.*, *26*, 96–114, 1996b, doi:10.1175/1520-0485(1996)026<0096:SPAMWS>2.0.CO;2.

Paillet, J., & H. Mercier, An inverse model of the eastern North Atlantic general circulation and thermocline ventilation, *Deep-Sea Res. I*, *44*, 1293–1328, 1997, doi:10.1016/S0967-0637(97)00019-8.

Peliz, A., T. L. Rosa, A. P. Santos, & J. L. Pissarra, Fronts, jets, and counter-flows in the Western Iberian upwelling system, *J. Marine Syst.*, *35*, 61 – 77, 2002, doi:10.1016/S0924-7963(02)00076-3.

Peliz, A., J. S. Dubert, & D. B. Haidvogel, Subinertial response of a density-driven eastern boundary poleward current to wind forcing, *J. Phys. Oceanogr.*, *33*, 1633–1650, 2003.

Peliz, A., J. Dubert, A. M. P. Santos, P. B. Oliveira, & B. Le Cann, Winter upper ocean circulation in the Western Iberian Basin - fronts, eddies and poleward flows: an overview, *Deep-Sea Res. I*, *52*, 621–646, 2005, doi:10.1016/j.dsr.2004.11.005.

Penduff, T., A. C. de Verdière, & B. Barnier, General circulation and intergyre dynamics in the eastern North Atlantic from a regional primitive equation model, *J. Geophys. Res. Oceans*, *106*, 22313–22329, 2001, doi:10.1029/2000JC000346.

Pérez, F. F., A. F. Ríos, B. A. King, & R. T. Pollard, Decadal changes of the θ -S relationship of the eastern North Atlantic Central Water, *Deep-Sea Res. I*, *42*, 1849–1864, 1995, doi:10.1016/0967-0637(95)00091-7.

Pérez, F. F., R. T. Pollard, J. F. Read, V. Valencia, J. M. Cabanas, & A. F. Ríos, Climatological coupling of the thermohaline decadal changes in Central Water of the Eastern North Atlantic, *Sci. Mar.*, *64*, 347–353, 2000, doi:10.3989/scimar.2000.64n3347.

Pickart, R. S., & S. S. Lindstrom, A comparison of techniques for referencing geostrophic velocities, *J. Atmos. Ocean. Tech.*, *11*, 813-824, 1994.

Pickart, R. S., F. Straneo, & G. W. K. Moore, Is Labrador Sea Water formed in the Irminger basin?, *Deep Sea Res., Part I*, *50*, 23–52, 2003, doi:10.1016/S0967-0637(02)00134-6.

Pingree, R. D., Component of Labrador Sea-Water in Bay-Of-Biscay, *Limnol. Oceanogr.*, *18*, 711–718, 1973, doi:10.4319/lo.1973.18.5.0711.

Pingree, R. D., Winter warming in the southern Bay of Biscay and Lagrangian eddy kinematics from a deep-drogued Argos buoy, *J. Mar. Biol. Assoc. U. K.*, *74*, 107–128, 1994, doi:10.1017/S0025315400035700.

Pingree, R. D., & B. Le Cann, Structure, strength and seasonality of the slope currents in the Bay of Biscay region, *J. Mar. Biol. Assoc. U. K.*, *70*, 857–885, 1990, doi:10.1017/S0025315400059117.

Pingree, R. D., & B. Le Cann, Anticyclonic eddy X91 in the southern Bay of Biscay, May 1991 to February 1992, *J. Geophys. Res.*, *97*, 14353–14367, 1992a, doi:10.1029/92JC01181.

Pingree, R. D., & B. Le Cann, Three anticyclonic Slope Water Oceanic eDDIES (SWODDIES) in the Southern Bay of Biscay in 1990, *Deep-Sea Res. A*, *39*, 1147–1175, 1992b, doi:10.1016/0198-0149(92)90062-X.

Pollard, R. T., & S. Pu, Structure and circulation of the upper Atlantic Ocean northeast of the Azores, *Prog. Oceanogr.*, *14*, 443–462, 1985, doi:10.1016/0079-6611(85)90022-9.

Pollard, R. T., M. J. Griffiths, S. A. Cunningham, J. F. Read, F. F. Pérez, & A. F. Ríos, Vivaldi 1991 – a study of the formation, circulation and ventilation of eastern North Atlantic Central Water, *Prog. Oceanogr.*, *37*, 167–192, 1996, doi:10.1016/S0079-6611(96)00008-0.

Polyakov, I., V. Alexeev, U. Bhatt, E. Polyakova, & X. Zhang, North Atlantic warming: patterns of long-term trend and multidecadal variability, *Clim. Dyn.*, *34*, 439–457, 2010, doi:10.1007/s00382-008-0522-3.

Quaresma, L. S., & A. Pichon, Modelling the barotropic tide along the West-Iberian margin, *J. Marine Syst.*, *109-110*, S3 – S25, 2013, doi:10.1016/j.jmarsys.2011.09.016.

Read, J. F., & W. J. Gould, Cooling and freshening of the subpolar North Atlantic Ocean since the 1960s, *Nature*, *360*, 55–57, 1992, doi:10.1038/360055a0.

Rhines, P. B., & R. Schopp, The wind-driven circulation: quasi-geostrophic simulations and theory for nonsymmetric winds, *J. Phys. Oceanogr.*, *21*, 1438-1469, 1991, doi:10.1175/1520-0485(1991)021<1438:TWDCQG>2.0.CO;2.

Richardson, P. L., A. S. Bower, & W. Zenk, A census of Meddies tracked by floats, *Prog. Oceanogr.*, *45*, 209–250, 2000, doi:10.1016/S0079-6611(99)00053-1.

Risien, C. M., & D. B. Chelton, A Global Climatology of Surface Wind and Wind Stress Fields from Eight Years of QuikSCAT Scatterometer Data, *J. Phys. Oceanogr.*, *38*, 2379–2413, 2008, doi:10.1175/2008JPO3881.1.

Rubio, A., D. Gomis, G. Jordá, & M. Espino, Estimating geostrophic and total velocities from CTD and ADCP data: Intercomparison of different methods, *J. Marine Syst.*, *77*, 61 – 76, 2009, doi:10.1016/j.jmarsys.2008.11.009.

Ruiz-Villarreal, M., C. González-Pola, G. Díaz del Río, A. Lavín, P. Otero, S. Piedracoba, & J. M. Cabanas, Oceanographic conditions in North and Northwest Iberia and their influence on the Prestige oil spill, *Mar. Pollut. Bull.*, *53*, 220–238, 2006, doi:10.1016/j.marpolbul.2006.03.011.

Santos, A., H. Martins, H. Coelho, P. Leitão, & R. Neves, A circulation model for the European ocean margin, *Appl. Math. Model.*, *26*, 563 – 582, 2002, doi:10.1016/S0307-904X(01)00069-5.

Sarafanov, A., On the effect of the North Atlantic Oscillation on temperature and salinity of the subpolar North Atlantic intermediate and deep waters, *ICES J. Mar. Sci.*, *66*, 1448–1454, 2009, doi:10.1093/icesjms/fsp094.

Sarafanov, A., A. Falina, A. Sokov, & A. Demidov, Intense warming and salinification of intermediate waters of southern origin in the eastern subpolar North Atlantic in the 1990s to mid-2000s, *J. Geophys. Res.*, *113*, 2008, doi:10.1029/2008JC004975.

Sarafanov, A., H. Mercier, A. Falina, A. Sokov, & P. Lherminier, Cessation and partial reversal of deep water freshening in the northern North Atlantic: observation-based estimates and attribution, *Tellus A*, *62*, 80–90, 2010, doi:10.1111/j.1600-0870.2009.00418.x.

Sarafanov, A. A., A. V. Sokov, & A. S. Falina, Warming and salinification of Labrador Sea Water and deep waters in the subpolar North Atlantic at 60°N in 1997-2006, *Oceanology*, *49*, 193–204, 2009, doi:10.1134/S0001437009020040.

Slater, D., The transport of Mediterranean Water in the North Atlantic Ocean, Ph.D. thesis, University of Southampton, UK, 2003.

Solomon, S., D. Qin, M. Manning, M. Marquis, K. Averyt, M. M. B. Tignor, H. L. Miller, & Z. Chen (Eds.), *Climate Change 2007 - The Physical Science Basis: Working Group I Contribution to the Fourth Assessment Report of the IPCC (Climate Change 2007)*, Cambridge University Press, 2007.

Somavilla, R., C. Gonzalez-Pola, C. Rodriguez, S. A. Josey, R. F. Sanchez, & A. Lavin, Large changes in the hydrographic structure of the Bay of Biscay after the extreme mixing of winter 2005, *J. Geophys. Res.*, *114*, 2009, doi:10.1029/2008JC004974.

Srokosz, M., Baringer, M., Bryden, H., Cunningham, S., Delworth, T., Lozier, S., Marotzke, J. & and R. Sutton, Past, Present, and Future Changes in the Atlantic Meridional Overturning Circulation, *Bull. Amer. Meteor. Soc.*, *93*, 1663-1676, 2012, doi:10.1175/BAMS-D-11-00151.1.

Stramma, L., & H. J. Isemer, Seasonal Variability of Meridional Temperature Fluxes in the Eastern North-Atlantic Ocean, *J. Mar. Res.*, *46*, 281–299, 1988, doi:10.1357/002224088785113577.

Stramma, L., & G. Siedler, Seasonal Changes in the North Atlantic Subtropical Gyre, *J. Geophys. Res.*, *93*, 8111–8118, 1988.

Sundby, S., & K. Drinkwater, On the mechanisms behind salinity anomaly signals of the northern North Atlantic, *Prog. Oceanogr.*, *73*, 190–202, 2007, doi:10.1016/j.pocean.2007.02.002.

Sy, A., M. Rhein, J. R. N. Lazier, K. P. Koltermann, J. Meincke, A. Putzka, & M. Bersch, Surprisingly rapid spreading of newly formed intermediate waters across the North Atlantic Ocean, *Nature*, *386*, 675–679, 1997, doi:10.1038/386675a0.

Thomson, R. E., S. Tabata, & D. Ramsdem, Comparison of sea level variability on the Caribbean and the Pacific coasts and the Panama canal, in *Time series of ocean measurements*, vol. 2 of *IOC Technical Series*, pp. 33–37, UNESCO, 1985.

Torres, R., & E. D. Barton, Onset and development of the Iberian poleward flow along the Galician coast, *Cont. Shelf. Res.*, *26*, 1134–1153, 2006, doi:10.1016/j.csr.2006.03.009.

Vage, K., R. S. Pickart, V. Thierry, G. Reverdin, C. M. Lee, B. Petrie, T. A. Agnew, A. Wong, & M. H. Ribergaard, Surprising return of deep convection to the subpolar North Atlantic Ocean in winter 2007-2008, *Nat. Geosci.*, *2*, 67–72, 2009, doi:10.1038/ngeo382.

van Aken, H. M., The hydrography of the mid-latitude Northeast Atlantic Ocean. I: The deep water masses, *Deep-Sea Res. I*, *47*, 757–788, 2000a, doi:10.1016/S0967-0637(99)00092-8.

van Aken, H. M., The hydrography of the mid-latitude Northeast Atlantic Ocean. II: The intermediate water masses, *Deep-Sea Res. I*, *47*, 789–824, 2000b, doi:10.1016/S0967-0637(99)00112-0.

van Aken, H. M., The hydrography of the mid-latitude Northeast Atlantic Ocean - Part III: The subducted thermocline water mass, *Deep-Sea Res. I*, *48*, 237–267, 2001, doi:10.1016/S0967-0637(00)00059-5.

van Aken, H. M., M. F. de Jong, & I. Yashayaev, Decadal and multi-decadal variability of Labrador Sea Water in the north-western North Atlantic Ocean derived from tracer distributions: Heat budget, ventilation, and advection, *Deep-Sea Res. I*, *58*, 505 – 523, 2011, doi:10.1016/j.dsr.2011.02.008.

Varela, R. A., G. Roson, J. L. Herrera, S. Torres-Lopez, & A. Fernandez-Romero, A general view of the hydrographic and dynamical patterns of the Rias Baixas adjacent sea area, *J. Mar. Sys.*, *54*, 97–113, 2005, doi:10.1016/j.jmarsys.2004.07.006.

Vargas-Yáñez, M., G. Parrilla, A. Lavín, P. Vélez-Belchí, C. González-Pola, & A. Hernández-Guerra, Eddy-induced variability in a transatlantic section: Argo observing system-gyroscope 0302 cruise comparison, *J. Atmos. Ocean. Tech.*, *22*, 1069–1079, 2005, doi:10.1175/JTECH1761.1.

Visbeck, M., Deep velocity profiling using lowered Acoustic Doppler Current Profiler: Bottom track and inverse solutions, *J. Atmos. Ocean. Tech.*, *19*, 794–807, 2002, doi:10.1175/1520-0426(2002)019<0794:DVPULA>2.0.CO;2.

von Storch, H., & F. Zwiers, *Statistical Analysis in Climate Research*, Cambridge University Press, 2001.

Wooster, W. S., A. Bakun, & D. R. Mclain, Seasonal upwelling cycle along eastern boundary of North-Atlantic, *J. Mar. Res.*, *34*, 131–141, 1976.

Wunsch, C., The interpretation of short climate records, with comments on the North Atlantic and Southern Oscillations, *Bull. Amer. Meteor. Soc.*, *80*, 245–255, 1999, doi:10.1175/1520-0477(1999)080<0245:TIOSCR>2.0.CO;2.

Wunsch, C., Mass and volume transport variability in an eddy-filled ocean, *Nat. Geosci.*, *1*, 165–168, 2008, doi:10.1038/ngeo126.

Yaremchuk, M. I., D. A. Nechaev, & K. R. Thompson, Seasonal variation of the North Atlantic Current, *J. Geophys. Res.*, *106*, 6835–6851, 2001, doi:10.1029/2000JC900166.

Yashayaev, I., & B. Greenan, Environmental Conditions in the Labrador Sea in 2010, *Tech. rep.*, Northwest Atlantic Fisheries Organization (NAFO), 2011.

Yashayaev, I., & B. Greenan, Environmental Conditions in the Labrador Sea during 2011, *Tech. rep.*, Northwest Atlantic Fisheries Organization (NAFO), 2012.

Yashayaev, I., & J. W. Loder, Enhanced production of Labrador Sea Water in 2008, *Geophys. Res. Lett.*, *36*, 2009.

Yashayaev, I., & J. W. Loder, Environmental Conditions in the Labrador Sea in 2009, *Tech. rep.*, Northwest Atlantic Fisheries Organization (NAFO), 2010.

Yashayaev, I., M. Bersch, & H. M. van Aken, Spreading of the Labrador Sea Water to the Irminger and Iceland basins, *Geophys. Res. Lett.*, *34*, 2007, doi:10.1029/2006GL028999.